UNIVERSITÉ DE MONTRÉAL

CLASSIFICATION OF ALZHEIMER'S DISEASE AND MILD COGNITIVE IMPAIRMENT USING LONGITUDINAL FDG-PET IMAGES

SEYED HOSSEIN NOZADI
DÉPARTEMENT DE GÉNIE INFORMATIQUE ET GÉNIE LOGICIEL
ÉCOLE POLYTECHNIQUE DE MONTRÉAL

MÉMOIRE PRÉSENTÉ EN VUE DE L'OBTENTION
DU DIPLÔME DE MAÎTRISE ÈS SCIENCES APPLIQUÉES
(GÉNIE INFORMATIQUE)
JUIN 2017

UNIVERSITÉ DE MONTRÉAL

ÉCOLE POLYTECHNIQUE DE MONTRÉAL

Ce mémoire intitulé :

CLASSIFICATION OF ALZHEIMER'S DISEASE AND MILD COGNITIVE IMPAIRMENT USING LONGITUDINAL FDG-PET IMAGES

présenté par : NOZADI Seyed Hossein
en vue de l'obtention du diplôme de : Maîtrise ès sciences appliquées
a été dûment accepté par le jury d'examen constitué de :

M. BILODEAU Guillaume-Alexandre, Ph. D., président
M. KADOURY Samuel, Ph. D., membre et directeur de recherche
M. TOEWS Matthew, Ph. D., membre

DEDICATION

To my lovely Mom,
and in memory of my wonderful Dad,
dearly missed

ACKNOWLEDGEMENTS

Foremost, I would like to express my sincere gratitude to my research director Prof. Samuel Kadoury for the continuous support of my master's program, for his patience, motivation, enthusiasm, and immense knowledge. His guidance and his following up helped me a lot while researching and writing this thesis. I would like to thank my thesis committee : M. Bilodeau Guillaume-Alexandre, Ph.D. and M. Toews Matthew, Ph.D. for accepting to be the part of the jury. Also, a lot of thanks to my colleague Mahsa Shakeri for being supportive during all my experiments and working in the lab. I am also very thankful to my lab mates, Poayhoon, Robert, Eugene, and Shashank, for their help and collaboration.

I do appreciate my best encourager during my study, Alejandro Mendoza, for giving me good motivation and supporting me mentally to do my best in this work. Last but not least, I would like to thank my family, my parents for their endless support and prayers for me.

Data collection and sharing for this project was funded by the Alzheimer's Disease Neuroimaging Initiative (ADNI) (National Institutes of Health Grant U01 AG024904) and DOD ADNI (Department of Defense award number W81XWH-12-2-0012).

RÉSUMÉ

La maladie d'Alzheimer (MA) est la principale cause de maladies dégénératives et se caractérise par un début insidieux, une perte de mémoire précoce, des déficits verbaux et visuo-spatiaux (associés à la destruction des lobes temporal et pariétal), un développement progressif et une absence de signes neurologiques tôt dans l'apparition de la maladie. Aucun traitement n'est disponible en ce moment pour guérir la MA. Les traitements actuels peuvent souvent ralentir de façon significative la progression de la maladie. La capacité de diagnostiquer la MA à son stade initial a un impact majeur sur l'intervention clinique et la planification thérapeutique, réduisant ainsi les coûts associés aux soins de longue durée. La distinction entre les différents stades de la démence est essentielle afin de ralentir la progression de la MA.

La différenciation entre les patients ayant la MA, une déficience cognitive légère précoce (DCLP), une déficience cognitive légère tardive (DCLT) ou un état cognitif normal (CN) est un domaine de recherche qui a suscité beaucoup d'intérêt durant la dernière décennie. Les images obtenues par tomographie par émission de positrons (TEP) font partie des meilleures méthodes accessibles pour faciliter la distinction entre ces différentes classes. Du point de vue de la neuro-imagerie, les images TEP par fluorodésoxyglucose (FDG) pour le métabolisme cérébral du glucose et pour les plaques amyloïdes (AV45) sont considérées comme des biomarqueurs ayant une puissance diagnostique élevée. Cependant, seules quelques approches ont étudié l'efficacité de considérer uniquement les zones actives localisées par la TEP à des fins de classification.

La question de recherche principale de ce travail est de démontrer la capacité des images TEP à classer les résultats de façon précise et de comparer les résultats de deux méthodes d'imagerie TEP (FDG et AV45). Afin de déterminer la meilleure façon de classer les sujets dans les catégories MA, DCLP, DCLT ou CN en utilisant exclusivement les images TEP, nous proposons une procédure qui utilise les caractéristiques apprises à partir d'images TEP identifiées sémantiquement. Les machines à vecteurs de support (MVS) sont déjà utilisées pour faire de nombreuses classifications et font partie des techniques les plus utilisées pour la classification basée sur la neuro-imagerie, comme pour la MA. Les MVS linéaires et la fonction de base radiale (FBR)-MVS sont deux noyaux populaires utilisés dans notre classification. L'analyse en composante principale (ACP) est utilisée pour diminuer la taille des données suivie par les MVS linéaires qui sont une autre méthode de classification. Les forêts d'arbres décisionnels (FAD) sont aussi exécutées pour rendre les résultats obtenus par MVS comparables. L'objectif général de ce travail est de concevoir un ensemble d'outils déjà exis-

tants pour classer la MA et les différents stades de DCL. Suivant les étapes de normalisation et de prétraitement, une méthode d'enregistrement TEP-IRM multimodale et déformable est proposée afin de fusionner l'atlas du MNI au scan TEP de chaque patient et de développer une méthode simple de segmentation basée sur l'atlas du cerveau dans le but de générer un volume étiqueté avec 10 régions d'intérêt communes. La procédure a deux approches : la première utilise l'intensité des voxels des régions d'intérêt, et la seconde, l'intensité des voxels du cerveau en entier.

La méthode a été testée sur 660 sujets provenant de la base de données de l'(Alzheimer's Disease Neuroimaging Initiative) et a été comparée à une approche qui incluait le cerveau en entier. La précision de la classification entre la MA et les CN a été mesurée à 91,7% et à 91,2% en utilisant la FBR et les FAD, respectivement, sur des données combinant les caractéristiques multirégionales des FDG-TEP des examens transversal et de suivi. Une amélioration considérable a été notée pour la précision de classification entre les DCLP et DCLT avec un taux de 72,5%. La précision de classification entre la MA et les CN en utilisant AV45-TEP avec les données combinées a été mesurée à 90,8% et à 87,9% pour la FBR et les FAD, respectivement. Cette procédure démontre le potentiel des caractéristiques multirégionales de la TEP pour améliorer l'évaluation cognitive. Les résultats observés confirment qu'il est possible de se fier uniquement aux images TEP sans ajout d'autres bio-marqueurs pour obtenir une précision de classification élevée.

ABSTRACT

Alzheimer's disease (AD) is the most general cause of degenerative dementia, characterized by insidious onset early memory loss, language and visuospatial deficits (associated with the destruction of the temporal and parietal lobes), a progressive course, and lack of early neurological signs early in the course of disease. There is currently no absolute cure for AD but some treatments can slow down the progression of the disease in early stages of AD. The ability to diagnose AD at an early stage has a great impact on the clinical intervention and treatment planning, and hence reduces costs associated with long-term care. In addition, discrimination of different stages of dementia is crucial to slow down the progression of AD. Distinguishing patients with AD, early mild cognitive impairment (EMCI), late mild cognitive impairment (LMCI), and normal controls (NC) is an extremely active research area, which has garnered significant attention in the past decade. Positron emission tomography (PET) images are one of the best accessible ways to discriminate between different classes. From a neuroimaging point of view, PET images of fluorodeoxyglucose (FDG) for cerebral glucose metabolism and amyloid plaque images (AV45) are considered a highly powerful diagnostic biomarker, but few approaches have investigated the efficacy of focusing on localized PET-active areas for classification purposes.

The main research question of this work is to show the ability of using PET images to achieve accurate classification results and to compare the results of two imaging methods of PET (FDG and AV45). To find the best scenario to classify our subjects into AD, EMCI, LMCI, and NC using PET images exclusively, we proposed a pipeline using learned features from semantically labelled PET images to perform group classification using four classifiers. Support vector machines (SVMs) are already applied in a wide variety of classifications, and it is one of the most popular techniques in classification based on neuroimaging like AD. Linear SVMs and radial basis function (RBF) SVMs are two common kernels used in our classification. Principal component analysis (PCA) is used to reduce the dimension of our data followed by linear SVMs, which is another method of classification. Random forest (RF) is also applied to make our SVM results comparable. The general objective of this work is to design a set of existing tools for classifying AD and different stages of MCI. Following normalization and pre-processing steps, a multi-modal PET-MRI registration method is proposed to fuse the Montreal Neurological Institute (MNI) atlas to PET images of each patient which is registered to its corresponding MRI scan, developing a simple method of segmentation based on a brain atlas generated from a fully labelled volume with 10 common regions of interest (ROIs). This pipeline can be used in two ways: (1) using voxel intensities

from specific regions of interest (multi-region approach), and (2) using voxel intensities from the entire brain (whole brain approach).

The method was tested on 660 subjects from the Alzheimer's Disease Neuroimaging Initiative database and compared to a whole-brain approach. The classification accuracy of AD vs NC was measured at 91.7 % and 91.2 % when using RBF-SVM and RF, respectively, on combining both multi-region features from FDG-PET on cross-sectional and follow-up exams. A considerable improvement compare to the similar works in the EMCI vs LMCI classification accuracy was achieved at 72.5 %. The classification accuracy of AD versus NC using AV45-PET on the combined data was measured at 90.8 % and 87.9 % using RBF-SVM and RF, respectively. The pipeline demonstrates the potential of exploiting longitudinal multi-region PET features to improve cognitive assessment. We can achieve high accuracy using only PET images. This suggests that PET images are a rich source of discriminative information for this task. We note that other methods rely on the combination of multiple sources.

TABLE OF CONTENTS

LIST OF TABLES

LIST OF FIGURES

LIST OF SYMBOLS AND ABBREVIATIONS

French

MA	Maladie d'Alzheimer
TEP	Tomographie par émission de positrons
INM	Institut neurologique de Montréal

English

3D	Three dimensional
AD	Alzheimer's disease
$A\beta$	$\beta-$amyloid
AAL	Automated anatomical labelling
AAN	American academy of neurology
ACC	Accuracy
ADNI	Alzheimer's disease neuroimaging initiative
AIR	Automated image registration
ANN	Artificial neural network
ANT	Advanced normalization tools
APOE	Apolipoprotein E
APP	Amyloid precursor protein
BET	Brain extraction tool
CSF	Cerebral spinal fluid
CT	Computerized tomography
EMCI	Early mild cognitive impairment
FAST	FMRIB's automated segmentation tool
FDA	Food and Drug Administration
FDG	Fluoro-deoxy-D-glucose
FLIRT	FMRIB's linear image registration tool
FMRI	Functional magnetic resonance imaging
FMRIB	Functional Magnetic Resonance Imaging of the Brain
FN	False negative
FSL	FMRIB Software Library
FWHM	Full width at half maximum

GM	Grey matter
ICPR	International conference on pattern recognition
IRTK	Image registration toolkit
KNN	K-nearest neighbor
LMCI	Late mild cognitive impairment
MATLAB	MATrix LABoratory (software's name)
MCI	Mild cognitive impairment
MMSE	Mini–mental state examination
MNI	Montreal neurological institute
MR	Magnitude Resonance
MRI	Magnitude resonance image
NC	Normal control
NIFTI	Neuroimaging informatics technology initiative
NIH	National institutes of health
PC	Principal component
PCA	Principal Component Analysis
PET	Positron emission tomography
PLR	Penalized logistic regression
RBF	Radial basis function
RBF-SVM	Radial Basis Function-Support Vector Machine
RF	Random forest
ROI	Region of interest
RTM	Registration transformation matrix
SEN	Sensitivity
SLR	Sparse Logistic Regression
SPE	Specificity
SPECT	Single Photon Emission Computed Tomography
SPM	Statistical parametric mapping
SPSLR	Spatially Regularized Sparse Logistic Regression
SVD	Singular value decomposition
SVM	Support Vector Machine
VBM	Voxel-based morphometry
WM	White matter

CHAPTER 1 INTRODUCTION

Alzheimer's disease (AD) is one of the most common causes of dementia in the aging population and is known as a neurodegenerative disorder. Typically, AD follows certain stages, which will bring about changes in a person's life. Mild cognitive impairment (MCI) is the preclinical stage of Alzheimer's disease (Dessouky and Taha, 2013) and is an intermediate stage of normal aging dementia between expected age-related dementia and the serious decline of dementia. MCI is classified into early stage and late stage before converting to AD. The early stage of MCI (EMCI) refers to any aged person who has mild impairment. Some common symptoms are recognized in this stage, like forgetfulness, changes in mood and behaviour, as well as problems with memory, language, thinking, and judgment that are greater than normal age-related changes. The next stage of MCI is late stage (LMCI), which brings a greater decline in the person's cognitive and functional abilities (Mayo Clinic Staff, 2017).

In developed countries, due to good treatment and the high rank of health, people can live longer. However, their lifestyles and habits influence disease risk. Moreover, some vascular system problems (hypertension, type 2 diabetes, and obesity) increase the risk of dementia including AD (Kalaria et al., 2008). As of today, there is still no absolute cure for AD but some treatments like cholinesterase inhibitors, a type of drug approved for Alzheimer's disease given to people with MCI whose main symptom is memory loss (Lee et al., 2011), can slow down the progression of the disease in the early stages of AD (Salmon, 2008), (Cabral and Silveira, 2013). Therefore, being able to differentiate and diagnose the different stages of AD can help improve on time treatment for the early stages. The early detection of AD as well as finding a successful treatment to slow down the progression of symptoms are still challenges.

In the last few years, the development of automated diagnostic tools has attracted great attention. Classification between the different stages of AD and normal control (NC) is popular, and different approaches were developed to get better results of classification (Fox et al., 1996), (Zhang et al., 2011a), (Habeck et al., 2008), (Smailagic et al., 2015). The PET images are one of the best accessible ways to discriminate between different classes. Therefore, classification of AD and MCI based on PET images has been the main objective of several works (Gray et al., 2012), (Rodrigues and Silveira, 2014), (Aidos et al., 2014a). In this work, PET images are used as the main biomarker to discriminate between the different stages of MCI and AD versus NC.

1.1 Definition and Basic Concept

Alzheimer's disease (AD) is a brain disorder that is not part of normal aging, although the greatest known risk factor is increasing age (Alzheimer's Association, 2016). Since there is an abundance of published information about AD, emphasis will be put on basic information related to the work of this thesis.

Neuroimaging, with its strong ability to produce high-quality images of the brain, has been a true revolution in medicine. Computerized tomography (CT), magnetic resonance imaging (MRI), positron emission tomography (PET), and single photon emission computed tomography (SPECT) are the most common imaging techniques used to provide detailed and non-invasive visualization of internal anatomy and physiology. For instance, to help evaluate organ and tissue functions, PET uses small amounts of radioactive materials called radiotracers, an adapted camera, and a computer. By identifying body changes at the cellular level, PET may detect the early onset of the disease before it is evident on other imaging tests. Among the modalities above, PET provides very good and complimentary information for diagnosis of AD (Bauer, 2014).

There is no definite cure for AD. Likely there is some treatment for early stage of AD and in case of diagnosing the AD in early stage and recommending the treatment planing we can reduce the costs associated with the long term care.

The PET exam is usually used after ensuring that patient does not have any other neurological disorders using clinical tests and CT or MRI scans. When the patient is diagnosed with any stage of AD, a long-term follow up is arranged along with treatment planning, when applicable. In this case, using only PET imaging can be a possible solution to track the patient's disease progression as well as to diagnose patients who are not able to have a MRI due to metal parts like a heart battery. Therefore, we used PET images at two time points : first visit (or baseline) and second visit, which is approximately after 12 months.

There is different way for AD diagnosis, brain imaging (structural, functional or metabolic examination) can help to get more accurate and robust diagnosis. MRI is already tested by several publications and it gives high results, but still neurological finding regions which are more affected by AD is under question. PET is looking at metabolic activity of radioactive compound inside of the body and specifically in brain to find out the most affected regions by AD.

Most of the published works on classification between AD and MCI vs NC. However, differentiating between the different stages of MCI is more relevant in treatment planning.

1.2 Problem and Research Question

Medical signs, which are limited to the medical observations of the patient, can be measured accurately and reproducibly (Strimbu and Tavel, 2011). Biomarkers, on their side, refer to signs measured with medical tools such as clinical exams, blood tests, imaging, and neuroimaging. Neuroimaging is focused on early detection among the most promising areas of research (Alzheimer's Association, 2016). Recently, standard workup for AD includes structural imaging with MRI or CT to rule out other conditions that may cause symptoms similar to Alzheimer's with different treatment. Structural imaging can reveal tomors, evidence of small or large strokes, damage from severe head trauma or a buildup of fluid in the brain. Whereas, PET suggests that those with Alzheimer's typically have reduced brain cell activity in certain regions. For example, studies with fluorodeoxyglucose (FDG)-PET indicate that Alzheimer's disease is often associated with reduced use of glucose (sugar) in brain areas important in memory, learning and problem solving. However, as with the shrinkage detected by structural imaging, there is not yet enough information to translate these general patterns of reduced activity into diagnostic information about individuals. Accurate and reliable classification of AD, EMCI, LMCI, and NC requires a targeted combination of biomarker results for treatment planning and follow up of the patients. To have a more accurate and robust method for this purpose, many researchers suggested solutions and methods, which have valuable results (Pontecorvo and Mintun, 2011), (Jack et al., 2004),(Carbonell et al., 2015). Nevertheless, among all these researchers and publications, few considered PET images as the only biomarker. In addition, PET images are categorized by their radiotracers, which are β-Amyloid (AV45) and fluorodeoxyglucose (FDG). Specifically, AV45-PET images are still not a frequently used biomarker for AD diagnosis, despite giving good information for discrimination between different stages.

Therefore, focusing on longitudinal PET images with two radiotracers (FDG and AV45) only for classification without any other biomarkers is still a relevant topic to investigate the high accuracy of classification. Using PET images is one step of the diagnosis of AD for patients who are referred to the medical team. Without PET images, there is a lack of non-invasive information to discriminate between the different stages of MCI and AD. Therefore, the hypothesis in this project is to use only PET images to investigate : 1) the regions of interest (ROIs), which are the most affected by AD and the different stages of MCI, compared to the whole brain, 2) the best classifier(s) using different methods to achieve the best possible accuracy, 3) the best method for classification of longitudinal data using a combination time points. In brief, our research question is to achieve the most accurate and robust classification

between AD, EMCI, LMCI, and NC using only PET images.

1.2.1 Motivation

In diagnostic imaging, Positron Emitted Tomography (PET) is one of the most effective imaging modalities for assessing neurological disorders. For Alzheimer's disease (AD), PET imaging was shown to be able to detect the onset of neurological disorders with increased levels of amyloid accumulation (Serrano-Pozo et al., 2011). Early detection provides patients with access to therapies that are more effective in the early stages of the disease. Distinguishing between the different stages of cognitive impairment currently depends on clinical history and some neuropsychological, biological, and molecular genetic examination. PET shows different patterns of hypometabolism in this disorder that might aid differential diagnosis (Morin et al., 2012). Imaging by different modalities such as CT and MRI provides rich anatomical information. Nevertheless, in the case of AD, PET images may also provide evidence of disease progression. In additional, PET images include complementary information to the best-established structural brain imaging measurements of disease progression (i.e., MRI measurements of hippocampal volume) (Weiner and Khachaturian, 2005). PET imaging with fludeoxyglucose (FDG) radio tracer can highlight different levels of pathology in dementia disorders, which may aid diagnosis. Therefore, FDG-PET provides slightly better discrimination than MRI (Mosconi et al., 2006) (Kawachi et al., 2006) (De Santi et al., 2001) (Matsunari et al., 2007) (Ishii et al., 2007) (Barrack, 2013).
Different anatomical regions used in previous works with multi-region approach to classify the subjects. However, integrated spesific anatomical regions detected by previous works could obtain better accuracy which attracted our attention to focus on certain offered ROIs in literature which are not tested together.
This project focused on the diagnostic value of PET imaging alone, particularly on two radiotracers of PET, namely FDG and AV45. FDG-PET has been used to study neurodegenerative diseases for over two decades. Indeed, a particular application for FDG-PET is recognizing AD because of the sharp contrast in their pattern of glucose hypometabolism. Therefore, FDG-PET is a valuable technique for diagnosing AD (Silverman et al., 2001) and for evaluating the efficacy of drugs that aim at modifying the progression of AD (Alexander et al., 2002). Decreased FDG-PET uptake reflects metabolic deficits due to synaptic dysfunction and possibly tau-mediated neuronal injury (Vemuri and Jack, 2010). Since the researchers could have complementary information of glucose metabolism from PET images could discriminate between AD and different stages of MCI versus NC, adding more biomarkers and using PET imaging in combination with MRI may improve discrimination performance over

what they achieved with only PET images. Even though there is other demographic and clinical information available, the present work focused on having a better understanding of the diagnostic accuracy of AV45 or FDG-PET imaging in AD, independently of other available modalities, cognitive examinations, and neuropsychological testing correlation. Future work could combine additional information.

1.2.2 Contribution

The contribution of this work is in validating the direct use of voxel intensity to discriminate between four classes (AD, LMCI, EMCI,NC) which is not used as a feature in the literature : (Aidos et al., 2014a)(Gray et al., 2012) (Rodrigues and Silveira, 2014) (Cabral and Silveira, 2013) (Carbonell et al., 2015). We extracted the anatomical structure of the brain by labelling 116 regions, which were extracted by applying the Automated Anatomical Labelling atlas (based on the MNI152 atlas) in PET images after registering them to their corresponding MRI scans. This differs from other works which performed segmentation using the watershed algorithm on FDG-PET images (Aidos et al., 2014a), multi-atlas propagation with enhanced registration (Gray et al., 2012), automated atlas-based segmentation developed by Desikan et al. (Rodrigues and Silveira, 2014) and by a ratio of voxel intensities (Cabral and Silveira, 2013), (Carbonell et al., 2015). Specifically, the majority of prior methods used, as ROIs the frontal, superior parietal, lateral temporal, lateral occipital, medial temporal, anterior cingulate and posterior cingulate cortex regions. Our method uses features extracted from ROIs using a single atlas-based segmentation, which enabled us to create the 2D matrices of the voxels in the multi-region approach to compare the images together. Our work employs two different classification approaches (multi-region, whole-brain) for two time points (baseline and second visit) and combination of the two time points for FDG-PET and AV45-PET images. We obtained the highest classification accuracy by combining the two time points, which is in line with published studies (Gray et al., 2012) (Cabral and Silveira, 2013) (Aidos et al., 2014a). An important consideration of the described multi-regional approach is that it requires MR imaging data. Structural imaging, which helped us to localize the anatomical regions, is routinely used to identify brain lesions. To clarify that we only used MRI to find the anatomical regions in the brain and the data for classification obtained from PET images only. MR imaging data also provides regional volumes and volume changes, which may be beneficial in combination with PET images. We additionally attempt the less commonly reported classification task of separating EMCI from LMCI patients. Our accuracy of 72% is encouraging compared with the most directly comparable studies based on PET imaging data and similar methodologies.

1.3 Research Objectives

In this work, we proposed a pipeline using the available image processing tools for each step (such as registration and segmentation) to classify our subjects into four different classes (AD, EMCI, LMCI, and NC). The main biomarker to do this classification is brain PET images (FDG-PET and AV45-PET). Our objectives are the following :

— To collect and analyze our cohort data downloaded from a pre-processed Alzheimer's Disease Neuroimaging Initiative (ADNI) database, which encompasses patients with both PET images (FDG & AV45) and structural MRI for two time points (baseline exam and after 12 months approximately) ;

— To register PET images by their corresponding MRI to find the brain anatomical structures and to segment the images into different regions including our ROIs ;

— To classify our subjects into four classes using different classifiers ; and

— To evaluate the results of classifiers and to compare the results of the two approaches (multi-regions and whole-brain).

1.4 Thesis Structure

This thesis is composed of eight chapters. Following the introduction, Chapter 2 provides background information and describes some useful terms for understanding this thesis. Chapter 3 presents a critical literature review of works with their methods, which are compared or applied to the current work. The included methods and their results of classification accuracies are state of the art. Chapter 4 explains our methodology and our proposed pipeline, particularly the two important steps of registration and segmentation. Chapter 5 presents our manuscript entitled "Identification of AD/LMCI/EMCI Patients from Semantically Parcelled AV45 and FDG-PET Images "submitted to the *IEEE Journal of Biomedical and Health Informatics* (March, 2017). This paper details the method of classification of our subjects and compares the results of different approaches using AV45 and FDG-PET. Chapter 6 then presents additional results of all our experiments, including our validation results, tuning parameters for classifiers, and classification results of different test methods. Chapter 7 discusses our method and results and Chapter 8 is the conclusion of this work.

CHAPTER 2 LITERATURE REVIEW

2.1 Human Brain

The human brain is one of the most complex organs in the body and is responsible for reasoning, memory, and coordination of bodily functions (MILLER et al., 2005). Each of the brain's parts perform a different function. We have different classifications of brain parts ; from the anatomical view, we can divide our brain into different parts.
The brain stem is deep in the centre of the brain between the spinal cord and the rest of the brain. The brain stem is an extremely important part of the brain as it serves to control motor and sensory systems, which controls many basic functions, such as breathing and sleeping, as well as the heart rate and blood pressure. It is also the seat of our most fundamental emotions like happiness, sadness, fear, love, or hate ; they all seem to reside in the brainstem (Watson et al., 2010). The basal ganglia on top of the brainstem coordinate messages between multiple other brain areas. In other words, it acts as a gateway to the higher cortical regions. All sensory information from our body passes through the thalamus and is directed to the correct regions of the cortex for further processing. The hippocampus, surrounding the thalamus, is a crucial part of the brain and the seat of our special working memory. It allows us to remember where we put those keys or how to get back home from work or school. At the base and the back of the brain, the two lobes of the cerebellum are responsible for coordination and balance of movement, allowing us to move multiple sets of muscles in a coordinated fashion so that we can walk and talk, take things up, and set things down (Hoffman, 2014). Therefore, the major parts of the brain are the cerebellum, cerebrum (cerebral hemisphere), diencephalon (hypothalamus), and brain stem, as shown in Figure 2.1.

The outermost layer of brain cells are called the cerebral cortex. The cerebral hemispheres are divided into four lobes, as shown in Figure 2.2. The different lobes perform very different functions. The occipital lobe contains the brain's visual processing system. The parietal lobe is concerned with processing sensory information and integrating it with the visual information from the occipital lobe ; it also manages handwriting and body position. The temporal lobe is the centre for memory and learning that contains the hippocampus and a number of other regions that are required to recognize different objects, faces, sounds, and environments. The frontal lobe is an important part of the brain and is responsible for problem solving, judgement, and motor function. It is associated with personality, language and social behaviour. It is the decision-making centre and contains the motor cortex, which

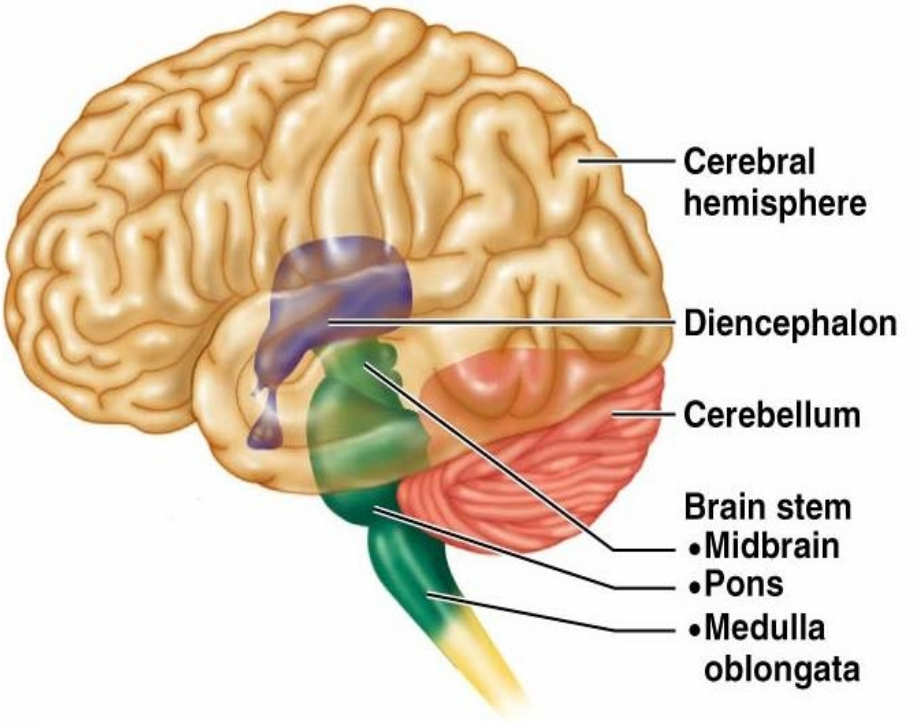

Figure 2.1 The major parts of human brain (http ://www.edoctoronline.com, 2016)

controls the movement.

2.1.1 Brain Structure

A human bain contains about 86 billion neurons (Pelvig et al., 2008). These cells are very specialized with long extensions through which they communicate with each other and form a large and complex network. These networks are the basis of how the brain works. The processes comprise two basic types ; dendrites receive incoming information from other neurons, and signals pass through the cell body of the soma to the other neurons. Figure 2.3 displays the structure of the neuron (Dayan and Abbott, 2001).

2.1.2 Neuronal Communication

Neurons usually use electrical signals to communicate ; however, the act of passing the signal from one neuron to another is a chemical process (Dayan and Abbott, 2001). Neurons are connected to each other via synapses. This is formed by the terminal of the axon of neuron A and the small membranous protrusion from a dendrite for neuron B, which is called a spine. Electrical signals from the axon pass through the dendrite, firing a chemical message called a neurotransmitter. Neurotransmitters are stored in small vesicles inside the axon terminal

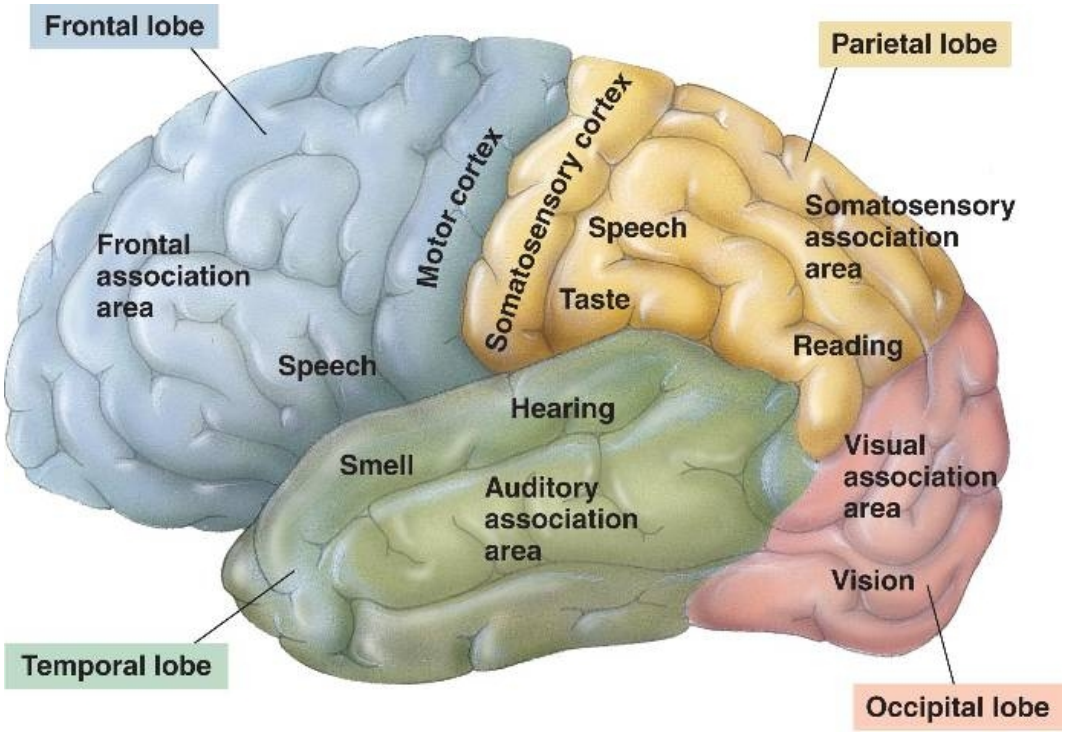

Figure 2.2 Four lobes of each hemisphere of the cerebral cortex (frontal, parietal, temporal, and occipital)(CaliSun, 2013).

(also called the synaptic bouton). When a signal arrives down the axon, one or more of these vesicles join with the outer membrane of the bouton and release its contents into a small gap between the axon and dendrite ; this is the synaptic cleft. On the other side of the synaptic cleft, the receptor molecules bind with the transmitter in much the same way as a key fits into a lock. There are actor molecules, actor poles through the outer membrane of the dendritic spine allowing charged atoms or ions to cross, this entry of charged ions into the spine re-creates the signal that was sent from the previous neuron. Consequently, information is passed from one neuron to the next and around the neuronal network. Although we described the synapse between two neurons, in reality, each neuron communicates with many others, over thousands of spines. In this way, an extraordinary complex system can be built that allows us to see, hear, and experience the world around us (Jahn, 2016). Figure 2.4 illustrates chemical synapse.

2.1.3 Neurodegenerative Disease

Degenerative nerve disease or neurodegenerative disease is a general term for several disorders and abnormalities that primarily affect the neurons in the human brain (Przedborski et al.,

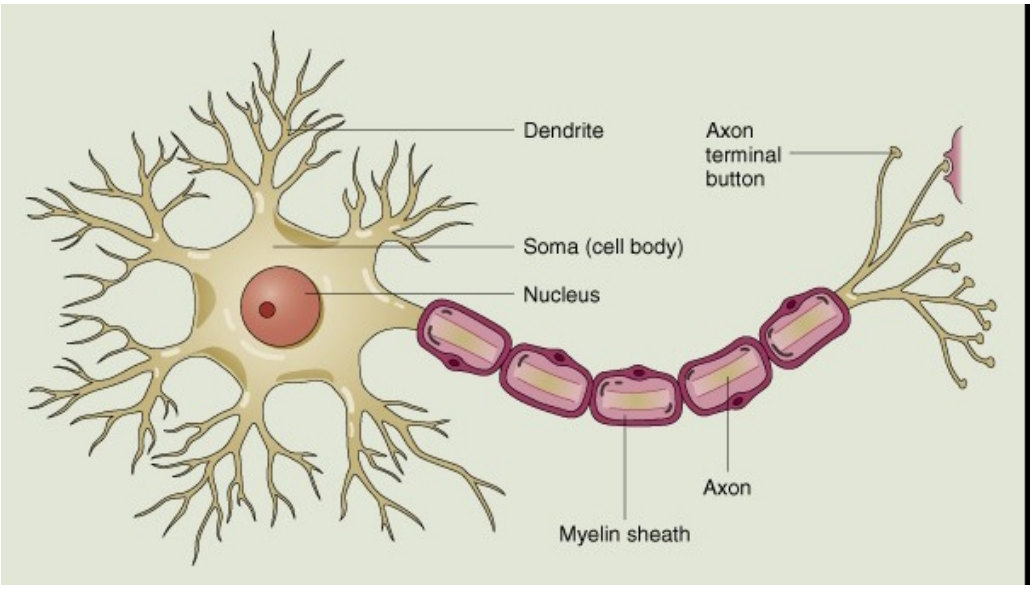

Figure 2.3 Structure of neuron (adapted from (Kirwan, 2016)).

2003). Consequently, it affects many of our body's activities, such as balancing, moving, talking, breathing, and heart functioning. Neurons are normally not replaceable, and they cannot reproduce themselves (Gage, 2004), so when they degenerate, they can not be replaced by new neurons. Additionally, as we know, neurons are the building blocks of the nervous system, which includes the brain and spinal cord. Neurodegenerative diseases are mostly incurable, and debilitating conditions result in progressive degeneration and or the death of nerve cells. This causes problems with movement or mental functioning. Dementias are responsible for the greatest proportion of such disease, with AD representing approximately 70 % of cases (Neurodegenerative Diseases Research, 2014).

The most popular neurodegenerative diseases are :

— Alzheimer's disease (AD) and other dementias,
— Parkinson's disease and related disorders,
— Prion disease,
— Motor neuron diseases,
— Huntington's disease,
— Spine cerebellar ataxia, and
— Spinal muscular atrophy.

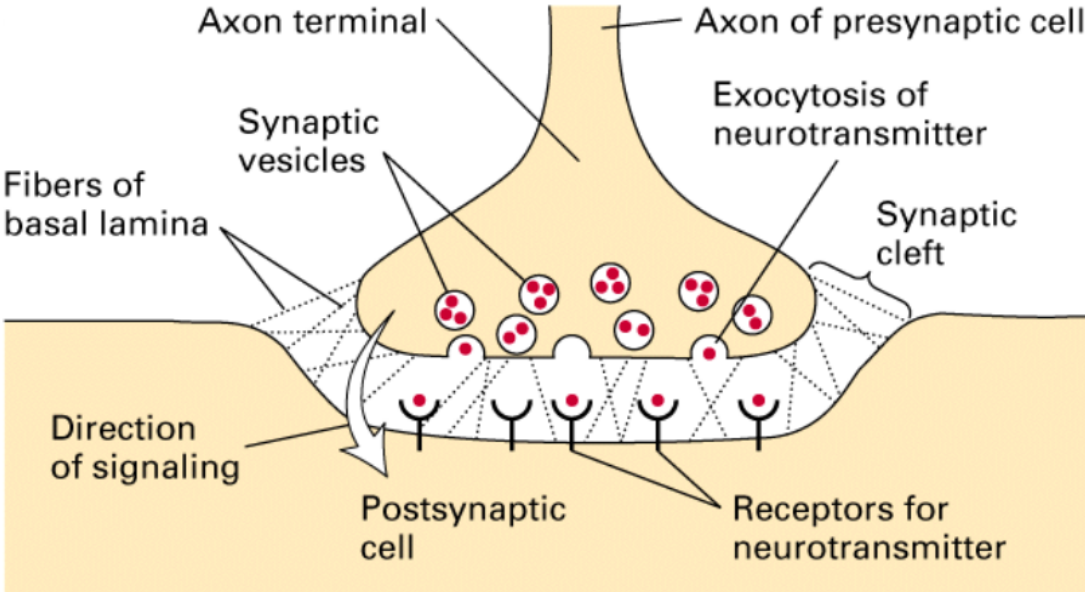

Figure 2.4 A chemical synapse (Lodish et al., 2000).

Alzheimer's disease

Alzheimer's disease (AD) was described for the first time in 1907 by the German psychiatrist Alois Alzheimer. In performing a histopathologic study on the brain of his patient, Auguste D., suffering from dementia, he brought to light the presence of two types of lesions in the brain : senile plaques and neurofibrillary tangles. Thus, he reached the conclusion that a distinct disease of the cerebral cortex exists. A hundred years later, due to current scientific techniques, research has made a great leap in understanding the disease. We know that the brain is made of neurons and that these are interconnected in a vast network. These connections (nano synapses) can transmit the information from one neuron to another. In Alzheimer's disease, 10 to 15 years before the development of apparent symptoms, two main lesions form in the brain, one is senile plaque composed of β-amyloid (Aβ) protein, and the other one comprises neurofibrillary tangles composed of τ protein (Budson and Kowall, 2011).

Senile plaque formation

There is a large protein on the surface of the neuron called the amyloid precursor protein (APP). Normally, APP is sectioned by an enzyme on the surface of the neurons and it releases the protein called Aβ. Then, the Aβ protein is cleared in the body. In the case of AD, there is an accumulation of Aβ since the clearing rate of the amyloid is decreased substantially, leading to the formation of plaques. The protein assembles to form indiscernible fibrosis and

creates senile plaque (Crews and Masliah, 2010).

Neurofibrillary tangle formation

When a neuron communicates with another neuron, the signal passes through the skeleton of the neuron composed of microtubules. These microtubules are stabilized by normal τprotein. In AD, τprotein becomes defective and gets detached from the microtubules. Thus, the skeleton of the neuron dissociates, as it is no longer maintained. Defective τprotein then assemble to form filaments in the neuron without the skeleton. The neuron degenerates, and connection between the neurons is lost. The abnormal accumulation of τ filaments and neurons creates neurofibrillary tangles and eventually causes the death of the neurons (Crews and Masliah, 2010).

Lesions spread out in the brain

Neurofibrillary tangles and senile plaque do not follow the same pathway in the brain over time. Neurofibrillary tangles first develop in the hippocampus, which is essential to memory and learning and then reach the whole brain following a centrifugal movement. The process causes brain atrophy, which engenders global dysfunction. The progression of the lesions corresponds with symptoms of the disease, which begins with memory problems, followed by problems of language, recognition, and inability to form gestures. Senile plaques develop differently. They are initially observed in the cortex, next in the hippocampus, and then the senile plaques reach the whole brain following a centripetal movement. Their progression does not correspond to the symptoms of the disease (Budson and Kowall, 2011).
Figure 2.5 illustrates different key players in the pathogenesis of AD. In brief, the aggregation and accumulation of Aβ in the brain may result from increased neuronal production of Aβ, decreased activity of Aβ degrading enzymes, or alterations in transport processes that shuttle Aβ across the blood-brain barrier. The Aβ oligomers impair synaptic functions, whereas fibrillar amyloid plaques displace and distort neuronal processes. The Aβ oligomers interact with cell surface membranes and receptors, altering signal-transduction cascades, changing neuronal activities, and triggering the release of neurotoxic mediators by microglia (resident immune cells). The lipid carrier protein apoE4 increases Aβ production and impairs Aβ clearance. When produced within stressed neurons, apoE4 is cleaved into neurotoxic fragments that destabilize the cytoskeleton and, like intra-cellular Aβ, impair mitochondrial functions. The τprotein and a synuclein can also self-assemble into pathogenic oligomers and can form larger intra-neuronal aggregates, displacing vital intra-cellular organelles (Ott et al., 2011).

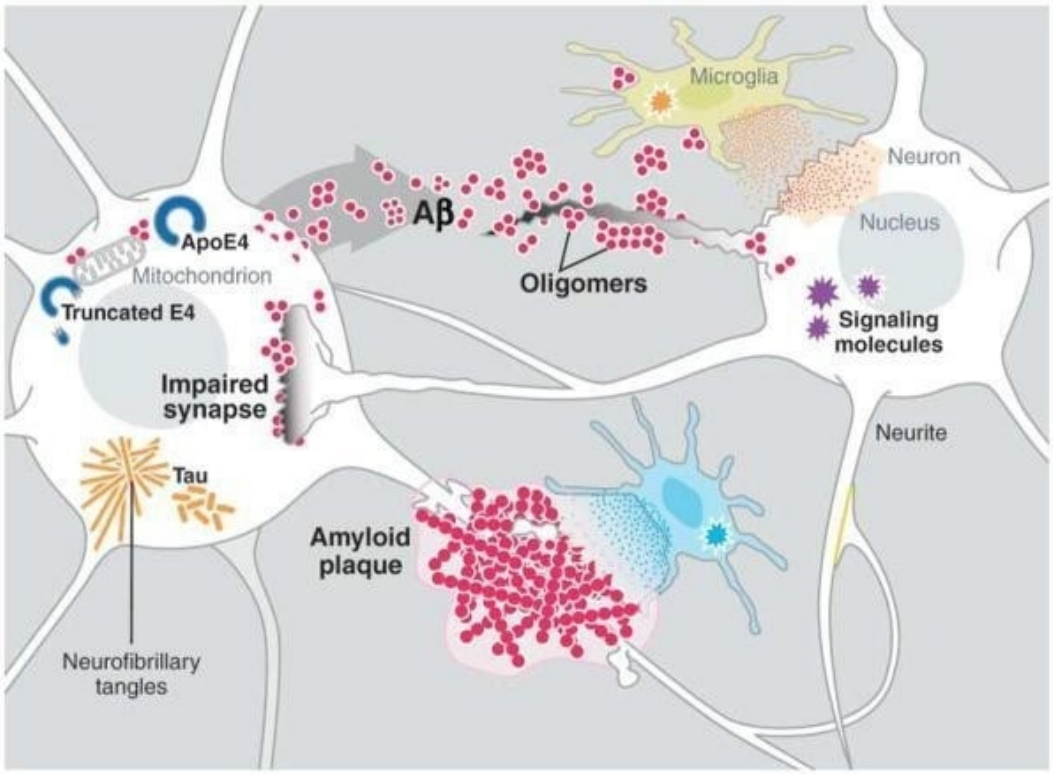

Figure 2.5 Example of key players in the pathogenesis of Alzheimer's disease (Roberson and Mucke, 2013).

2.1.4 Diagnosis of Alzheimer's Disease

Diagnosing AD with 100 percent accuracy is possible by post-mortem microscopic examination of the brain (Love, 2005). In terms of in vivo diagnosing, some neuropsychological tests, checking the familial history of the patient, and neuroimaging can help discover whether the patient's brain is inflicted by AD and recognize its progress and level. Moreover, AD should be differentiated from other neurodegenerative dementia like frontotemporal dementia, Lewy-Body dementia, and Creutzfeldt-Jakob disease. In neuroimaging like MRI, PET, and SPECT, we have more detailed information of the brain and some regions that are more relevant to investigate. Then, it is necessary to look for some regions of interest (ROIs), which are involved in learning and memory as well as decreased glucose metabolism and uptake of radioligands, which detect some proteins that are not normal. The CSF is another biomarker that may show abnormalities like low levels of Aβ protein. In AD versus Normal control the levels of τ and phospho-τ are higher (Ott et al., 2011). In addition, AD has different stages from the beginning of the illness to its merciful end. Some experts believe in following a simple three-phase model, such as early, moderate, and end stage, whereas others have found

a breakdown to be a more useful tool to understand the progression of the illness.
Dr. Barry Reisberg of New York University breaks the progression of AD into seven stages. In each stage, the patient has different symptoms and less ability, progressing as far as losing the ability to swallow (Reisberg, 2016). Here is a summary of the seven stages of AD based on the ideas of Dr. Reisberg. In the first stage, there is no impairment ; the patient does not have memory problems, and no symptoms are seen. The second stage is a very mild decline in which minor memory problems start, such as losing things around the house. In this situation, the patients still do well on memory tests, and the disease can easily be distinguished as normal age-related memory loss. In the third stage, there is a mild decline and the friends and family members of the individual may begin to notice memory and cognitive problems. In addition, cognitive tests are affected in this stage, and there is some difficulty in finding the right word during conversations and remembering names of new acquaintances. In stage four (moderate decline), clear-cut symptoms of AD are apparent. Patients have difficulty with simple arithmetic, may forget details about their life histories, have poor short-term memory or inability to manage finances and pay bills. During the fifth stage (moderately severe decline), patients need help with many daily activities. They have significant confusion ; they are unable to recall simple details about themselves, such as their own phone number. Additionally, dressing appropriately is difficult for them, but they typically can still bathe and use the toilet independently. They still know their family members and some details about their personal histories. In the next stage, severe decline occurs in which patients at this level need constant supervision and frequently require professional care. Some symptoms, such as confusion or unawareness of the environment and surroundings or major personality changes and potential behaviour problems, are significant. They need assistance with activities of daily life, such as toileting and bathing. In the final stage (very severe decline), patients are nearing death because AD is a terminal illness. They lose the ability to respond to their environment or communicate. While they may still be able to utter words and phrases, they have no insight into their condition and need assistance with all activities of daily life. At the end of the illness, patients may lose their ability to swallow (Reisberg, 2016).

2.1.5 Risk Factor of Alzheimer's Disease

Scientists have identified factors that increase the risk of AD. The most important risk factors are age, genetics, family history, heredity, and environmental or infectious mechanisms (Brayne, 1993). Some studies have also shown the number of years of education (Katzman, 1993), history of head injury (Heyman et al., 1984) are associated with a greater risk of AD. Advancing age is the greatest known risk factor for AD (Tyas et al., 2001). Another strong risk factor is family history. Those who have a parent, brother, sister, or child with AD are more

likely to develop the disease. The risk increases if more than one family member has the illness. When diseases tend to run in families, either heredity (genetics) or environmental factors or both may play a role. Scientists identified several risk genes implicated in AD. However, there are three genes in which mutations with the strongest influence are involved, resulting in early onset autosomal dominant familial AD. These are the APP or apolipoprotein E-e4 (APOE-e4), presenilin-1 (PS-1) and presenilin-2 (Tilley et al., 1998). Scientists estimate that APOE-e4 is the main genetic determinant of AD (Chalovich and Eisenberg, 2005).

2.2 Neuroimaging Modalities

Generally, for any evaluation of dementia, routine structural imaging studies are recommended to facilitate the diagnosis of dementia. The most popular structural imaging is MRI scans (or CT if MRI is not available), which should be performed at least once in the diagnostic examination of patients (Silverman, 2009). To distinguish vascular lesions and neurodegenerative dementia, structural imaging is strongly recommended. To differentiate between various forms of dementing disorders, such as neoplastic infiltration in lymphomas or Creutzfeldt-Jakob disease, neuroimaging can indicate reliable pathological processes in the brain. From the other point of view, functional imaging with PET using isotopes, such as 18F-2-fluoro-deoxy-D-glucose (FDG) or other radio tracers, has become the test of choice for the differential diagnosis of neurodegenerative disorders (Román and Pascual, 2012). In this section, we present a short introduction of routine imaging.

2.2.1 Magnetic Resonance Imaging (MRI)

Magnetic resonance imaging (MRI) is a test that uses a magnetic field and pulses of radio wave energy to make pictures of organs and structures inside the body. To produce detailed pictures of organs, MRI uses a powerful magnetic field, radio frequency pulses, and a computer. Figure 2.6 illustrates one MRI scanner with different main parts. The images produced by MRI have details of soft tissues, bone, and virtually all other internal body structures. Furthermore, MRI is able to detect brain abnormalities. The brain imaging has complimentary information of some diseases associated with MCI and can be used to predict which patients with MCI may eventually develop AD. The MRI allows for accurate measurement of the three-dimensional (3D) volume of brain structures, especially the size of the hippocampus and related regions and therefore can be used as the primary choice of neuroimaging examination for AD (Van de Pol et al., 2007). An MRI scan of the brain may be normal in the early stages of AD, but in later stages, MRI may show a decrease in the size of different areas of the brain (Weiner and Khachaturian, 2005).

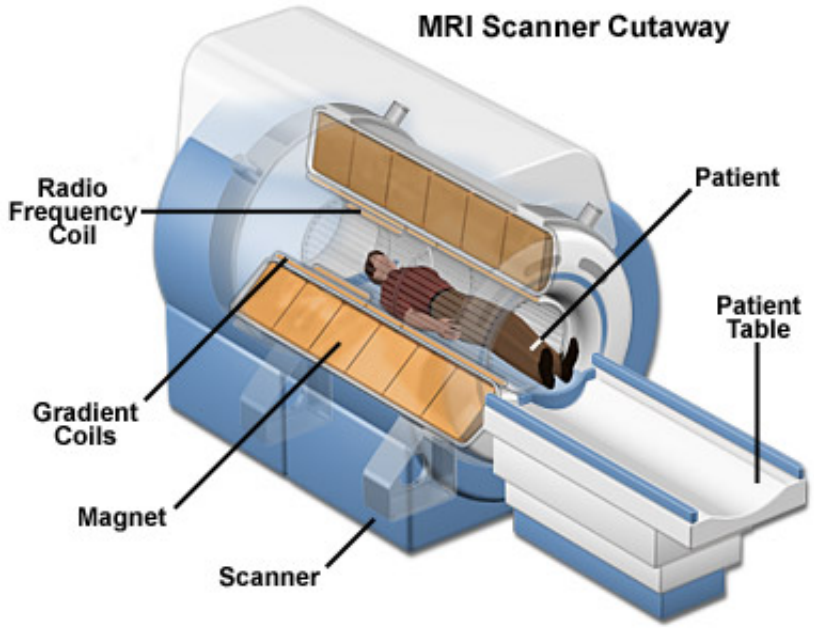

Figure 2.6 MRI scanner structure (Orthopaedics, 2017)

The American Academy of Neurology (AAN) suggests that neuroimaging may be most useful in patients with dementia characterized by an early onset or an unusual course (Petersen et al., 2001). Longitudinal MRI scans can provide brain volume change, which Fox et al. (1996) used with an automated technique to subtract MRI scans obtained at an average of one year apart. They observed that there was a significant difference between the rate of change in patients with AD and the rate in the control subjects. The disease usually begins in the medial temporal lobe, particularly the entorhinal cortex and hippocampus. Later, when subjects are in the MCI stage, the disease spreads to the basal temporal lobe and paralimbic cortical areas, such as the posterior cingulate gyrus and precuneus (Vemuri and Jack, 2010). Figure 2.7 illustrates the typical MRI scans in normal subjects and in patients with MCI or AD. As seen in the figure, there is increasing medial temporal atrophy (specifically, the hippocampus and ventricular enlargement) in MCI and AD when compared with NC.

The MRI scans have two separated targets to acquire the images. The first is recognizing several brain anatomical structures, which are called structural MRI (sMRI) and second is to detect changes in blood oxygenation and flow, which is called functional MRI (fMRI).

2.2.2 Positron Emission Tomography (PET)

The PET scan is a nuclear medicine imaging technique that not only provides 3D images but also enables in vivo examination of brain functions. It allows for non-invasive quantification

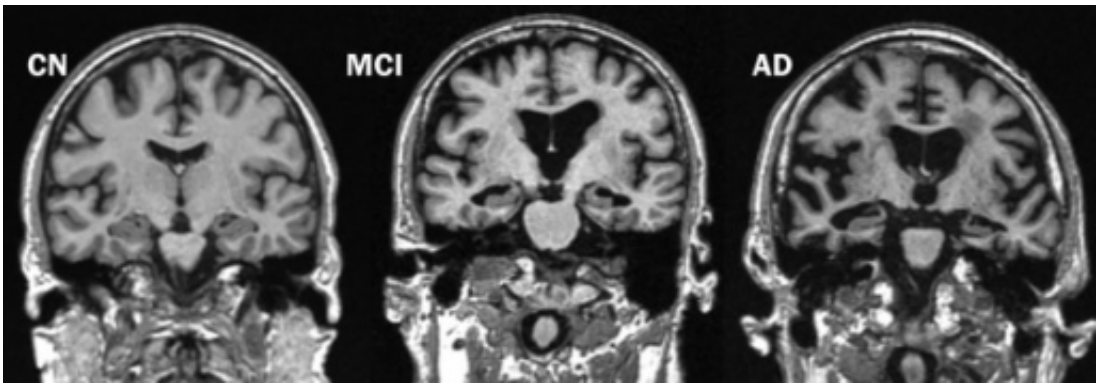

Figure 2.7 Progressive atrophy (medial temporal lobes) in an aged normal subject (NC), MCI subject (MCI) and an AD subject (Vemuri and Jack, 2010).

of cerebral blood flow, metabolism, and receptor binding. The most common basic imaging methods currently use metabolic imaging (PET and SPECT) in the diagnosis of dementia (Silveira and Marques, 2010). The PET scan produces the 3D images using radioactive tracers, which are usually administered to a patient through intravenous injection. The tracers are made up of carrier molecules that are tightly bonded to a radioactive atom, called an isotope. The carrier molecule can interact with or bind to specific proteins or sugars in the body. The carrier molecule that will be used depends on what is being investigated. If looking for AD or the progression of early stage of AD, FDG, a modified form of glucose, which gets absorbed by tissues, may be used. When tissues do not absorb glucose, it may indicate a low rate of metabolism in the brain. Table 2.1 displays three common isotopes, which are usually used for scanning to diagnose AD (Román and Pascual, 2012).

Table 2.1 Physical properties of some common isotopes used in PET scanning

Isotopes	Name Half-life (min)	Energy range (Kev)
^{11}C	Carbon-11 (20.4)	960
^{15}O	Oxygen-15 (2.1)	1720
^{18}F	Flourine-18 (109.8)	640

The radiation from the tracers poses little danger to the patient since they quickly pass it out of the body. The isotope produces small particles called positrons, which interact with surrounding electrons. This interaction results in the complete annihilation of both particles, releasing two photons that speed off in opposite directions. The detectors in the PET scanner measure these photons and use this information to create an image of the distribution of the tracer in the body. Figure 2.8 displays how the PET modality works.

Among different radiotracers, FDG-PET has been used extensively to study AD, and it is

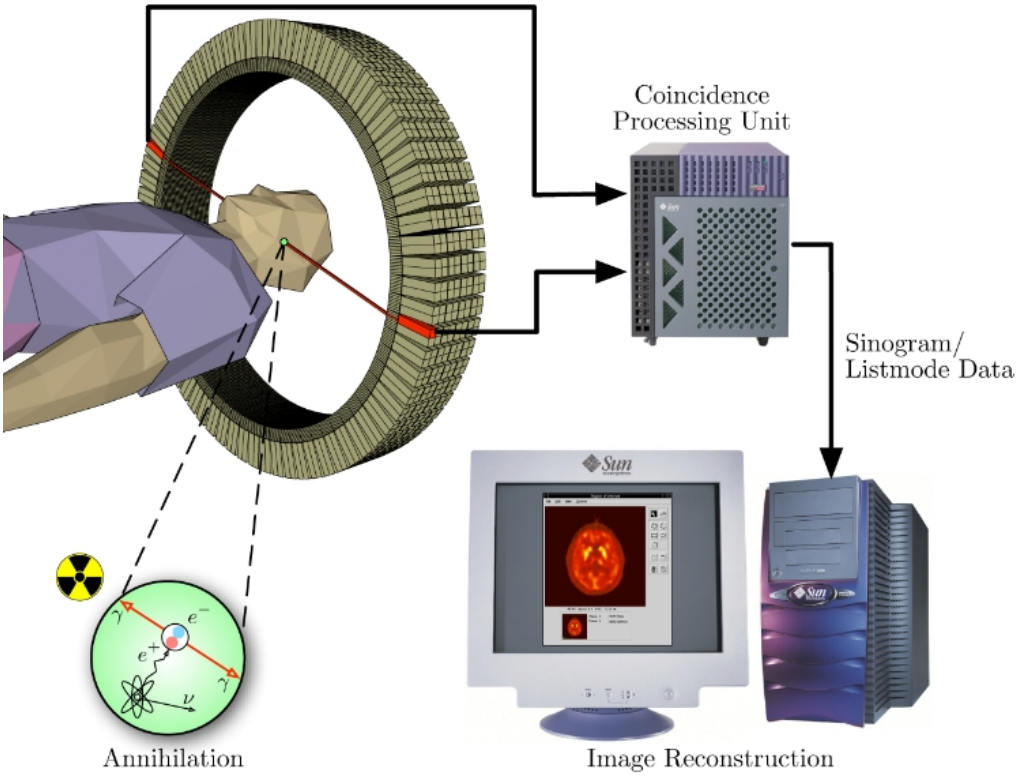

Figure 2.8 Schema of a PET acquisition process (Maus, 2003)

evolving into an effective tool for early diagnosis and differentiation of AD from other types of dementia. The FDG-PET has been used to detect persons at risk for AD, even before the onset of symptoms (Silverman et al., 2001). The carrier molecules 18F 2-fluorodeoxyD-glucose (FDG, a modified form of glucose) are absorbed by normal neurons, which means they are not degenerated (Silverman, 2009). The PET scanners provide clear benefits, such as the following :

— Earlier tissue tumour detection ;
— Improved accuracy of therapies based on tumour evolution and tracking ;
— Lower radiation exposure for patients compared to PET-CT (Kim et al., 2016)
— Better brain imaging when combined with MRI.

A sugared radionuclide tracer is introduced in the human body, typically in the blood circulation. Figure 2.9 displays a brain scan using PET with the isotope marker 18fluoro-deoxy-glucose (FDG-PET) on the left and amyloid plaques (AV45-PET) on the right side. In the FDG-PET image, red areas indicate good utilization of glucose by the brain in contrast with the yellow to blue areas in the posterior parietal regions characteristic of AD. In the AV45-PET image, the red areas indicate accumulation of amyloid plaque, which is more significant

in the AD image, while in the NC image, amyloid is negative.

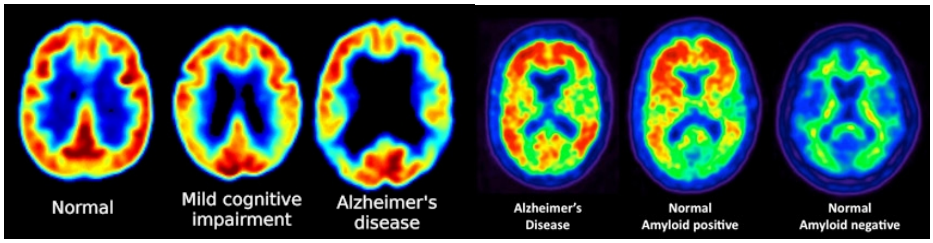

Figure 2.9 FDG-PET images showing reduced glucose metabolism in temporal and parietal regions in patients with MCI and Alzheimer's disease (left) . PET scans revealing amyloid plaques, (warm colours, ie. red and orange)(right). Person with no symptoms of cognitive problems, but with evident levels of amyloid plaque in the brain (middle scan) (Baker, 2010).

2.2.3 Quantification of PET Imaging

The PET scan is one of the main functional neuroimaging techniques used in AD. The FDG-PET provides measurements of regional glucose metabolism, which, in AD, is indicated by the presence of a temporal parietal decline in glucose metabolism. In brief, the diagnostic accuracy of PET is similar to the accuracy of a pathologically confirmed clinical diagnosis of AD (Román and Pascual, 2012). A few years before the onset of symptoms, the concentration of Aβ starts to decrease in the CSF (Bateman et al., 2012). Atrophy of the grey matter (GM) in AD can be quantified with automated methods to measure cortical thickness. In AD, loss of cortical neurons is accompanied by atrophy of white matter (WM) due to axonal disconnection and loss of anisotropy of affected axonal bundles.

2.3 Classification

Classification means naming and categorizing things based on physical or non-physical attributes to two or more individual groups. One of the most common data mining techniques is classification. A classification process yields a discrete value representing the probability that a case belongs to a particular group. Classification will be executed in accordance with some knowledge about the data, such as density, texture etc. (Japan Association of Remote Sensing., 1996), (Joshi et al., 2010). Hence, a training set is used to identify specific parameters. Training data requires sample input data, domain expertise, and a classification assignment to the data. A classification problem occurs when an object needs to be assigned into a predefined group or class based on a number of observed attributes related to that object. In this chapter, we review some classification methods, which are used in different

related research. After that, we note some methods that are common to use and have very good results, especially in the field of image processing.

2.3.1 Support Vector Machines (SVMs)

Support vector machines (SVMs) are already applied in a wide variety of classifications, and it is one of the most popular techniques in classifications based on neuroimaging like AD. Linear and nonlinear algorithms are already developed, and they are available as functions in different programming, like MATLAB, Python, C++, etc.

Linear SVM

The goal of SVM is to find the optimal separating hyperplane between binary classes. To achieve this goal, maximized margin criteria should be followed (Cortes and Vapnik, 1995). To explain more, we assume training data as vectors $X_i \in R^d, i = 1, 2, ..., l$ in two classes, and the label vector $y \in \{1, -1\}^l$, SVM requires to solve the following optimization problem :

$$_{W \in H, b \in R, \xi_i \in R} Min(\frac{1}{2} W^T.W + C \sum_{i=1}^{l} \xi_i) \tag{2.1}$$

Subject to

$$y_i(W^T \varphi(X_i) + b) \geq 1 - \xi_i, \xi_i \geq 0, i = 1, 2, ..., l \tag{2.2}$$

where $W \in R^d$ is the weight vector, $C \in R_+$ is the constant regularization, the mapping function φ projects the training data into a suitable feature space, and H is to allow the non-linear decision to surface (Cortes and Vapnik, 1995). Following the SVM problem definition in brief, we have the following :

$$f(x) = W^T x + b \tag{2.3}$$

Formulated as solving an optimization problem over w, we have :

$$_{w \in R^d} Min(\|W\|^2 + C \sum_{i}^{N} max(0, 1 - y_i f(x_i)) \tag{2.4}$$

The SVM can be formulated to learn a linear classifier :

$$f(x) = \sum_{i}^{N} \alpha_i y_i (x_i^T x) + b \tag{2.5}$$

by solving an optimization problem over α_i (Bishop, 2006). More details about derivations of the algorithm can be found in the work by Cortes and Vapnik (1995) and Guo (2014) (Cortes and Vapnik, 1995) (Guo, 2014).

Radial Basis Function (RBF)

Support vector machines (SVMs) with the Gaussian (RBF) kernel have been also widely applied in many classification problems in different fields (Howlett and Jain, 2001). Model selection in this class of SVMs involves two hyper parameters : the penalty parameter C and σ the kernel width σ.
Usually, the decision is on the use of a linear or an RBF (aka Gaussian) kernel. Typically, the best possible predictive performance is better for a nonlinear kernel (or at least as good as the linear one), as it has been shown that the linear kernel is a degenerate version of RBF. Hence, the linear kernel is never more accurate than a properly tuned RBF kernel (Keerthi and Lin, 2003). Based on the SVM equation, we can reformulate it for the RBF kernel as shown below :

$$f(x) = \sum_{i}^{N} \alpha_i y_i \exp(\frac{-\|x - x_i\|^2}{2\sigma^2}) + b \tag{2.6}$$

Then RBF kernel is defined as :

$$K_{RBF}(x, x_i) = \exp(-\gamma \|x - x_i\|^2) \tag{2.7}$$

Where γ is a parameter that sets the spread of the kernel.

2.3.2 Principal Component Analysis (PCA)

Principal component analysis (PCA) is a method to reduce the number of features used to represent data. This dimensionality reduction can provide a simpler representation of the data, specifically on a 3D matrix of voxel intensity of each image. Moreover, reduction in memory and faster classification are some advantages of using PCA (Pedersen et al., 1993). Given data points. $x_1, x_2, ..., x_n$ with each vector x_i being p-dimensional. We want to transform that into $\lambda_1, \lambda_2, ..., \lambda_n$ with each vector λ_i q-dimensional. $q < p$. The dimensionality of the data is reduced. In example, we are trying to reduce two-dimensional data to one dimension. Each 2D data point can be projected onto a subspace which is a line. We can find the sum of squared distance (i.e. reconstruction error) from the data to its projection on the subspace. So,

$$f(\lambda) = \mu + v_q\lambda \tag{2.8}$$

In this rank q model, the mean is μ is a p-dimensional vector vector which represents the offset in p-space. v_q is a $p \times q$ covariance matrix with q orthogonal unit vectors. Its q vectors are the principal components of the data. Finally, λ is the q vector. Creating a good low-dimensional representation of the data requires a careful selection of μ , v_q and λ. One possible way to do this is to minimize the reconstruction errors given by,

$$\underset{\mu,\lambda_{1\ldots N},v_q}{min} \sum_{n=1}^{N} (\|x_n - \mu - v_q\lambda_n\|)^2 \tag{2.9}$$

In Equation 2.9, μ is the interception of the lower space in the higher space. Next, $\lambda_{1\ldots N}$ is the q_dimensional coordination of x , or where x lies on the line in Figure 2.10. The p_dimensional plane, using v_q and μ is defined. Lastly, the quantity inside the sum is the distance between the original data and the low-dimensional representation reconstructed in the original space.

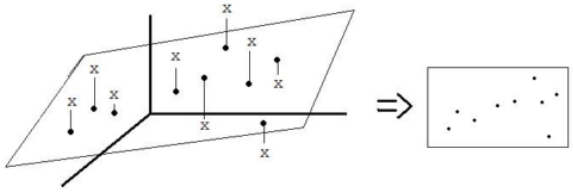

Figure 2.10 Projecting R^3 data to R^2 (Pop, 1993).

Singular Value Decomposition (SVD) is a widely used implementation of PCA. It is based on variance and principal components (PCs), which are determined by the dataset matrix (Pedersen et al., 1993). Using the reshaped matrix of the voxel of each subject to the vector, the dataset matrix is produced. The data matrix contains one volume dataset per column for all subjects. Consider the following :

$$X = UDV^T \tag{2.10}$$

Where

- X is a $N \times p$ matrix.
- U is an $N \times p$ orthogonal matrix, and the columns are linearly independent.
- D is a positive $p \times p$ diagonal matrix with $d_{11} \geq d_{22} \geq ... \geq d_{pp}$.
- V^T is a $p \times p$ orthogonal matrix.

We represent each data point as linear combinations (Pedersen et al., 1993).
$x_1 = u_{11}d_1\acute{v}_1 + u_{12}d_2\acute{v}_2 + ... + u_{1p}d_p\acute{v}_p$
$x_2 = u_{21}d_2\acute{v}_1 + u_{22}d_2\acute{v}_2 + ... + u_{2p}d_p\acute{v}_p$
...
After applying PCA on the dataset, the PC coefficients are returned as a $p \times p$ matrix. Each column of coefficients contains coefficients for one PC. The columns are in the order of descending component variance.

2.3.3 Random Forest (RF)

Random forests (RF) (Breiman, 2001) are an improvement of classification and regression trees method (Breiman et al., 1984). The RF algorithm works as a large collection of correlated decision trees. Decision trees are compact tree-like representations of conditions that specify when decisions should be taken together with the actions/decisions. Decision trees consist of intermediate nodes and leaf nodes. The outgoing edges from intermediate nodes are labeled by conditions. The leaf nodes are labeled by decisions or actions. Decision trees are used by starting at the root and then navigating down on true conditions until a leaf is reached. The action or decision in the leaf is then taken. Decision tree classifiers are decision trees used for classification, which were first introduced by Breiman (Breiman et al., 1984). In other words, RF is the result of the combination of bagging (Breiman, 1996) and the random selection of features (Dietterich, 2000). The algorithm for inducing an RF was developed by Leo Breiman and Adele Cutler, and "Random Forests" is their trademark (Liaw and Wiener, 2002). Every tree is built using a deterministic algorithm in two stages. First, at each node, a good split is chosen from a random subset of the predictors rather than all of them. Second, every tree is built using a bootstrap sample of the observations. The combination of learning models increases the classification accuracy. When we use different learning models, we can increase the accuracy of classification, which is the main idea of the bagging technique. Bagging averages noisy and low bias models to create another model with a lower variance, in terms of classification. The RF definition by Breiman is a classifier with a collection of tree-structured classifiers $\{h(x, \theta_k), k = 1, ...\}$ where the $\{\theta_k\}$ independently identically distributed random vectors, and each tree casts a vote for the predicted class for input x (Breiman, 2001). The RF algorithm uses the decision trees to make a classification, which is why it is based on the bagging technique. The random forests classification and regression algorithm draws n_{tree} bootstrap samples from the original data. For each of them, it grows an unpruned classification or regression tree with modification. If the tree is too big, the lower branches are modeling noise in the data, called over-fitting ; it then becomes necessary to prune back unnecessary splits ; pruning methods use some form of cross-validation

and it may need to tune amount of pruning. At each node, rather than choosing the best split among all predictors, randomly sample m_{try} of the predictors and choose the best split from among those variables. (Bagging can be thought of as the special case of random forests obtained when $m_{try} = p$, the number of predictors) Splitting criteria for regression is residual sum of squares :

$$RSS = \sum_{left}(y_i - Y_L)^2 + \sum_{right}(y_i - Y_R)^2 \tag{2.11}$$

Where
Y_L = Mean y - value for left node
Y_R = Mean y - value for right node

and for classification is gini criterion :

$$Gini = \eta_L \sum_{k=1,\ldots,K} p_{kL}(1 - p_{kL}) + \eta_R \sum_{k=1,\ldots,K} p_{kR}(1 - p_{kR}) \tag{2.12}$$

Where
p_{kL} = proportion of class k in left node
p_{kR} = proportion of class k in right node

At the end, it predicts new data by aggregating the predictions of the n_{tree} trees (i.e., majority votes for classification, average for regression).
A part of the RF algorithm is estimating the prediction error on the training data. To obtain this prediction first, we need to predict the data at each bootstrap iteration and not in the bootstrap sample (what Breiman calls “out-of-bag”, or OOB, data) using the tree grown with the bootstrap sample. Next, it needs to aggregate the OOB predictions (the out-of-bag OOB data, approximately one-third of the observations, are then used to estimate the prediction accuracy). We then calculate the error rate, and call it the OOB estimate of error rate. Our experience has been that the OOB estimate of error rate is quite accurate, given that enough trees have been grown (otherwise the OOB error estimate can be biased upward ; more details in (Bylander, 2002)). Parameter Tuning : Random Forest effectively has only one tuning parameter, m_{try}. This parameter is the number of descriptors randomly sampled as candidates for splitting at each node during tree induction. It can range from 1 to p, the total number of descriptors available. The latter case is equivalent to bagging. In our Random Forest classification experiments we used Breiman’s algorithm (Breiman, 2001) as

implemented in MatLab with 60 trees and 2 features to split each node, based on results suggesting that performance was highly insensitive to this parameter.

RF function

For better understanding of how the RF classification works, we start with an example. Here, we have a matrix S, which is a matrix of training samples that we will submit to the algorithm to create a classification model.

$$S = \begin{bmatrix} f_{A1} & f_{B1} & f_{C1} & C_1 \\ . & . & . & . \\ . & . & . & . \\ . & . & . & . \\ f_{AN} & f_{BN} & f_{CN} & C_N \end{bmatrix}$$

In this case f_{A1}, f_{B1}, f_{C1} are a set of extracted features ; for example, f_{A1} is feature A of the first sample, and we continue in all the samples up to N, so that f_{CN} is feature C of the Nth sample, and in the last column, the $C_1 ... C_N$ are labels for the rows. Therefore, the aim is to create a RF to classify this sample set. From sample set S, we can create many subsets with random value as shown below :

$$S_1 = \begin{bmatrix} f_{A12} & f_{B12} & f_{C12} & C_{12} \\ f_{A15} & f_{B15} & f_{C15} & C_{15} \\ . & . & . & . \\ . & . & . & . \\ . & . & . & . \\ f_{A42} & f_{B42} & f_{C42} & C_{42} \end{bmatrix} \quad S_2 = \begin{bmatrix} f_{A2} & f_{B2} & f_{C2} & C_2 \\ f_{A6} & f_{B6} & f_{C6} & C_6 \\ . & . & . & . \\ . & . & . & . \\ . & . & . & . \\ f_{A20} & f_{B20} & f_{C20} & C_{20} \end{bmatrix} \quad S_M = \begin{bmatrix} f_{A4} & f_{B4} & f_{C4} & C_4 \\ f_{A9} & f_{B9} & f_{C9} & C_9 \\ . & . & . & . \\ . & . & . & . \\ . & . & . & . \\ f_{A12} & f_{B12} & f_{C12} & C_{12} \end{bmatrix}$$

$S_1, S_2, ..., S_M$ are randomly selected samples which may belong to multiple subsets and are used to create the decision trees. In the first subset S_1, we used the line number 12, 15, and 35 with some other random elements. Thus, we get a subset from the main sample set S, and from this element, we create a decision tree number 1, then we make another random subset S_2 with different values, and we can see that we have the sample number 2, 6, and 20 and many others. With these values, we can create a decision tree number 2. From the S_M subset, we can create the decision tree number M. After we create these decision trees, we will repeat it using different samples from each of the sample sets. We created a subset with random samples. Then, with all these decision trees, we have different variations of the main classification. We will then use all these decision trees to create a ranking of classifiers.

In Figure 2.11 we showed five different patterns of class prediction, only to see how the class prediction will work. In this case, we have five decision trees, and our forest is composed of five trees.

If we have a new element to classify, then we need to check five trees for their prediction. The first tree responded that the classification of this sample is class 1. Then, we checked the second decision tree, and its answer is class number 3. The answer of the third and fourth trees are class number 1, and the last tree responded as class number 2. Thus, we have five independent decision trees, which were created using sub-samples of the entire sample set, and we can now count the number of votes for each class. It is obvious that we have three votes for class 1 and one vote for class 3 and one vote for class 2, so the result will be class 1. This RF classified all the elements, and class 1 was the selected for this classification. The difficulty for this technique is to create many decision trees and use them for a fast and accurate method of classification.

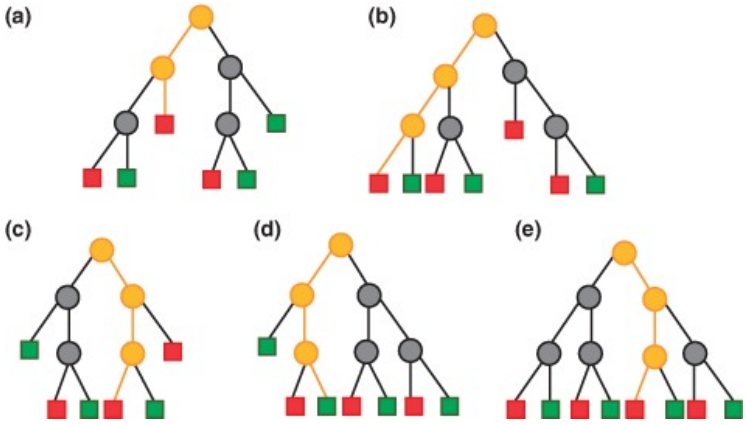

Figure 2.11 Five different pattern of class prediction (Mitchell, 2014)

2.3.4 Artificial Neural Networks (ANN)

Traditional statistical classification patterns, such as discriminant analysis, based on the Bayesian decision theory (Duda et al., 2001) are often used. The accuracy of these patterns depends on the various assumptions or conditions, which are selected by users who have a knowledge of both data properties and model capabilities before the models can be successfully applied. However, recently, researchers are motivated to use neural classification as an alternative to various conventional classification methods. This alternative solution has some benefits : first, artificial neural networks (ANNs) are data-driven self-adaptive methods in the sense that they can adjust themselves to the data without any explicit specification of functional or distributional form for the underlying model. Second, they are universal functional

approximators in the sense that neural networks may be particularly useful to approximate functions with varying levels of accuracy. Third, deep nonlinear neural networks are flexible in modelling real-world complex relationships. Finally, ANNs can estimate posterior probabilities, which provide the basis for establishing classification rules and performing statistical analysis (Richard and Lippmann, 1991)(Cybenko, 1989)(Hornik, 1991)(Hornik et al., 1989). Recently, different techniques for neural classification of AD are available. We review the ANN, which is used for the first time to discriminate AD vs NC.

Artificial Neural network function

Some computer scientists had the idea that we could make a computer that is modelled after the system of neuron connections (Furber and Temple, 2007). The idea behind the artificial neural networks (ANN) is that we have nodes and connections between those nodes. This is similar to the neurons in the brain and their synapses. A typical neural network has few dozen to hundreds, thousands, or even millions of artificial neurons called nodes arranged in a series of layers, each of which connects to the layers on either side. Since we are used to the computer model of computation, well-defined input and output nodes are preferred. Input nodes, are designed to receive various forms of information from the outside. Other nodes sit on the opposite side of the network and signal how it responds to the information it has learned ; those are known as output nodes. In between the input and output nodes are one or more layers of hidden nodes. Information is fed into the network via the input nodes, which trigger the layers of hidden nodes, and these in turn arrive at the output nodes. This common design is called a feedforward network. We also prefer to have directed connections, so that we know which way information is going. Moreover, we want connections to have different values ; thus, some connections should be more important than others. Here, the connection values are called weights. The purpose of having different connection weights is to allow our nodes to behave individually. In neurons, when one node is stimulated by two different nodes, it can decide which one is more important by the connection weights ; for example, as seen in Figure 2.12, if we have nodes A and B, which are giving the values green and orange to node C, since the connection weights between B and C are much larger than those in the connection between A and C, node C decides B is more important and takes its value. In some cases, we would like to be able to decide for several nodes, whether they want to accept their choice. Thus, to decide which input to accept, each node is given what is called a transfer function. The transfer function is a mathematical equation. After a node decides, it sets its value and then takes it to the next item with the same value. Choosing whether to accept the trade in value is most useful for the output nodes since these are the nodes that produce the results that are actually required. Usually, though, the transfer function will return a value

that is a combination of the node's current value and true value. Thus, using the connection weight and transfer functions, the ANN takes the inputs and produces outputs. This is the same task that the computer would do, but it is done in a way that is similar to the way that neurons work. Since the input and output nodes are the ones that matter to us, we consider the nodes in the middle to be hidden nodes. They do most of the work but get the least credit.

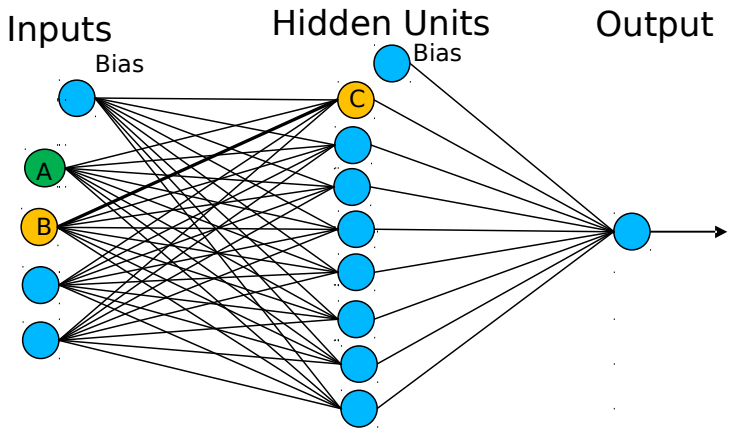

Figure 2.12 Example of neural network.

Now, as we know the basics, one of the more important questions is how the connection weights are determined. It turns out that the ANN can learn them, but ANN are extremely demanding in terms of training time. Their learning is through a process called back-propagation. Back-propagation networks require extensive computational resources, needing possibly thousands of iterations to learn. We start with random connection weights. Then, for a given set of inputs, we determine the set of desired outputs. In terms of using random weights, we first let the network calculate the outputs. Then, we compare the outputs calculated by ANN with the desired outputs that we defined. Since we gave the network random weights, we obviously cannot expect them to be equal, so we find their difference. We call this difference the error in the network. Now, we have their error, and we need to adjust the connection weights to try to produce the smallest errors. This is the where the back-propagation comes in. The output nodes tell the hidden nodes about the error, and together they decide how to adjust the connection weights between them. The new weights are calculated using an equation based on the old weight, the node's input value, the error, and the learning rate.

$$\Delta w_{ij}(t+1) = (1-\alpha)\eta\delta_j o_i + \alpha\Delta w_{ij}(t) \tag{2.13}$$

where :
$\Delta w_{ij}(t+1)$ is the change in weight $w_{ij}(t+1)$ in the connection of node i to node j at time $(t+1)$,
η a learning rate ($\eta < 0$), δ_j the error signal of node j and o_i the output of node i, which is also an input of the current node (node j),
α the influence of the inertial term $\Delta w_{ij}(t)$ (in $[0, 1]$). This corresponds to the weight change at the previous point in time.

With the weights adjusted, the hidden nodes calculate their own errors using a similar formula as before. Then, these nodes with their newer calculated errors push the errors back through the hidden nodes and adjust the weights behind them. This goes on until all the weights have been adjusted, and all the nodes have been assigned an error. The idea is to determine which nodes are most to blame for the error in the output and to try to adjust their weights the most. Now, that all the paths are updated, the network tries out the original inputs again and tries to calculate some outputs, the calculated outputs should be closer to the desired outputs than before. However, there are still some errors ; thus, the whole process should be repeated again and again. As stated, ANN takes a lot of time to train. This is because the ANN must repeat the process above for each different input set, and there are usually many inputs to achieve a better training. To try to produce the desired output more quickly, we could try adjusting the learning rate and change the number of nodes, but it would still take millions of attempts for the ANN to get the desired output for even a simple problem (Rojas, 1996).
In standard back-propagation, too low a learning rate makes the network learn very slowly ; in contrast, too high a learning rate makes the weights and objective function diverge, meaning there is no learning at all. If the objective function is quadratic, as in linear models, good learning rates can be computed from the Hessian matrix (Bertsekas and Tsitsiklis, 1996). In machine learning, ANNs are a family of models inspired by biological ANNs and are used to estimate functions that can depend on many inputs and are generally unknown. Therefore ANN training is strictly a “supervised learning” process. The learning is essentially by example, with no guidance from the user as to the criteria to employ (Kippenhan et al., 1992). An ANN is an interconnected group of nodes, namely, input, hidden, and output nodes. The structure of an ANN suitable for the classification task is shown in Figure 2.12 The three-layer feedforward network has four input units.

2.4 Registration

Image registration, as a crucial step for image analysis (Kiebel et al., 1997), also known as image fusion, matching, or warping, can be defined as the process of putting two images of the same thing into spatial alignment. In other words, a process of transforming or aligning different sets of data into one coordinate system is image registration. In general, we can divide its applications into four main groups, in which valuable information is conveyed in more than one image, like images acquired at different times, from distinct viewpoints, or by different sensors and scenes. For medical purposes, the data are the medical images from different digital modalities. Registration, alignment, geometrical correspondence, matching, and motion estimation are some crucial steps in registration between two images (Oliveira and Tavares, 2014).

Generally, we can classify the registration methodology into physical categories : rigid and non-rigid registration or mathematical categories, linear and nonlinear registration or complexity categories, and parametric and non-parametric registration categories (Chumchob and Chen, 2009). Nevertheless, the majority of the registration methods consist of feature detection, feature matching, transform model estimation, and image resampling and transformation (Zitová and Flusser, 2003). Registration based on these four steps starts determining what kinds of features are appropriate for the given task. The features should be easily detectable and frequently spread over the images with enough common elements, even in the case in which the images do not cover the same scene. In the feature matching step, we establish the correspondence between the features detected in the sensed image and those detected in the reference. Then, we need to estimate the type and parameters of the mapping functions, aligning the sensed image with the reference image. Finally, the sensed image is transformed by means of the mapping functions. Image values in non-integer coordinates are computed by the appropriate interpolation technique. In addition, there is four simple transformations : translating, rotating, scaling, and shearing for aligning datasets.

In the case that images are acquired in the same scene with different sensors (modalities), we need to integrate the images from different sources to obtain more detailed scene representation. The goal of registration in medical images for MRI with sensors monitoring metabolic body activities in PET is to find the anatomical body structure (Zitová and Flusser, 2003). Therefore, inter-modality registration to find anatomical information in some functional images like PET is necessary (Friston et al., 1995). Medical image registration has been developed for almost all anatomic parts or organs of the human body like the brain (Ashburner, 2007). Hence, registration of functional PET and T1-weighted MR images is recommended for image processing in this area.

2.5 Segmentation

Segmentation partitions an image into distinct regions containing each pixels with similar attributes. This attributes can be simply established by sets of semantically meaningful, homogeneous, and no overlapping regions of similar attributes or descriptors on the objects represented in the images. The attributes include intensity, depth, colour, texture, points, edges, lines, contours, surfaces, areas, volumes, medial axes, etc. Additionally, the descriptors can be included by distances, lengths, angles, moments, or shape signatures. In some cases, descriptors involve even more complex structures containing information about the objects, such as graphs, skeletons, or diagrams in the images. The segmentation result is either an image of labels identifying each homogeneous region or a set of contours, which describe the region boundaries (Oliveira and Tavares, 2014).

In the last few decades, non-invasive brain imaging technologies have rapidly improved, and this has caused dynamism in analyzing and studying the brain anatomy and function (Despotovic et al.). Functional and structural brain imaging is one of the most important steps in neuroscience and experimental medicine (Heckemann et al., 2006). In the same way, image segmentation is playing an expanding role in medical image analysis, since its quality affects the accuracy of the subsequent analysis (Kalini, 2004). Specifically, the anatomical structure of the brain is one of the popular uses of image segmentation, and in this case, the MR image is one of the first main materials to be used for brain segmentation (Fischl et al., 2002a). Recently, there has been a number of automated segmentation methods (Fischl et al., 2002a), (Fischl et al., 2002b), (Pham et al., 2000) as well as manual segmentation used by clinicians who must manually extract their ROIs. However, manual segmentation is time-consuming and prone to errors due to various inter or intra operator variability studies. All these difficulties in MRI image segmentation, especially when the subject is the brain, drive us to use automated methods for segmenting each structure precisely and quickly.

The most common segmentation method of brain MRI can be classified into two groups : basic tissue classification and anatomical segmentation procedures (Heckemann et al., 2006). In basic tissue classification, typically, the image of the brain is divided into three main tissue types : WM, GM, and CSF (Despotovic et al.). This classification assigns a label, such as a tissue class, to each element in the image, where the classes are defined in advance. There are some automated methods for tissue classification, such as BET and FAST, from the FSL library (Smith et al., 2004), Exbrain (Lemieux et al., 2003). The brain structures have no border or boundaries to be distinguished from other structures ; therefore, anatomical segmentation is comparatively difficult to use for tissue classification. Most procedures involving labelling the brain structures offer the interactive input of human knowledge for each case

individually (Hammers et al., 2003). The diversity of shapes and the numerous various appearances of anatomical structures make this segmentation one of the most challenging and essential topics in medical image processing (Elnakib et al., 2015). Lewandowski et al. (2015) categorized image segmentation methods into :

— Rule-Based Segmentation ;
— Segmentation by Optimal Statistical Inference ;
— Atlas-Based Segmentation ;
— Segmentation with Deformable Models.

In atlas-based segmentation approaches, anatomical atlases are used as reference images. The first step after choosing the atlas is nonlinear registration to the target image. Next, labels are transferred from the atlas to the image using the same geometric mapping as the registration. Finally, the target regions are obtained from the labelled map. Obviously, segmentation accuracy depends on the accuracy of registration (Morin et al., 2012), (El-Baz et al., 2015). Wachinger and colleagues (2015) proposed a method to increase the efficiency of the atlas-based segmentation using sparse correspondences between keypoints that represent automatically identified distinctive image locations in the test and training images. This method consists of three steps : (i) keypoint matching, (ii) voting-based keypoint labeling, and (iii) keypoint-based probabilistic transfer of organ label maps (Wachinger et al., 2015).

CHAPTER 3 CRITICAL LITERATURE REVIEW OF ALZHEIMER'S CLASSIFICATION METHODS

In this chapter, we have an overview of various publications in the field, and we introduce their methods and present their results. However, before that, we need to review the previous classification techniques using brain images. Therefore, this chapter comprises sections based on using two modalities that produce the 3D images of brain, including complementary information to discriminate between different stages of AD and NC.

3.1 Magnetic Resonance Imaging (MRI)

3.1.1 Structural MRI

In this part of the review, we discussed the roles and limitations of sMRI for AD. The two most pathological dementia features are cortical atrophy and vascular changes (Chetsadaporn et al., 2015). As we mentioned in the previous chapter, MRI is recommended for distinguishing vascular lesions and neurodegenerative dementia. As mentioned previously, MRI images present rich anatomical information, and it is useful to extract some features which can be identified as a saliency criterion of the image (Toews et al., 2010) Structural MRI has the ability to visualize specific atrophy patterns in the brain ; hence, it is important for the differential diagnosis of AD (Wattjes, 2011). From the sMRI point of view, brain atrophy and neuronal loss, as common MRI biomarkers in some special parts of the brain, are key criteria for the diagnosis of AD. Atrophy starts from the entorhinal area and continues in the hippocampus, amygdala, and parahippocampus along with disease progression (Johnson et al., 2012), (Vemuri and Jack, 2010).Other brain regions, such as the posterior temporal, parietal cortex, and mesial temporal lobe, are affected by progress of AD (Chetsadaporn et al., 2015). When changes in different individual brain regions occur, it is possible to assess the degree of atrophy visually. Volumetry is the most common quantitative metric used in AD (Vemuri and Jack, 2010). Voxel-based morphometry (VBM) is a validated method to assess atrophy over the entire 3D sMRI scan (Ashburner and Friston, 2000). Moreover, VBM has an alternative, which is manual segmentation of ROIs instead of the voxel-based approach. Toews and colleagues (2010) proposed a fully data- driven technique to find the anatomical structural patterns in 3D images by using feature-based morphometry (FBM). To classify the subjects based on their image, FBM can promote an image model which is more related to the most probable class. The authors used this technique to obtain high accuracy of

classification between AD and NC (Toews et al., 2010). Multivariate analysis and machine learning-based algorithms recently attracted the investigator's (Chupin et al., 2009),(Suk and Shen, 2013) attention to compare brain volume changes by forming a disease model against which individual subjects may be compared. In addition, there are several techniques based on sMRI, which are used to discriminate healthy controls from subjects with AD and to predict conversion from MCI to AD. Comparing the shape of the hippocampus, evaluating the power of hippocampal volume, and measuring cortical thickness, tensor-based morphometry, and manifold-based learning are some examples of methods used with sMRI scans (Wolz et al., 2011). Local image texture features is used for characterizing Alzheimer's disease (AD) in brain MRI. One of the most discriminative techniques regarding subject groups (AD vs NC) is using computed texture features from local sub-volumes of MR images (Chaddad et al., 2016). Finding well-known ROIs for most studies on the automated detection and characterization of AD from MRI data is the important step of their methodology (Maani et al., 2015). In another work (Chaddad et al., 2016) using multitextural information like 3D Gray-Level Co-Occurrence Matrix, the Laplacian of Gaussian filter and the 3D discrete wavelet transform determine discriminative brain regions in a data-driven manner, without having to segment specific ROIs. Table 3.1 presents some studies that used sMRI with different techniques to distinguish AD or its progression from the early onset stage.
In (Desikan et al., 2009), volume and mean thickness of 34 neuroanatomic ROIs were investigated on MRI images. To better discriminate MCI, in addition to the cortex thickness, hippocampal volume and supramarginal gyrus thickness were used which yielded over than 91% of accuracy in their results. In other work (Klöppel et al., 2008), following segmentation of grey matter, normalization and combining images of different groups were implemented. Then they tested several method of classification, especially linear kernel of SVM. With this method the authors could differentiate AD- patients versus controls with 95% accuracy. Jacobian determinants method was used for scaled grey-level intensity in some ROIs, specifically medial temporal lobe, to separate the probable AD and age-matched normal controls with 92% accuracy in one work of Duchesne et al. (2008). As well as last work SVM classifier obtained the best results of this method (Duchesne et al., 2008). The work of (Liu et al., 2016) investigated on some ROIs based on AAL to find the classification features. Their method proposed using hierarchial network to extract the ROIs. The parcellated whole brain into 90 regions based on AAL in first layer of network and some regions merged to obtain 54 region in next layer. In next layer 14 regions found after merging between two previous layers' ROIs and the last layer containing one ROI that was whole brain. They computed the connectivity between each pair of regions in terms of Pearsons correlation coefficient. In their method Features selected based on Feature ranking approach. The results of their work obtained by

multiple kernel boosting, which is about 95 % accuracy of classification between AD and NC, and about 72 % between MCI convertable and MCI non convertable. Ben Ahmad et al. (2014) presented an automatic classification framework for AD recognition in structural MRI. Hippocampal area is the ROI in this work. Their proposed method extract the visual information from MRI using the approximation of image signal by Circular Harmonic Functions. Where the probabilistic outputs of classifies on both local features and the amount of CSF were fused, a late fusion scheme could perform the final classification of the MRI scans. The experimental results of their work show 87% of classification accuracy on AD versus NC and 78 % and 72 % for MCI versus NC and MCI versus AD respectively on ADNI database (Ben Ahmed et al., 2014). Rao et al. (2011) applied Sparse Logistic Regression (SLR) to classify 69 AD and 60 NC subjects based on voxel-wise grey matter volumes derived from structural MRI. Penalized Logistic Regression (PLR) and Spatially Regularized Sparse Logistic Regression (SPSLR) are two different formulations of SLR which applied to solve the problem of having large number of voxels in comparison to the number of training subjects. The input features in the classifiers for this work were the standardized grey matter voxel intensities. Their results present about 85 % of overal classification accuracy for AD and NC (Rao et al., 2011). (Vemuri et al., 2010) compared the annual change in MRI and CSF biomarkers for their subjects based on intergroup discrimination, correlation with concurrent cognitive or functional changes and some other biomarkers. This paper didn't use some common feature from imaging to discriminate between different classes of ADNI subjects. Whereas, it compared the Annual change in CSF and MRI biomarkers across clinical groups for the pairwise discrimination between groups. The importance of reviewing this work is to investigate clinically about the ADNI subjects consisting of AD, MCI and NC cohorts with both baseline and 12-month follow-up. There results of this work presents that the annual change did not differ by clinical group in pairwise comparisons. From the findings, it's possible to indicate that Aβ deposition itself is not directly responsible for clinical symptoms, but rather initiates a pathologic cascade that later results in clinical symptoms. Another work (Walhovd et al., 2010) combined MRI, FDG-PET and CSF biomarkers in diagnostic classification to examine : 1) most sensitive measures to diagnostic status, 2) the effects of providing unique information in diagnostic classification 3) most predictive measures of clinical decline. Their ROIs included by hippocampus, entorhinal, parahippocampal, retrosplenial, precuneus, inferior parietal, supramarginal, middle temporal, lateral and medial orbitofrontal cortices. They performed regression analyses to determine measures' sensitivity to diagnostic status and some clinical measures. The results of this work indicated that each of the biomarkers have potential to inform diagnosis and enrich clinical trials. Moreover, hippocampal volume was the most sensitive to diagnostic group. Quantitative MRI morphometry and regional

metabolism by co-registered FDG-PET data, both together provided better prediction of clinical decline than CSF biomarkers. As conclusion of this work, MRI scans are often routinely required as part of the diagnostic work-up.

Table 3.1 Summary of studies using MRI in Alzheimer's disease

Author(s)	Year	Subjects	Diagnostic measures	Associations
Chaddad et al. (Chaddad et al., 2016)	2016	62 AD, 62 NC	more than 70% AD/NC	Texture features are computed from local sub-volumes on T1-MRI scans
Liu et al. (Liu et al., 2016)	2016	200 AD, 120 MCIc, 160 MCInc, and 230 NC	94.65% AD/NC, 89.63% AD/MCI 85.79% MCI/NC 72.08% cMCI/ncMCI	In the hierarchical network, using ROIs and are also used the spatial-correlations for the better classification accuracy
Ben Ahmed et al. (Ben Ahmed et al., 2014)	2014	35 AD, 111 MCI, 72 NC	87% AD/NC, 78% MCI/NC	late fusion of classification results on two biomarkers : hippocampus and CSF obtained high accuracy
Rao et al. (Rao et al., 2011)	2011	69 AD, 60 NC	85% AD/NC overal	classification accuracies for SLR and SRSLR with both performing better than PLR and MLDA
Toews et al. (Toews et al., 2010)	2010	100 AD, 98 NC	80% AD/NC equal error classification rate	Feature-based morphometry, a group-related anatomical structure in volumetric imagery
Vemuri et al. (Vemuri et al., 2010)	2010	71 AD, 149 MCI, 92 NC	Sample size required to detect treatment effects in AD MRI : 100; CSF >10	Longitudinal annual changes were observed only in MRI and not in CSF. Change in MRI was associated with change in cognitive measures.
Walhovd et al. (Walhovd et al., 2010)	2010	38 AD, 73 MCI, 42 NC	AD/NC : MRI : 85% CSF :81.2%, CSF+MRI :88.8%	In MCIs, only baseline MRI and FDG were correlated to (or predictive of) future clinical decline during 2 years

In assessing degenerative dementia as a result of AD, early stages using sMRI may not be as specific as advanced and quantitative PET imaging. Richard et al. (2013) assessed the efficacy of adding sMRI scans to a memory test to predict the progression of MCI to AD and found no significant increases in the accuracy of the diagnosis. Therefore, sMRI does not provide adequate diagnostic insight into the progression of MCI to AD (Richard et al., 2013).

In summary, sMRI is an appropriate biomarker to reflect the disease stage and intensity, which is extremely useful. It must be noted that it is an independent non-invasive measure of neuronal loss and thus provides a supplementary measure based only on anatomy. Numerous publications show that sMRI is a stable biomarker of AD progression.

3.1.2 Functional MRI (fMRI)

Functional MRI (fMRI) is one of the forms of neuroimaging for measuring brain activity. It detects the changes in blood oxygenation and flow. When a brain area is more active, the related neurons consume more oxygen, and consequently, in response to the increased demand, blood flow increases to the active area. Then, fMRI produces activation maps showing which parts of the brain are involved in a particular mental process. In AD field, fMRI researchers used memory tests and focused on an activation pattern of fMRI. In fMRI maps, there are some brain regions that have higher activation than others. Some studies focused on similar

ROIs, which are affected by AD in sMRI, and did not have satisfactory results. Accordingly, frontal and mesial temporal lobes have lower activation, and the ventral lateral prefrontal cortex has higher activation (Lenzi et al., 2011). Likewise, the hippocampus is still an ROI (Miller et al., 2009).

There are some advantages in assessing AD using fMRI. It is non-invasive and does not involve radiation ; hence, fMRI can be done multiple times during the disease. It also has excellent spatial and good temporal resolution, although sometimes imaging quality can be affected by any degree of head motion. This matter can be more intense for patients with more advanced dementia who cannot perform the task in an adequate manner. It is easy for the experimenter to use and interpret the fMRI scans (Chetsadaporn et al., 2015).

3.2 Positron Emission Tomography (PET)

From a neuroimaging point of view, the PET image is another main biomarker for AD diagnosis (Román and Pascual, 2012). The PET images are acquired for two methods, which are popular and include PET imaging using amyloid plaque ligands (AV45-PET) and FDG-PET. The FDG-PET images are the most common tracers for understanding which region of the brain has a higher accumulation of glucose. The reason we do not have more publications about classification of AD and MCI using AV45-PET compared to FDG-PET is that AV45-PET images were used by researchers and were not clinically approved for AD diagnosis. On January 20, 2011, there was a recommendation to use the AV45-PET scan technique to diagnose AD, which was approved by the Food and Drug Administration (FDA). Whereas Fludeoxyglucose ^{18}F Injection ([^{18}F]FDG) have been approved by the FDA as a new drug application on August 5, 2004 (Food and Drug Administration, 2014).

In many studies by various researchers (Aidos et al., 2014a), (Gray et al., 2012), (Rodrigues and Silveira, 2014), (Cabral and Silveira, 2013), FDG-PET is used as the main biomarker for classification of AD. Recently published AD and MCI criteria showed that AV45-PET tends to have an increased weight in the diagnosis of some special regions of the brain (McKhann et al., 2011), (Albert et al., 2011). Therefore, some researchers (Saint-Aubert et al., 2013), (Pontecorvo and Mintun, 2011), (Vlassenko et al., 2012) have used AV45-PET to differentiate between AD, MCI, and NC. However, there is less research that has used FDG-PET and AV45-PET to compare results. The PET images should be registered to the subject's corresponding brain extracted sMRI results. Generally, this registration is used as a first step of pre-processing on PET images to represent the structure of the brain. A six-parameter rigid body transformation and affine transformation are the most common methods in this part (Kiebel et al., 1997). In the work by Rodrigues and Silveira (2014), registration between MRI

and PET needs to extract the brain tissue in all MR images (skull-stripping) and segment all MR images to GM and WM . Then, they used SPM8 as the registration tool for 223 subjects (Rodrigues and Silveira, 2014). Pre-processed FDG-PET images were co-registered with the corresponding pre-processed MR images with IRTK tools using rigid and affine registration (Gray et al., 2012) for 221 subjects. In some research with different methods (Stühler and Merhof, 2012), the registration PET and brain atlas were used to prepare the PET images for extracting the features.

A feature indicates a distinctive attribute or aspect of something and in computer vision, and image processing is the relevant data to find the computational attribute for the subjects. Depending on the field of work, features may vary, such as points, edges, or objects from the image structure point of view or a general neighbourhood operation or feature detection applied to the image (Guyon and Elisseeff, 2006). In image processing, features can discriminate between different images that are basically acquired in the same way. Here, in this section of literature, we focused on medical images that are acquired by PET and MRI to differentiate between NC and other diagnosed stages of AD. For analyzing MRI images, there are some feature extraction methods : rates of change in several structural measures, including whole-brain (Fox), entorhinal cortex (Frisoni et al., 2010), hippocampus (Thompson et al., 2004) and temporal lobe volumes (Hua et al.) as well as ventricular enlargement (Hua et al.), (Jack et al., 2004) that correlate closely with changes in cognitive performance, supporting their validity as markers of disease progression. In addition, PET images have very good information to be extracted, such as the ratio of voxel intensities (Fox et al., 1996), (Smailagic et al., 2015) and mean voxel intensity (VI) in each ROI (Smailagic et al., 2015). There are several studies that used VI as feature and that published acceptable results (Gray et al., 2013), (Aidos et al., 2014a), (Habeck et al., 2008), (Román and Pascual, 2012), (Zhang et al., 2011a) or combination of some of these features.

We can classify things into different groups. Image classification is used to assign corresponding classes based on image features and its homogeneous characteristics (Japan Association of Remote Sensing., 1996). As mentioned in previous chapters, using PET scans as an objective diagnostic tool for dementia can give us a metabolic pattern of the brain in vivo, which facilitates classifying different stages of dementia. To discriminate normal and abnormal FDG-PET scans, we can use different methods of classification. The performance of each method is dependent on the number of features that are obtained from all patient information and their images.

After extracting the features from the images and before applying the methods for classification, in different works, they have different ways to prepare their information. In different works, there is specific technique to extract the features from the images and to prepare

the data for training the classifiers. For this purpose, Aidos et al. (2014) used whole-brain and some regions of FDG-PET images. To extract the features, they used two approaches (manual and automated). Using VI, they reduced the number of voxels by giving some values to each region, and they trained the classifiers SVM, K nearest neighbour, and naïve Bayes. The results were 85% accuracy for AD vs NC, 65% and 79% depending on the classifier and approach for MCI vs NC. Their results indicated that their automated approach and using a small number of features can discriminate subjects with AD from MCI (Aidos et al., 2014a).Aidos et al. (2014) also proposed the method started by segmentation of each 3D image, followed by construction of a probability matrix indicating the degree of belonging of each voxel to a region found by segmentation. Then, they used a feature extraction method, with SVM. The results had an accuracy rate of 89% in AD vs NC problem. In the case of AD vs MCI, the worst results were approximately 64% when the best result was higher than 76% between MCI subjects and NC subjects (Aidos et al., 2014b). Gray et al. (2012) proposed a method using longitudinal MRI and FDG-PET images to extract the features from 83 anatomically defined regions to train the SVM classifier in three individual categories (baseline, 12-months, and combined). This work also investigated differentiating between progressive and stable MCI, which had the best results with 65% accuracy. Furthermore, they reported 88% accuracy for AD/NC and 81% for MCI/NC with the combined approach (Gray et al., 2012). Another work used FDG-PET images in two time points (baseline and after 12 months) as well. The features were extracted from the difference rates of VI between two time points, and they sorted the number of features using tuned RBF-SVM as a classifier, giving the overall results of 92.6% for NC/AD and 70.2% for NC/MCI for their best method of combining the longitudinal and cross-sectional data (Rodrigues and Silveira, 2014).
Table 3.2 presents some studies that used PET images to distinguish different stages of AD from NC.

Table 3.2 Summary of studies using PET in Alzheimer's disease

Author(s)	Year	Subjects	Diagnostic measures	Associations
Carbonell et al. (Carbonell et al., 2015)	2015	23 AD, 125 LMCI, 151 EMCI, 155 NC	73% AD/NC, 94% EMCI/LMCI	determination of an optimal target ROI on AV45-PET images
Rodrigues & Silveira (Rodrigues and Silveira, 2014)	2014	48 AD, 109 MCI, 66 NC	93% AD/NC, 67% MCI/NC	the best classification results were achieved by combining cross- sectional and longitudinal information
Aidos et al. (Aidos et al., 2014a)	2014	59 AD, 59 MCI, 59 NC	85% AD/NC, 65% MCI/NC 79% MCI/NC (other classifier)	to identify ROIs by segmenting 3-D FDG-PET and extracting features proposed methodology outperforms using VI despite a small number of features
Gray et al. (Gray et al., 2012)	2012	50 AD, 53 sMCI, 64 pMCI, 54 NC	88% AD/NC, 65% MCI/NC	our combined method shows considerably better performance compared to the case of using an individual modality of biomarkers
Salas-Gonzalez et al. (Salas-Gonzalez et al., 2010)	2010	53 AD, 114 MCI, 52 NC	95% AD/NC, 88% MCI/NC 86% AD/MCI/NC	selection of voxels of interest using the t-test and a posterior reduction achieves better compared to the voxel-as-features and a PCA- based approach

Cabral and Silveira (2013) used FDG-PET images and VI of each brain scan as the classification features. To select the subset of features, they ranked the features according to their mutual information with the class label, selecting the highest-ranking features. They used two classifiers (SVM and RF) and one proposed method to combine the outputs of several classifiers and to increase performance by exploring the diversity of the base classifiers in terms of random features. They achieved, based the classifiers across all tested features, 66.55% and 64.63% averaged for ensembles of SVM and RF (Cabral and Silveira, 2013).
Establishing relationships between multiple features facilitates finding a good classification between some datasets, but people are often prone to making mistakes during analysis, and it makes it difficult to find solutions for certain problems. Machine learning can help to decrease the number of mistakes and improve the efficiency of systems (Kotsiantis, 2007).
One model for the classification of AD focuses on the selection of the most influential risk factors using various attribute evaluation schemes, for instance, the ranker search method. It was found that some specific genetic factors, diabetes, age, and smoking were the strongest risk factors attributing to AD (Joshi et al., 2010). A detailed study on the various risk factors for AD has been proposed by many researchers (Luchsinger et al., 2001). It is often useful to apply different supervised machine learning methods for classification, such as the decision tree (Pushpa et al., 2006), bagging, RF tree, RBF networks, and multilayer perceptron. Moreover, ANN is another method of AD classification which is also used (Joshi et al., 2010).
There was one work that focused on EMCI and LMCI, which used AV45-PET images to classify their subjects (Carbonell et al., 2015). Carbonell et al. (2015) developed a statistical approach using amyloid-PET images to optimize the selection of regions of interest and corresponding standardized uptake value ratio cut-off for the automated classification of subjects into amyloid-low and amyloid-high. Amyloid-high or amyloid-positive in PET is almost always associated with low CSF amyloid-β42 in individuals with symptomatic Alzheimer's disease. There are individuals (typically cognitively normal) with similarly low levels of CSF amyloid-β42 but who are amyloid-low or amyloid-negative by PET. The authors used ADNI subjects with different diagnosis, and grouped the subjects into different levels of cognitive impairment : cohort 1 included EMCI and LMCI subjects and cohort 2 a combination of NC and AD subjects. In order to achieve segmented MRI images into gray matter, white matter, cerebrospinal and partial volume estimation, they used a 9-parameter affine transformation on MRI images and mapped them on MNI reference. Projection of segmented mid-cortical surface on PET images after correction and registration to the subject MRI image gave them voxel wise SUVR corresponding to each ROI. For each subject mean SUVR across the whole cerebral cortex was calculated. Regularized Discriminant Analysis (RDA) served to determine the optimal threshold in order to separate subjects based on whole cortex SUVR

(SUVR_WC) measurements. Additional statistical testing including cognitive performance measures (MMSE, Alzheimer's disease assessment scale-cognitive subscale (ADAS-Cog), CSF ($A\beta_1 - 42$), gender, clinical classification and APOE genotype were considered to obtain the results of discrimination between $A\beta_H$ and $A\beta_L$ for each cohort (classification between EMCI and LMCI (cohort 1), also for AD vs. NC (cohort 2)).
In the subject characteristic results, which is not completely relevant to our work, the authors did not find significant association between clinical classification and APOE, similarly to gender. In contrast there was a statistically significant age difference between EMCI and LMCI subjects, also the initial SUVR_WC measurements, cognitive measures and CSF biomarkers. Statistically significant association between clinical classification (NC vs. AD) and APOE was reported, but not for gender. SUVR_WC and cognitive measurements, also CSF biomarkers were significant for cohort 2. The results of anatomical target ROI, which is more relevant part of this publication and our work, the performance of the proposed approach on target ROI compared to the results of subject classification based on SUVR value. For cohort 1, the accuracy of 0.942 with the cut-off value of 1.10 and 0.985 with 1.24 cut-off value reported. In addition accuracy of 0.966 with cutoff of 1.10 for cohort 2 is reported. Conclusion : Based on this paper, the authors did not investigate the classification between different stages of AD among their subjects directly, however their results displayed that several iterations of the discriminant analysis improved the classification of subjects into amyloid-low and amyloid-high groups. Determination of the cut-off value for classification of the subjects based on the optimal target ROI SUVR measurement is their main key of their statistical approach.
Among all previous works, Carbonell et al. (2015), achieved 94% classification accuracy to discriminate between low and high amyloid accumulation with the cohort of EMCI vs LMCI (cohort1), which is different to the classification of cognitive class, and reported 73% for AD vs NC using amyloid PET images, which is lower than most of the state-of-the-art methods.

3.3 Multi-modality

Recent studies have demonstrated that multiple neuroimaging contains complementary information for diagnosis of AD and its classification into different stages with high accuracy. However, to obtain more reliable classification results, these multiple biomarkers need to be combined to provide an accurate diagnosis. In previous sections, we reviewed some modalities, such as sMRI, fMRI, FDG-PET, and AV45-PET, which yielded satisfactory results (Chetsadaporn et al., 2015). In this section, we studied some research that used multi-modality to achieve higher results. Some of the publications above had extra experiments to show the

results of combining two multi-modal images or combining more clinical and biological biomarkers. Different biomarkers can expose different aspects of pathological changes associated with AD. Some biological biomarkers have been developed for diagnosis of AD. Three CSF biomarkers are common in state of the art : total τ (T-τ), hyper-phosphorylated τ (P-τ) and the 42 amino acid isoforms of Aβ (Aβ42) (Tong et al., 2017).
Table 3.3 presents some studies that used multi-modal images to obtain higher accuracy.

Table 3.3 Summary of studies using multi-modal images in Alzheimer's disease

Author(s)	Year	Subjects	Diagnostic measures	Associations
Tong et al. (Tong et al., 2017)	2017	37 AD, 75 MCI, 35 NC	98.1% AD/NC, 82.4% for MCI/NC and 77.9% for AD/MCI/NC	significantly better using multi-modality biomarkers (PET, MRI and CSF)
Lele Xu et al. (Xu et al., 2015)	2015	113 AD, 110 MCI, 117 NC	94.8% AD/NC, 74.5% for MCI/NC and 77.8% for pMCI/sMCI	classification with multi-modality data were helpful
Saint-Aubert et al. (Saint-Aubert et al., 2014)	2014	22 AD, 17 NC Florbetapir (AV-45)		well discriminated using PET template-based quantification with the MRI-based cortical quantification method
Richard et al. (Richard et al., 2013)	2013	181 MCI	More than 95% accuracy	unlike PET MRI or CSF do not substantially affect diagnostic accuracy for predicting progression to AD with MCI
Zhang et al. (Zhang et al., 2011a)	2011	51 AD, 99 MCI, 52 NC	86.5% AD/NC, 76.4% for MCI/NC 93.2% AD/NC (3 biomarkers)	our combined method shows considerably better performance compared to the case of using an individual modality of biomarkers

3.4 Summary

In this section, we reviewed the publications in similar domains, and we selected some relevant research to present here. In these studies, different approaches were applied to prepare the images, to extract the features, to select the classifiers, and to use some extra biomarkers. The results were obtained in several manners, which are studied. Among all studied work, there are a few studies that pointed to the different stages of MCI (EMCI and LMCI). The studies that used MRI images only gave us a good historical review on methods for finding ROIs and different classifiers. In addition, it led to more understanding of the advantages and disadvantages of MRI compared to PET modality. The studies using FDG-PET images mostly focused on VI in multiple regions.
PET images provide a wealth of diagnostic functional information in various sites, particularly in the brain. A large number of prior work investigated different topics on PET images, including differentiating between brain disorders and health controls (AD vs NC) or other disordering by inferring sites of pathology based on characteristic signs and symptoms (AD vs FTD). FDG-PET provides a separate, simpler, more objective and quantitative way to make this same judgement. Good reliability and diagnostic accuracy was observed with traditional images. There are also many potential ways to analyze FDG-PET data. Thus, the most

accurate classification method via the PET images was necessary to be able to obtain the best result of classification for FDG-PET and AV45-PET images.

CHAPTER 4 GENERAL METHODOLOGY

This chapter comprises sections along with our proposed pipeline steps, which are formed by a set of tools. The pipeline schema is divided into two parts to present more details. Figure 4.1 presents the first part of our pipeline to select the features from extracted ROIs. Each step of this flowchart includes a tool chosen after validation and tests. The tool selection was done among several available ones, according to our needs and their advantages.

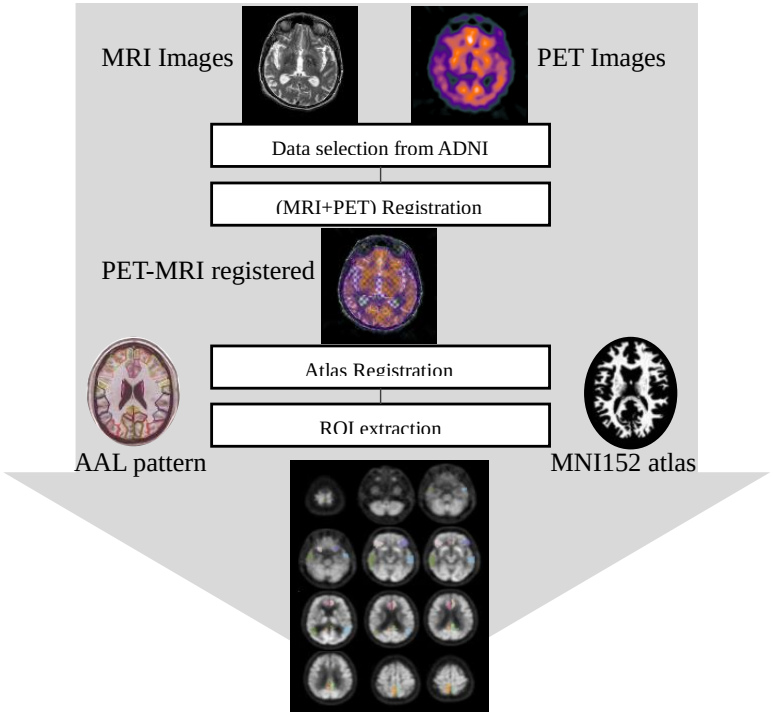

Figure 4.1 Pipeline of proposed method, Part I : Image processing.

Following a summary of data collection and image pre-processing, selection of the registration tool will be explained. It is followed by segmentation and extracting the features from registered images. Selecting the ROIs to prepare data for classifier training is the next section. Then, the second part of our pipeline presents the different classifiers, which are applied and mentioned in Chapter 2.

4.1 Data Collection and Image Pre-processing

First, the images were downloaded from the Alzheimer's Disease Neuroimaging Initiative (ADNI) database. The ADNI has three databases : ADNI1, ADNI2, and ADNI GO. Pre-processed PET and MRI images were selected from all three ADNI databases. The most available subjects that had complete information (such as clinical test (MMSE), FDG-PET, AV45-PET images, and T1 weighted MRI scans) were downloaded, which comprised 1088 subjects.

Subject images were pre-processed by ADNI. Pre-processing on PET images included four steps : 1) co-registration between extracted frames of PET scans to the first extracted frame of the raw image file to reduce the effect of patient motion, 2) averaging of the six 5-minute frames of the co-registered dynamic image set, 3) reorientation of the output images into a standard space ($160 \times 160 \times 96$ voxel in $1.5mm^3$) and 4) obtaining a uniform image isotropic resolution of 8 mm full width at half maximum (FWHM). The MRI images also were corrected using three steps : 1) Gradwarp, a system-specific correction of image geometry distortion due to gradient non-linearity, 2) non-uniformity correction, calibration, and correction of the image intensity non-uniformity, and 3) reduction of the intensity of non-uniformity and reduction of the residual intensity non-uniformity (ADNI, 2014).

Next, the ADNI cohort were analyzed to select the sample set with PET and MRI and classification evaluation (diagnostics results by ADNI). In this step, 428 subjects were excluded because some of the subjects did not have the corresponding MRI in a close enough time to the PET acquisition, or the AV45-PET for those subjects was not available. Finally, 660 subjects were selected for this work.

4.2 Registration

Registration is one of the most important parts of our proposed method, and we aimed to choose the most convenient tool for this step, which includes two separate registration steps. The first step parcels the native MRI of patient by performing a non-rigid registration with the MNI152 atlas. This allows to the segment the patient's image by anatomical regions of interest and extract the specifics region that will be analyzed with PET. The second step registers the parcelled MRI with the patient's PET scan.. Based on our literature, affine registration is one of the commonly used parametric models (Chumchob and Chen, 2009). An affine transformation corrects some global distortions in the images to be registered. Moreover, the rigid body method is accurate because there are only six rigid body parameters

required to map between the structural and functional images.
Many software solutions have been presented for medical image registration. For this work, we investigated and tried some of free open-source software packages, such as :

— Automated Image Registration (AIR) (Woods et al., 1998) – source code in C ;
— ITK (Ibanez et al., 2005) – source code in C++ ;
— FLIRT (Jenkinson and Smith, 2001) – source code in C++ ;
— Elastix (Klein et al., 2010) – source code in C++
— Statistical Parametric Mapping (SPM) (Ashburner and Friston, 1999) designed for the analysis of brain imaging data sequences.

We looked for an accurate and fast method to execute this step of our pipeline in appropriate time with less errors. We considered to find a solution that was 1) suitable for registration between PET and T1-MRI, 2) programmable and compatible with the rest of the pipeline, and 3) accurate for standard atlas and MRI with less cost function. Among all algorithms for registration after validation, we used affine geometric transformations and rigid body (six parameters) with several transformations and cost functions that have been published in functional brain imaging studies.

The Functional Magnetic Resonance Imaging of the Brain (FMRIB) Software Library (abbreviated FSL) is a known software library of analysis tools for different imaging data and specifically for fMRI, MRI, and diffusion tensor imaging. The FMRIB Analysis Group from Oxford University made a series of analysis and statistical tools for functional, structural, and diffusion MRI brain imaging data. The latest stable version in 2012 for Linux and Mac OS X was released. Several functional and structural functions for MR images are included using FSL tools. In addition, FMRIB's linear image registration tool (FLIRT) is the linear inter-modal and intra-modal registration tool.
Statistical parametric mapping (SPM) is another tool, which is recommended for PET images. Below, we compare two final chosen tools to select one, considering their cost functions and different transformations. We applied them for the real data to find the best solution for our pipeline.
The FSL has a few well-defined, easy-to-use programs with a small number of input parameters. The SPM works quite well, but due to its file format conventions, it is best if SPM is not mixed into a pathway with other packages. One should only consider using SPM if prepared to rigorously validate the left/right orientation for the data. The SPM is more GUI-oriented than FSL, which uses the NIFTI file format to make it easy to integrate into processing pipelines (brainimaging, 2017). Among all registration tools, such as AIR (Woods et al., 1998), FLIRT, SPM, and so many automatic and non-automatic tools, based on our state of the art, we chose FLIRT and SPM to test. In Chapter 6, we presented the results of our cross

validation for choosing FLIRT as our registration tool.

4.3 Segmentation

In this work, a more relevant method for our pipeline is using atlas-based segmentation. Because we need our images to be comparable and uniform to each others and to select the spesific regions as ROIs. For this purpose we used single atlas-based segmentation using MNI152 to segment the brain into 116 anatomical structures. As we mentioned in the last chapter, the accuracy of segmentation based on an atlas is dependent on the registration between the input image and atlas. This is another reason for scrutinizing to choose the best method of registration. When compared to other methods for image segmentation, the atlas-based segmentation has the ability to segment the image with no well-defined relation between regions and pixel intensities (Kalini, 2004).
The use of anatomical atlases as reference images to guide segmentation of new images is very popular in different medical applications. The atlas typically helps to localize the anatomical structures. All the known atlas-based methods can be classified into single and multi atlas-based segmentation. In this work, we used the single atlas method, and the way we applied the labels for each brain region is different from the regular method of atlas-based segmentation. Therefore, we proposed a simple anatomical segmentation based on the MNI152 atlas and AAL pattern of 116 labels. In general, the accuracy of the atlas-based segmentation depends on the accuracy of the atlas-to-target registration (Oliveira and Tavares, 2014) ; thus, we can rely on our method, as we validated the method of registration.
The next step of segmentation after registration between the subjects and atlas is extracting the regions that are ROIs by subtracting to the mask of ROIs individually. This is done by implementing a function using the NIFTI toolbox in MATLAB (version : NIFTI_20100413). After verification of the effect of each region on the classification accuracy (results in Chapter 6), we combined all regions and made a mask in the atlas space. Figure 4.2 illustrates the steps of creating a mask for all ROIs. To create our mask, we performed five steps : I) The PET image is registered into the MNI atlas, and the AAL was applied on the image. II) Each ROI was extracted from the whole labelled image (in different slices, different ROIs are seen). III) All 10 ROIs were added together (logically there is no overlap) and a mask is created for each subject individually. IV) the PET image registered with MNI was used to replace the raw voxel intensities. V) The mask is applied on the PET image, and it is available to create matrix X.

We use voxel intensity (VI) as a feature and after ROI selection we used the VI of those regions to train the classifiers. ROIs have different size in different images, then all ROIs resized to

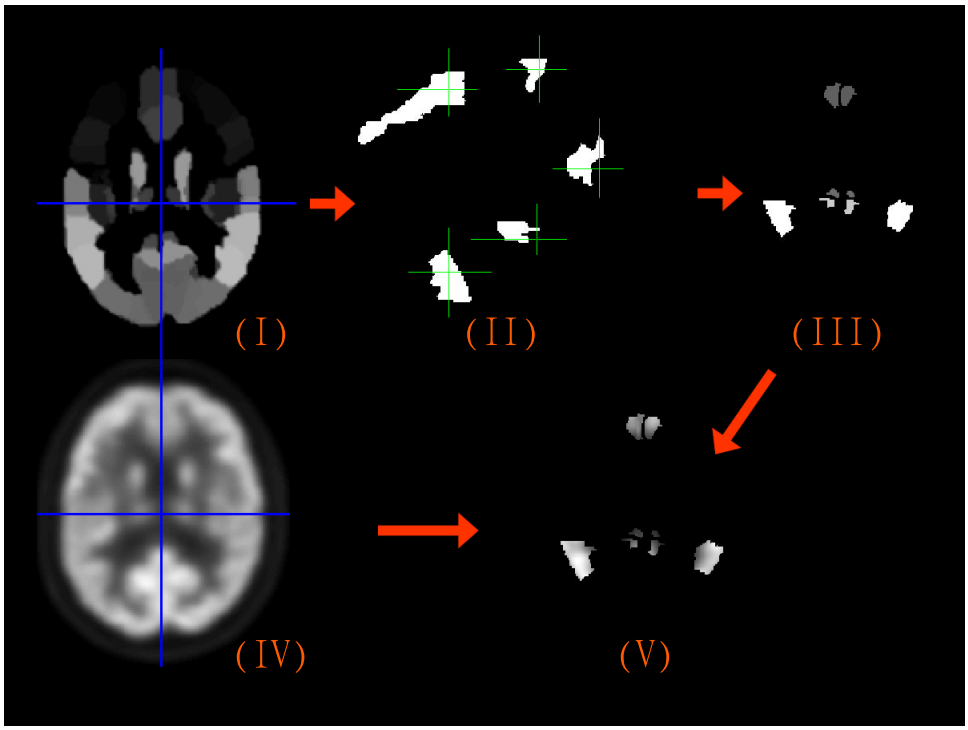

Figure 4.2 Steps of creating mask using individual ROIs.

maximum number of voxel. To find this number, we counted the maximum number of voxels among all subjects for each ROI. Based on the maximum identified values, we calculated the maximum length of the overall vector (reshaped 3D image voxels to 2D vector). Each subject ROI which did not reach the maximum value were zero-padded. Using this approach, we created the matrix X with vector of the subjects as rows and a maximum number of valued voxels ascolumns. Creating the matrix X for two approaches is explained in detail in Chapter 5. Therefore, the last step is classification and evaluation of the results, which is in the next section.

4.4 Classification

Our data for training the classifiers from the previous step were collected in matrix X, which had two versions for both approaches. Figure 4.3 shows the second part of our pipeline, which is training and testing the classifiers and cross validation. As mentioned previously, four different classifiers were selected for classification. Two matrices had 660 rows of data and depending on the approaches, the number of columns varied. To train all four classifiers, we chose 80% of the data randomly, and to test, we used the rest (20%) of the data. For each iteration, the sample sets changed, and we had at least five iterations per each classifier to

train and test. The results, which are presented in the result section, were obtained as an average of all iterations. All classifiers were implemented on MATLAB (2015) software and the results were stored on a spreadsheet for future data analysis.

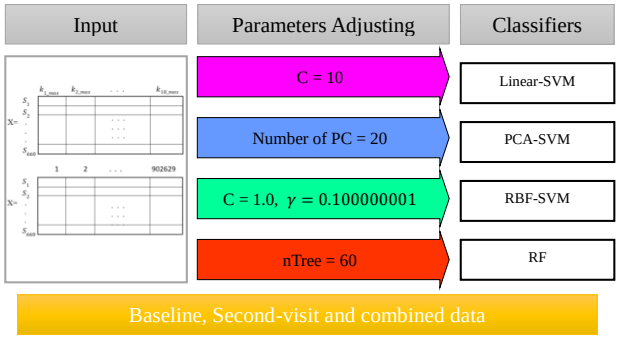

Figure 4.3 Pipeline of proposed method, Part II : Classification.

Linear SVM For linear kernels in SVM, we analyzed the C parameter. To find the optimal value for C, we used a 10-fold cross-validation on training data which is 80% of the total data. We selected the value for C using a grid search, followed by a refined search. The maximum in-sample validation accuracy were found at $C_{opt} = 10$. We used the same optimal parameter for linear SVM and PCA-SVM. To clarify the persentage of each subsets, we used 80% of total data as training set and the remained 20% as test set. We executed 10-fold cross-validation on training set which splited to 10 subsets. Of the 10 subsets, a single subset was retained as the validation data for testing the model, and the remaining 9 subsets were used as training data. The cross-validation process was then repeated 10 times, with each of the 10 subsets used exactly once as the validation data. The advantage of this method is that all observations are used for both training and validation, and each observation is used for validation exactly once.

PCA-SVM We derive the Principal Components (PCs) from the raw dataset while preserving 91% of the group variance. This implies that there is only a slight loss of discriminative information. Even when we were preserving 91% of the group variance, we could reduce the feature matrix from 6012 to 20 columns, thereby significantly reducing the computational time.

In our 50 iterations we removed the PCs and computed the average squared of the rest components in off-diagonal to find the minimum value and in rest of iterations we obtained ignorable change in minimum number. Therefore, in the first iteration, we first removed PC

from the correlation matrix and then the average squared of components in off-diagonal was computed. In the next iteration we removed the first two PCs and the same process repeated, and so forth. After twenty iterations, the first twenty PCs were removed from the correlation matrix and the above-mentioned processes repeated again. Obtained minimum of squared average value was a factor for selecting optimum PCs and implementing this method. We chose the optimum number of principal components such that the variance retained was 91% (Velicer, 1976). In MATLAB, the PCA function is predefined, we achieved PC = 20, and the results of the PCA were used to train the linear-SVM function to achieve the final results.

RBF-SVM The RBF-SVM classifier needs to be adjusted; therefore, we used a 10-fold cross validation approach to test the method. To do this, we chose randomly 10 subsets out of 660 subjects, of which 9 were used for training the SVM classifier and the remaining subset is used for test. The process is successively repeated 1000 times to avoid any possibility of bias. After all the optimum parameters, achieved :

$$C_{optimum} = 1.0, \gamma_{optimum} = 0.100000001, Score = 0.917 \tag{4.1}$$

Random forest To train the TreeBagger function in MATLAB, one of the crucial parameters is the number of trees (ntree). Based on the literature, this number should be greater than 50. To adjust the number of trees, a selected sub-sample was classified and evaluated 10 times. Each time the ntree was numbered in the range of [20 : 120 : 20], and the best accuracy of 91.2% was obtained when the ntree was equal to 60.

4.4.1 Classification Accuracy Calculation

To calculate the accuracy of each classifier, we present a common method. After applying the classifiers and all iterations of training and testing of the classifiers, the result data were saved. Table 4.1 shows an example of the data yielded by the linear SVM.

Table 4.1 Example of result data yielded by linear SVM on FDG-PET images.

	True	False
Positive	19	0
Negative	30	11

Accuracy (ACC), sensitivity (SEN), and specificity (SPE) are used to quantify the performance of the classifiers based on the results. The ACC, SEN, and SPE were calculated using

the following formulas :

$$ACC = \frac{TP + TN}{TP + TN + FP + FN} \tag{4.2}$$

$$SEN = \frac{TP}{TP + FN} \tag{4.3}$$

$$SPE = \frac{TN}{TN + FP} \tag{4.4}$$

where TP, FP, TN, and FN are the numbers of true positives, false positives, true negatives, and false negatives, respectively. Therefore, the ACC of our example in Table 4.1 is equal to 81.67%. In the case of presenting significant results, the p value was obtained by the t-test function of the spreadsheet (LibreOffice, version : 4.3.3.2).

CHAPTER 5 ARTICLE 1 : IDENTIFICATION OF AD/LMCI/EMCI PATIENTS FROM SEMANTICALLY PARCELLED AV45 AND FDG-PET IMAGES

Contribution of the first author in preparation and writing this paper is evaluated as 90%. This article has submitted to IEEE Journal of Biomedical and Health Informatics (March,2017)

Remarks : This paper presents a proposed pipeline of classification between AD and different sages of MCI, using PET images in two time points (baseline and second visit). The proposed method includes two approaches : first, multi-region approach using the region of ineterest in PET images to select the features for training the classifiers. Second, whole-brain approach using whole voxels of brain image to compare the results. Experiments revealed that the combination of two time points together obtain better results than single time point individually.

Identification of AD/LMCI/EMCI Patients from Semantically Parcelled AV45 and FDG-PET Images

Seyed Hossein Nozadi, Samuel Kadoury
for the Alzheimer's disease Neuroimaging Initiative [1]
Dept. of Computer and Software Engineering,
Ecole Polytechnique Montréal, Montreal, Canada

5.1 Abstract

Distinguishing patients with Alzheimer's disease (AD), Late mild cognitive impairment (LMCI), Early Mild Cognitive Impairment (EMCI) and normal controls (NC) is an extremely active research area, which has garnered significant attention in the past decade. Discrimination of different stages of dementia is crucial to slow down the progression of AD. Positron Emission Tomography (PET) is considered a highly powerful diagnostic biomarker, but few approaches

1. Data used in preparation of this article were obtained from the Alzheimer's disease Neuroimaging Initiative (ADNI) database (adni.loni.usc.edu). As such, the investigators within the ADNI contributed to the design and implementation of ADNI and/or provided data but did not participate in analysis or writing of this report. A complete listing of ADNI investigators can be found at : http ://adni.loni.usc.edu/wp-content/uploads/how_to_apply/ADNI_Acknowled gement_List.pdf

investigated the efficacy of focusing on localized PET-active areas for classification purposes. In this work, we propose a pipeline using learned features from semantically labelled PET images to perform group classification using Radial Basis Function (RBF) SVMs and Random Forests (RF). Following normalization and pre-processing steps, a deformable multi-modal PET-MRI registration method is proposed to fuse the MNI atlas to each patient-specific PET scan, generating a fully labelled volume from which 10 common regions of interest used for AD diagnosis are extracted. The method was tested on 660 subjects from the Alzheimer's Disease Neuroimaging Initiative database and compared to a whole brain approach. The classification accuracy of AD vs NC was measured at 91.2% when using RF combining both multi-region features from a cross-sectional and follow-up exam. A considerable improvement in the EMCI vs LMCI classification accuracy was achieved with a 72.5 % rate. The pipeline demonstrates the potential of exploiting longitudinal multi-region PET features to improve cognitive assessment.

IEEEkeywords Alzheimer's disease, Mild cognitive impairment, Classification, Longitudinal analysis, $[^{18}F]$ fluorodeoxyglucose, Positron emission tomography, Semantic segmentation

5.2 Introduction

Alzheimer's disease (AD) is one of the most common types of neurodegenerative disorders in the aging population (Liu et al., 2010). A recent research by the Alzheimer's association reports that AD is the sixth-leading cause of death in the United States and is rising every year considering its proportion in the causes of death (Alzheimer's Association, 2016). A typical AD starts with forgetfullness and progresses by affecting language, visuo-spatial and frontal lobe functions (Westman et al., 2011). Therefore the onset of forgetfullness is an important marker in the diagnosis of early stage AD, which is known as mild cognitive impairment (MCI) (Mucke, 2009). However, it could be due to age-related memory decline. Still, clinical and neuroimaging studies have demonstrated differences between MCI and normal control (NC) (Román and Pascual, 2012), (Silverman, 2009). The cognitive screening is a routine clinical method to detect, diagnose and classify dementia but the accuracy of classification is hindered due to the overlapping nature of the cognitive impairment. Different types of dementia are diagnosed by cognitive screening such as Mini–Mental State Examination (MMSE), which is usually sensitive to significant cognitive impairments, and in some patients can also detect MCI. Therefore, an integrated approach is needed to diagnose MCI in a more accurate manner.

MCI is divided into two stages such as early MCI (EMCI) and late MCI (LMCI) ; these

stages can either progress to the next stage (convertable MCI) or not (non-convertable MCI). Current treatments are effective for early MCI which is an active research area, whereas, there is still no complete cure for AD. This implies a great urgency to develop sensitive markers to detect and monitor early brain changes. The ability to diagnose and classify AD at an early stage helps in making a more informed decision at later stages for clinical intervention and treatment planning, thus having a great impact on reducing the cost of longtime care (Stoeckel and Fung, 2007). From a neuroimaging perspective, positron emission tomography (PET) of fluorodeoxyglucose (FDG) for cerebral glucose metabolism and β amyloid (also known as AV45 or florbetapir) can provide complementary information for the diagnosis of AD (Gray et al., 2012; Saint-Aubert et al., 2013; Bauer, 2014).

The classification of patients who are candidates under AD at its early stage versus NC is a topic looked by many studies conducted with PET imaging. To be able to classify patients, brain features of interest need to be extracted from the PET images. Features can discriminate between NC and other diagnosed stages of AD. By selecting the best features, we can make a better use of classifiers and subsequently, improve accuracy of the results. Feature-based methods can use brain volume (Cabral and Silveira, 2013), ratio of voxel intensities (Fox et al., 1996), (Smailagic et al., 2015), mean voxel intensity (VI) (Hinrichs et al., 2009) in each regions of interest (ROIs) and combinations of some of these features. Voxel intensity is one of the most important method in feature extraction (Zhang et al., 2011a), (Habeck et al., 2008). For instance, Smailagic et al. used VI to reduce the number of voxels by excluding lower intensity values from the PET images and simplify the classification process (Smailagic et al., 2015). Gray et al. differentiated AD and NC with an accuracy of 88%, whereas non-convertable MCI and NC yielded a 65% accuracy (Gray et al., 2012). The authors used FDG-PET images from the Alzheimer's Disease Neuroimaging Initiative (ADNI). Their method proposed to classify AD versus non-convertable MCI and convertable MCI to test regional feature sets based on signal intensities. In a work by Rodrigues and Silveira using the same longitudinal database, the best classification accuracy was obtained by combining two time points (baseline and after 12 months) (93% for NC vs AD) (Rodrigues and Silveira, 2014). In another study, Aidos et al. used VI in some ROIs which were manually selected by experts (Aidos et al., 2014a). By using an automated feature selection method to classify the subjects, they applied ROIs and mutual information to rank the features and identify the highest values to reduce the number of features. The best accurate classification rates among support vector machine (SVM), k-nearest neighbor (KNN) and naive Bayes were obtained by using ROIs with SVM or KNN for MCI, with rates ranging between 65% and 79%. An accuracy of 85% for AD vs NC was also obtained using the proposed method.

In this work, we concentrate solely on the diagnostic potential of PET images without using

additional biomarkers. In the first approach (hereafter called multi-region approach), we developed a method to segment the ROIs and extract the features while in the second, we used a similar method but for the entire brain (hereafter called whole-brain approach). Due to it's challenging nature, EMCI and LMCI is not frequently tested for classification. Generally, most studies compared AD, MCI and NC (Gray et al., 2012), (Cabral and Silveira, 2013), (Zhang et al., 2011a), (Zhang and Shen, 2012). However it must be noted that Carbonell et al. achieved 94% classification accuracy to discriminate between low and high amyloid accumulation in PET images from automatically identify ROIs, rather than LMCI vs EMCI, and they reported 73% for AD vs NC the same method, which is lower than most of the state-of-the-art methods.

Here we propose a fully automated pipeline to extract specific regions known for amyloid accumulation in order to classify the cognitive class. Therefore, we decided to group our data into four classes (AD, EMCI, LMCI, NC) using PET images only. Each subject had two PET scans at two time points (baseline and after approximately 12 months), FDG-PET and AV45-PET images. We believe longitudinal PET images provide additional information to acheive a high level of discrimination between EMCI vs NC, LMCI vs NC and EMCI vs LMCI. The main objective is to develop a method to select the best features using PET images only to classify AD, EMCI, LMCI and NC. To our knowledge, this work is unique because of the large sample size compared to those of previous works which used less than 250 subjects (Gray et al., 2012; Rodrigues and Silveira, 2014; Aidos et al., 2014a).

We propose to classify the subjects by using their PET images both at baseline and after approximately [2]12 months (hereafter called second visit). First, using the baseline images, a primary registration between magnetic resonance images (MRI) and PET images was performed to facilitate uniform measurements between the varying image resolutions and generating a gross alignment of the anatomical brain structure between all subjects. After registration between the PET and MRI images using FMRIB's Linear Image Registration Tool (FLIRT) (Jenkinson and Smith, 2001; Jenkinson et al., 2002), the resulting images were registered to the Montreal Neurological Institute (MNI) atlas (MNI152) in order to compare voxels among the subjects' image. Label assignment was performed with the automated anatomical labeling (AAL) atlas, yielding 116 different areas in the brain used for the multi-region approach. To extract features from each area, we used this AAL labeling method and selected 10 ROIs in each subject. The second visit images underwent the same process to extract the features and combined to the baseline for the multi-region approach for AV45-PET and FDG-PET images individually. The whole-brain approach used voxel-wise features from the entire volume for

2. The second scan of ADNI subjects was acquired between 6 to 18 months after baseline; this period of time is not the same for all subjects which gives an approximate 12-month period.

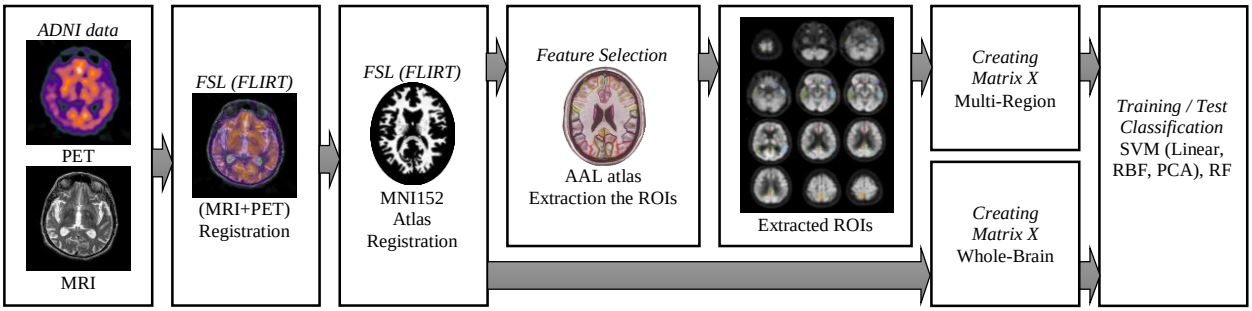

Figure 5.1 Pipeline of proposed method.

the same images and time points. For classification, we used as basis of comparison both linear and RBF SVMs, PCA and Random Forests (RF). The paper is structured as follows. Section II presents the materials and the methodology for the classification pipeline. Section III presents the experimental results, followed by a discussion. Section IV concludes the paper.

5.3 Materials and Methods

We propose a pipeline including PET and MRI registration, atlas registration, anatomical segmentation, feature selection and classification as shown in Figure 5.1. The following sections describe each component of the pipeline.

5.3.1 Data selection

The data used in this work was from the ADNI database (www.loni.ucla.edu/ADNI). ADNI is an ongoing effort launched in 2003, longitudinal, multicenter study designed to develop clinical, imaging, genetic, and biochemical biomarkers for the early detection and tracking of AD. It includes approximately 1800 subjects recruited from over 50 sites across the US and Canada in three database (ADNI, ADNI GO and ADNI 2) (Jagust, 2010), (http ://adni.loni.usc.edu/). Among all subjects which are available for download, this study used resting-state FDG-PET brain volumes acquired at two time points : baseline and second visit. The total number of subjects was 1046 patients, 386 patients were excluded because they did not have the complete PET series and/or corresponding MRI images at the same time. A final set of 660 subjects with PET and MRI images was selected, which amounted to 99 AD, 164 EMCI, 189 LMCI and 208 NC, and MMSE scores in both time points. Table 5.1 presents the characteristics of the patient cohorts.

Table 5.1 Characteristic of sample

Characteristics	AD	EMCI	LMCI	NC
n	99	164	189	208
Mean age	75.7±8.2	74.3±8.1	72.8±7.0	76.3±8.4
Gender (M/F)	57/42	94/70	101/88	119/88+1(undefined)
MMSE				
Baseline	22.9±2.2	28.5±1.4	27.6±1.8	29.1±1.2
second visit	20.4±4.1	27.7±2.7	24.4±4.9	28.3±2.3

5.3.2 PET & MRI datasets

PET protocol

Anatomical brain imaging (ex. MRI) and metabolic imaging (ex. PET) are two commonly used imaging modalities used in the diagnosis of dementia (Román and Pascual, 2012). PET creates three-dimensional (3D) metabolic images of the brain by using radioactive tracers, which are usually administered to patients through intravenous injection. This technique creates 3D images of the brain by detecting the emitted radiation of the intra-venously injected radiation tracers. The carrier molecules in the tracers binds to specific receptors. The routinely used PET tracer is FDG (a modified glucose) that binds to normal functioning cells, i.e., neurons in the brain. The radio-active past of the tracer emits positrons, which interacts with surrounding electrons resulting in 2 photons of 144 Kv. The principle of PET imaging is to localize the tracers from the detected photons, creating tomographic images. However, the distribution of the tracers depends on the functioning (metabolism) of the tissue thereby creating a functional imaging (Silverman, 2009).

PET is a functional neuroimaging technique used in AD, which produces a distribution map of glucose uptake. The absence of uptake in the temporal parietal lobe is an indication of AD (Román and Pascual, 2012). Importantly, the diagnostic accuracy of PET correlates with the histopathology confirming diagnosis of AD. Foster et al. demonstrated that FDG-PET improves the accuracy of differentiating AD from fronto-temporal dementia, especially when the symptoms and clinical tests are equivocal (Foster et al., 2007).

PET images were preprocessed in four steps. Scans were further processed to provide increasingly uniform datasets. The four steps were : 1) co-registration step to reduce the effect of patient motion and converted file into DICOM format ; 2) averaging of the 6 five-minute frames of the "co-registered dynamic" image set ; 3) reorientation of the output images into a standard space with $160 \times 160 \times 96$ voxel image grid of 1.5 mm cubic voxels ; and 4) acquiring a uniform image with isotropic resolution of 8 mm full width at half maximum (Jagust, 2010),

(http ://adni.loni.usc.edu/).

MRI protocol

The MR images were acquired on Phillips, GE and Siemens systems. Since the protocols for each scanner were different, a correction was provided by ADNI. These image corrections for each MPRAGE image were linked with related image files which have undergone specific image preprocessing correction steps. Corrections included geometry distortion, calibration and reduction of intensity of non-uniformity. More detailed information is available on the ADNI website (http ://adni.loni.usc.edu/). We used T1-weighted images which were selected and reviewed for quality and correction in terms of data format and/or alignment. MR images were used only to find the sub-cortical anatomical structures to increase the labelling accuracy of the ROIs. Finally, the MRI with $176 \times 256 \times 256$ resolution with 1 mm spacing were collected with the purpose of increasing the accuracy of registration and labelling.

5.3.3 Mask Extraction

PET - MRI registration

Accuracy of inter-modality registration between PET and MRI is a crucial step as it dictates the reliability of PET segmentation and subsequently provides better results for ROIs. The first step was to register the PET and its corresponding T1-w MRI. For this, we used FLIRT which is a robust, accurate and fully automated registration tool for brain images (Jenkinson and Smith, 2001), (Jenkinson et al., 2002). In our pipeline, skull stripping was not needed, so by reducing the total processing steps from the original images, we tried to keep as much detailed information of signal intensities as possible. We tested rigid body (6 parameters) and affine (12 parameters) transformation (mutual information and correlation ratio cost function done for each transformation). We used an affine transformation with correlation ratio for all 660 subjects in two time points as it provided the best inter-modality registration accuracy.

Atlas registration

The MNI152 atlas was created as a response to increasing demand for 3D standard templates to examine, validate and measure the accuracy of different image analysis procedures in a standardized space (Collins et al., 1998). This atlas is based on a brain phantom, which is made up of ten volumetric datasets in different tissues. This atlas is often considered as a gold standard to test brain analysis algorithms (Collins et al., 1998). Thus registration between the MNI152 atlas and the patient MRI facilitates the localization of the analyzed regions.

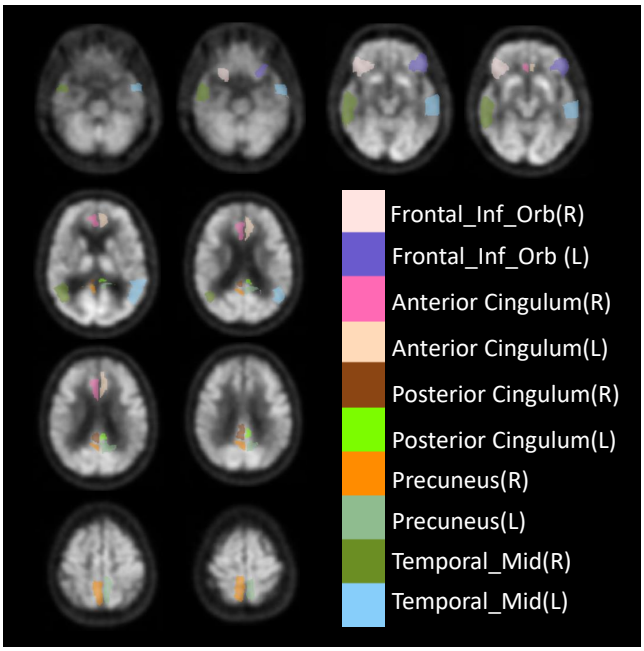

Figure 5.2 Regions of interest in AD diagnosis by using PET image.

Afterwards, AAL is used for labelling each region on the brain atlas. This labelling technique provides 116 cortical and subcortical labels, which are accurate and are perfectly compatible with the MNI152 atlas (Tzourio-Mazoyer et al., 2002). Registration with AAL enables to segment the whole brain structure and choose the ROIs. In order to perform voxel-wise analysis, all images were registered to the uniform size of the MNI template. Therefore, after PET and MRI registration, the resulting images were registered once more with MNI152 atlas (2 mm). Thus, we obtained all images with $91 \times 109 \times 91$ resolution, with 2mm isotropic voxel size. FDG-PET images in dementia show some regions presenting patterns of abnormality due to atrophy caused by the disease, namely in each brain hemisphere : 1) Anterior cingulum (right and left), 2) Posterior cingulum (right and left), 3) Inferior frontal gyrus/orbitofrontal (right and left), 4) Precuneus (right and left), 5) Lateral temporal (right and left). These patterns appear in multiple neurological disorders, including Alzheimer's disease. The main reason to draw the ROIs is to extract functional data from specific structural areas within the dataset. These ROIs were previously identified in the literature (Alexander and Moeller, 1994), (Markiewicz et al., 2009), (Apostolova and Thompson, 2008) and in the neuroscience field. The ten selected regions were extracted by selecting the specific labels after the AAL registration technique, and regional extraction in the original image volume space (Figure 5.2).

Extraction of ROIs

Regions in the 3D MRI of the brain can be labeled manually by experts, but segmenting and labeling these structures for large cohorts would require an extensive amount of time. Using an anatomical correspondence estimation relating the atlas to the target image space increases the accuracy of the resulting target labeling (Heckemann et al., 2006). The current literature on classification of AD did not use the previously mentioned regions which are more likely to be affected by AD (Lancaster et al., 1997a), (Fischl et al., 2002a). In order to accurately find the ROIs, we propose a method based on the MNI152 and AAL atlases. For the purpose of anatomical segmentation to extract the ROIs, we used registration by AAL (2 mm). From the 116 regions of the brain identified using our registration technique, five regions in each hemisphere were studied for the accumulation of glucose in each area.

Creating the masks based on ROIs was the next step in our pipeline before applying it on the processed images. Each voxel from the labelled ROIs obtained from segmentation were used in this process. In this step, we had 10 different patterns which had a labeled ROI. To create a single mask including all ROIs, we combined the 10 separate masks together. The mask represented a single pattern of all regions which had more probability of being affected by AD and specifically had less accumulation of glucose. After applying the mask, we then replaced the mask ROIs labels by the voxel values from the raw data for each subject. Following that, the data and images were ready for feature extraction.

5.3.4 Feature Selection

Preprocessed subject images each had 902629 voxels with corresponding intensity values. The training of the classifiers requires a reduced amount of labelled voxels for a cost-effective approach. Therefore, after replacing the ROI labels, we excluded the zero-valued voxels from the matrix. From the remaining values, assuming that the number of voxels differed for each region k_i, each subject dataset S, which included 10 ROIs, can be defined as follows :

$$S = \{k_1, k_2, k_3, ..., k_{10}\} \tag{5.1}$$

As we had 660 subjects and needed to have a vector of voxels for each subject, we reshaped the 3D matrix for all subjects, ROI's and voxels/per ROI, to a single feature vector. However, $\sum_{i=1}^{10} k_i$ for subject S_1 would be different from S_2 and other subjects. To solve this, we counted the maximum number of voxels among all subjects for each ROI. Based on the maximum

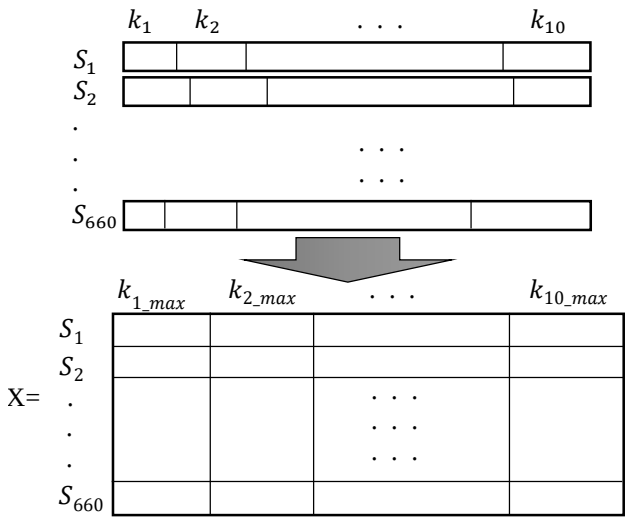

Figure 5.3 Creating matrix X from the reduced dimension dataset.

identified values, we calculated the maximum length of the overall vector such that :

$$\sum_{i=1}^{10}\sum_{j=1}^{N} max(k_{ij}), N = 660 \tag{5.2}$$

$$X = \{S_1 = \{k_1, k_2, k_3, ...,k_{10}\}, ..., S_{660} = \{k_1, k_2, k_3, ..., k_{10}\}\} \tag{5.3}$$

Each subject ROI which didn't reach the maximum value were zero-padded. Using this approach, we created the matrix X with vector of the subjects as rows and a maximum number of valued voxels (k_{max}) as columns(Figure 5.3).

In the proposed multi-region approach, we used matrix X which had a dimensionality of 22229×660 in order to train the classifiers. Whereas in the whole-brain approach, the size of the feature matrix was 902629×660. The objective was to learn the features from the VI in order to discriminate classes. The main difference between the two approaches was the total number of voxels used.

5.3.5 Classification

Once the voxel intensity extraction and feature selection steps were performed, the feature vector containing mean-centered voxel intensities was created for each of the 10 ROIs and

assembled for all cases. Supervised classification was performed using four different two-class methods, which included : a linear SVM, an RBF kernel SVM, a principal component analysis (PCA) model which reduced the feature space dimensionality, as well as a Random Forests classifier. Hyper-parameters of the RBF kernel were obtained using an exhaustive search grid (described in Section III), where the parameters were selected based on the maximum in-sample validation accuracy which outperformed polynomial kernels. The tuned hyper-parameters were then used to predict the out-of-sample accuracy values on the test set.

5.4 Results and Discussion

5.4.1 Parameter selection

We first present the methodology to determine the parameter settings of the classifiers. In order to train the RBF-SVM classifiers, two hyper parameters need to be determined : the penalty parameter C and the kernel width γ. Considering the number of features and data for training and testing, a properly tuned RBF kernel was shown in preliminary testing to be superior in terms of accuracy to linear kernels, even though they are simpler to use (Keerthi and Lin, 2003).

Cross-validation was used for tuning the RBF kernel. To evaluate the performance of different classification methods, and to find the best hyperparameters for SVM classifiers, we used a 10-fold cross-validation strategy in each iteration. To do so, we performed 1000 iterations using 10 randomly selected subjects each time. The range of values for C and γ were analyzed with a coarse search grid, followed by a refined search to find the optimal hyper-parameters. The maximum in-sample validation accuracy were found at $C_{opt} = 1$ and $\gamma_{opt} = 0.1$. The tuned hyperparameters were then used to predict the out-of-sample accuracy values on the test set. As for the PCA approach, principal components were calculated such that 95% of the group variance was retained. Finally, the number of trees grown in each forest (t) and the number of features (f) randomly selected at each tree node had to be determined. Based on out-of-bag classification errors to measure stability of training, we found that $t = 60$ and that $f = \sqrt{D}$ for all the experiments, where D is the initial dimensionality of the vectors, based on the findings of Liaw and Wiener (2002).

5.4.2 Results

We begin by presenting the results of the multi-region approach, followed by the whole-brain approach, both using FDG-PET images. This is followed by a more detailed analysis of the

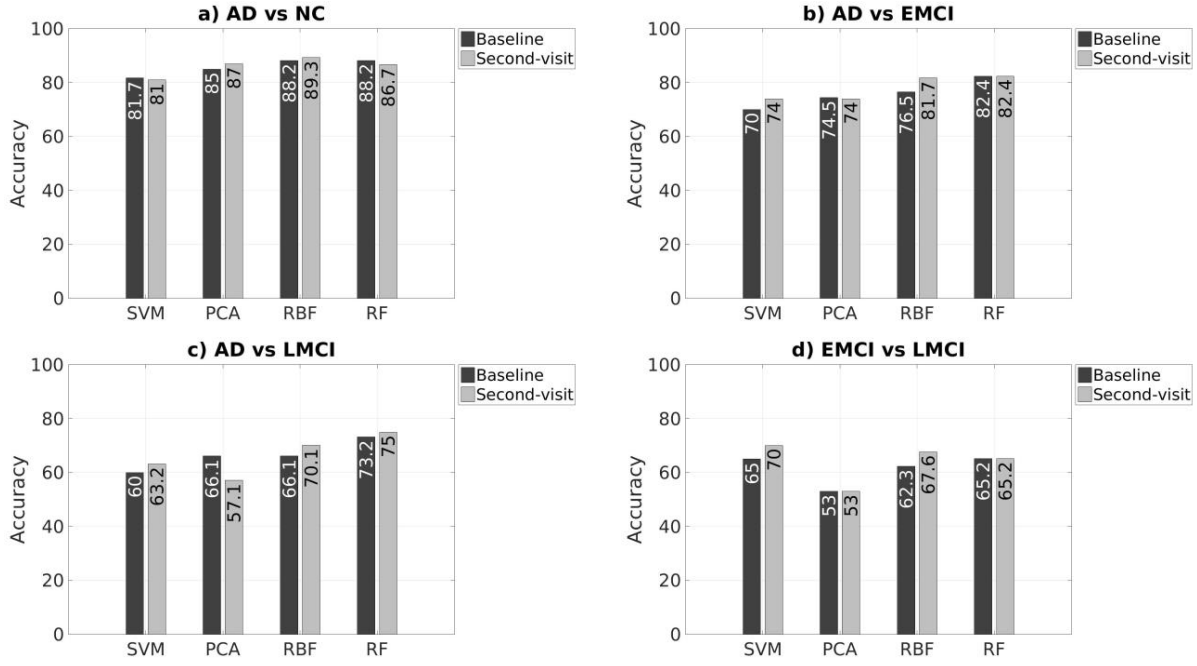

Figure 5.4 Classification accuracies using the multi-region approach for the four clinical group pairs based on the proposed classifiers (SVM, PCA, RBF, RF), using both baseline and longitudinal data.

longitudinal classification experiments, with the combination of two time points (baseline and 12-months). Finally, we present the comparative results between FDG-PET and AV45-PET.

In this work, we report the results of classification between six different paired classes of cognitive states using four classifiers in two approaches (multi-region and whole-brain). The results of four paired classes (AD vs NC, AD vs EMCI, AD vs LMCI, EMCI vs LMCI) of cognitive states are presented in 5.4 and Figure 5.5. Considering the whole set of classifications we produced, the tables with all accuracies and additional results are presented in the appendix.

Multi-region classification

We first used the proposed method to segment and classify the baseline based on regional signal intensities (ROIs). As showed in the boxplots in Figure 5.4 (a) and (b), RF and RBF-SVM demonstrated higher accuracies (over 80%). In Figure 5.4 (c) and (d), although values were globally lower, these classifiers still had the highest accuracies (over 65%), with the exception of the SVM classifier which has 70 % accuracy in the second visit (Figure 5.4(d)).

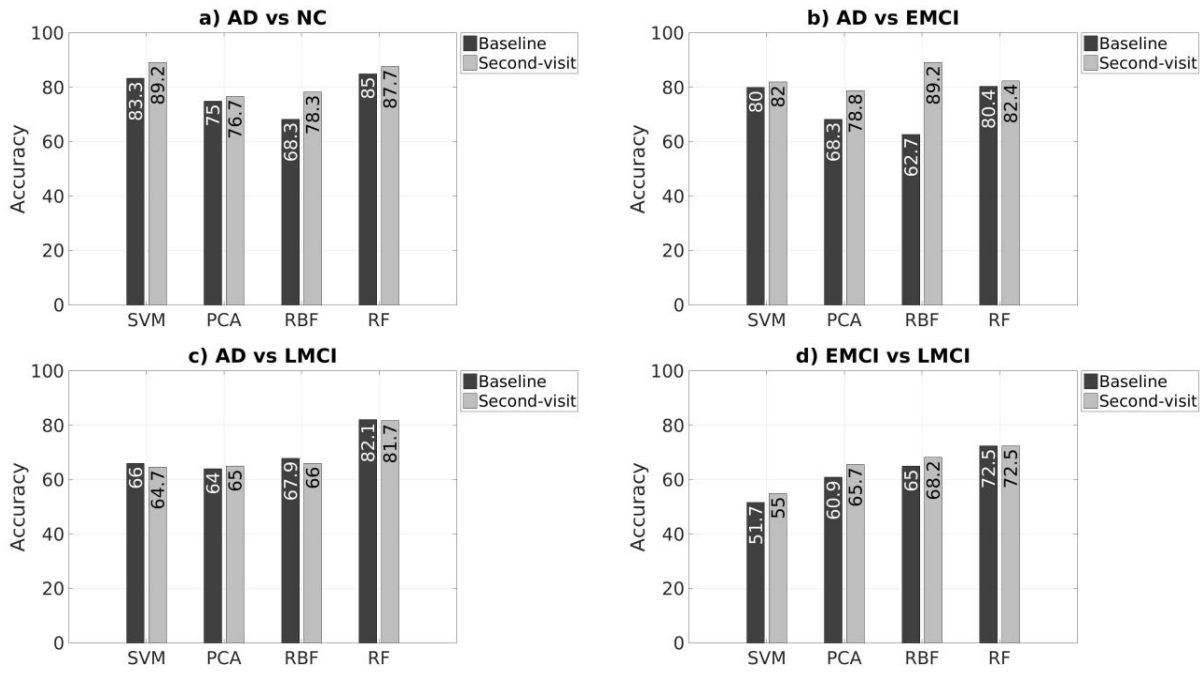

Figure 5.5 Classification accuracies using the whole-brain approach for the four clinical group pairs based on the proposed classifiers (SVM, PCA, RBF, RF), using both baseline and longitudinal data.

Whole-brain classification

In comparison to the region-based approach, the whole-brain technique does not perform as well for AD vs NC, and for AD vs EMCI as showed in Figure 5.5 (a) and (b). On the other hand, the RF classifier for the whole-brain approach demonstrated the highest accuracies for AD vs LMCI and EMCI vs LMCI (81.7% and 72.5% respectively) compared to the other classifiers which were between 55% and 68.2%. These results also outperform the region-based approach using the baseline scan for these last two pairs.

Combination of longitudinal data

The classification results using the combination of two time points in the multi-region approach were obtained by combining the second visit data to the baseline data. Based on the literature and the previous mentioned results, we applied RBF-SVM and RF on the combined data. The highest classification accuracy was obtained for AD vs NC based on FDG-PET images using RBF-SVM (91.7 %) and RF (91.2 %) methods. These results are shown in Table 5.2 and are higher than baseline and second visit results taken individually (Figure 5.4).

Figure 5.6 (a) shows the Receiver Operating Characteristic (ROC) curves, for the results based on Table 5.2. Classification accuracies of AD vs NC for FDG-PET in RBF-SVM and RF were similar but still significantly different based on student-t tests (P=0.01).

Table 5.2 Comparison in classification accuracy between FDG-PET and AV45-PET using combination of baseline and second visit time points for all diagnostic pairs.

	FDG-PET Results			AV45-PET Results		
	RBF-SVM	Random Forest	P-value	RBF-SVM	Random Forest	P-value
AD vs NC	91.7%	91.2%	0.010	90.8%	87.9%	0.024
AD vs EMCI	85.7%	85.7%	0.015	80.0%	88.0%	0.024
AD vs LMCI	87.5%	79.2%	0.016	88.9%	81.5%	0.027
EMCI vs NC	63.3%	56.7%	n.a.	57.7%	59.7%	n.a.
LMCI vs NC	63.5%	65.4%	n.a.	61.2%	55.7%	n.a.
EMCI vs LMCI	53.9%	64.1%	n.a.	52.2%	56.5%	n.a.

AV45-PET vs. FDG-PET

Finally, we compared the diagnostic accuracy between AV45-PET and FDG-PET images. Table 5.2 presents the results of the multi-region approach using combined data for AV45-PET images (right columns) compared to the results of FDG-PET images (left columns). These results demonstrate the high accuracy of RBF-SVM and RF classifiers for AD vs NC (90.8% vs 87.9%), AD vs EMCI (80.0% vs 88.0%) and AD vs LMCI (88.9% vs 81.5%). As for previously mentioned for the FDG-PET results, higher accuracies were achieved when using the combination of the two time points compared to individual time point results.
Figure 5.6 (b) illustrates the ROC curves for the classification results based on 5.2. Classification accuracies of AD vs NC for AV45-PET in RBF-SVM and RF were similar but still significantly different (P=0.02).

5.4.3 Discussion

To the best of our knowledge, this is one of the first studies to propose a PET classification method for stage identification in AD, comparing learned features from both AV45-PET and FDG-PET images, while using a multi-regional approach. The objective was to assess how a feature-learning approach focused on pre-defined sub-cortical regions with known decline in uptake for AD patients can help achieve better accuracy and minimize the errors of an automated classification of different stages of Alzheimer's, especially in the early stages of the disease. The classification results in this work are comparable and, in some cases, better than the performances reported in the literature (Gray et al., 2012), (Zhang et al., 2011a).

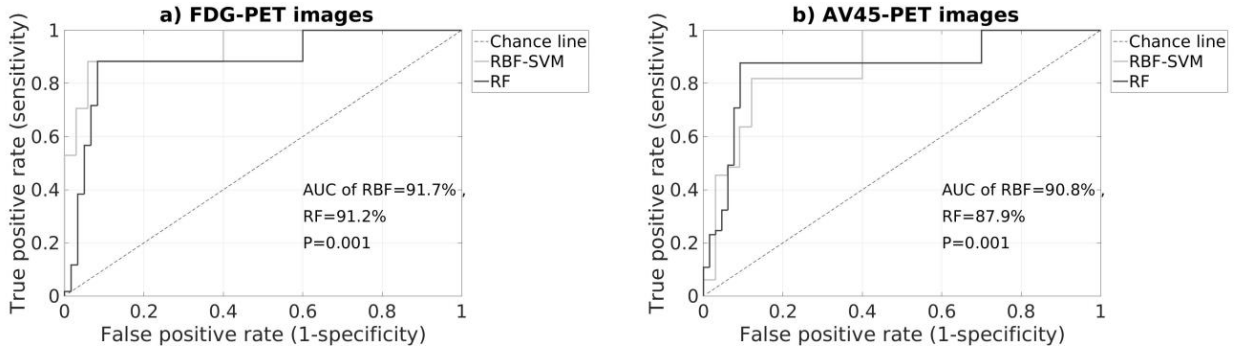

Figure 5.6 Receiver Operating Characteristic (ROC ; sensitivity vs specificity) curves for classification between AD vs NC using longitudinal data for (a) FDG-PET images and (b) AV45-PET images (b).

Generally, classification accuracy between AD and NC is a common banchmark to compare different methodology performances. Classification between the different stages of MCI, namely EMCI and LMCI, is a more challenging issue in this field. In fact, most publications discriminate the MCI and AD, with fewer attempts on EMCI or LMCI (Cabral and Silveira, 2013), (Zhang et al., 2011a), (Rodrigues and Silveira, 2014). Considering the importance of having the results of early and late stages of MCI versus NC, we conducted additional experiments to demonstrate that the models can indeed discriminate between early and late stages of MCI.

We demonstrated that AV45-PET images as well as FDG-PET images offer relevant information to yield classification results, which are comparable to models using imaging and non-imaging data (Zhang et al., 2011a), (Hinrichs et al., 2009). Results were slightly better with FDG-PET due to increased spatial resolution in the image, which helps to delineate the localized structures affected by AD.

Regarding the atlas registration step, it was crucial to choose an atlas offering all segments of the brain anatomy which would be included in our predefined ROIs. To achieve this purpose, we explored a number of different atlases such as the Harvard-oxford cortical and subcortical structural atlas (Gorgolewski et al., 2016), the Talairach atlas (Lancaster et al., 2000) (Lancaster et al., 1997b), the MNI152 structural atlas (Collins et al., 1998) and the automated anatomical labelling (AAL) atlas (Tzourio-Mazoyer et al., 2002). Among all four atlases, only MNI152 includes all 10 ROIs of interest which are labelled by AAL, which segments the brain image into 116 cortical and subcortical regions. Therefore, the MNI152 atlas combined with AAL was selected for the purposes of our pipeline.

The results obtained in this study using the ADNI-PET images were similar to previous works (Gray et al., 2012), (Aidos et al., 2014a), which also used VI as features. This confirms the high diagnostic power of uptake values in discriminating between different cognitive stages, particularly by integrating a progression component using time series features to the analysis.

To achieve these results, multi-modal registration played another key role to properly align both PET and MRI. The FLIRT tool is able to register intra and inter-modal brain images without extracting or segmenting the whole volume of the brain, which is convenient for processing large cohorts of patients with the proposed pipeline, by using automated registration for all subjects. Table 5.1 displays the MMSE for both groups of AD and NC for the two time points. It confirms a significant progression of the disease from baseline to second visit exam as observed in the results of the two approaches.

Results using PCA-SVM sees little changes in most diagnostic pairs between baseline and second visit, compared to RBF-SVM or RF classifiers. This indicates that the additional PET features provided in the longitudinal scans are non-linear features better detected by kernel- or learning-based methods. From these results, we can also interpret that combining second visit data provides additional information to discriminate between the classes compared to the baseline data. Finally, when comparing both the ROIs and whole-brain approaches, results at each time point individually were better with the ROIs method, except when using the linear SVM classifier. The combination between cross-sectional and longitudinal information achieved very good accuracy for AD compared with other classes but as presented in Table 5.2 for EMCI vs NC, LMCI vs NC and EMCI vs LMCI, it is not as adequate as with longitudinal data alone.

5.5 Conclusion

In this work, we compared both whole-brain and multi-region approaches to identify stages of AD using FDG-PET and AV45-PET. We observed that the classification accuracy of AD vs NC was improved using longitudinal images, as well as to other pairs of cognitive classes. Either FDG-PET or AV45-PET enabled to discriminate early and late MCI from AD, as well as to NC. The methodologies used in this work can contribute to improving the classification accuracy between different stages of AD by using the combination of two time points. Our results confirm that we can rely on PET images only, without the addition of other biomarkers to achieve high accuracy classification. Results were shown to be favorable or better compared to previous studies, especially for the more challenging classification problems such as NC vs. EMCI, AD vs. LMCI or EMCI vs. LMCI. Future work will involve

combining additional biomarkers such as cortical thickness data, volume, voxel-wise tissue probability and density of gray matter, in comparison with deep classifiers and other state-of-the-art AD classification approaches. In the context of Alzheimer's disease, the method can improve for the early detection of the disease with promising classification rates based on ground-truth knowledge.

Acknowledgment

Data collection and sharing for this project was funded by the Alzheimer's Disease Neuroimaging Initiative (ADNI) (National Institutes of Health Grant U01 AG024904) and DOD ADNI (Department of Defense award number W81XWH -12 -2 -0012). ADNI is funded by the National Institute on Aging, the National Institute of Biomedical Imaging and Bioengineering, and through generous contributions from the following : AbbVie, Alzheimer's Association ; Alzheimer's Drug Discovery Foundation ; Araclon Biotech ; BioClinica, Inc. ; Biogen ; Bristol -Myers Squibb Company ; CereSpir, Inc. ; Cogstate ; Eisai Inc. ; Elan Pharmaceuticals, Inc. ; Eli Lilly and Company ; EuroImmun ; F. Hoffmann -La Roche Ltd and its affiliated company Genentech, Inc. ; Fujirebio ; GE Healthcare ; IXICO Ltd. ; Janssen Alzheimer Immunotherapy Research & Development, LLC. ; Johnson & Johnson Pharmaceutical Research & Development LLC. ; Lumosity ; Lundbeck ; Merck & Co., Inc. ; Meso Scale Diagnostics, LLC. ; NeuroRx Research ; Neurotrack Technologies ; Novartis Pharmaceuticals Corporation ; Pfizer Inc. ; Piramal Imaging ; Servier ; Takeda Pharmaceutical Company ; and Transition Therapeutics. The Canadian Institutes of Health Research is providing funds to support ADNI clinical sites in Canada. Private sector contributions are facilitated by the Foundation for the National Institutes of Health (www.fnih.org). The grantee organization is the Northern California Institute for Research and Education, and the study is coordinated by the Alzheimer's Therapeutic Research Institute at the University of Southern California. ADNI data are disseminated by the Laboratory for Neuro Imaging at the University of Southern California.

CHAPTER 6 ADDITIONAL RESULTS

This chapter presents additional results on our experiments, which were achieved and were not presented in our submitted paper. Additional results include cross validation results of registration methods, different resolutions of our subject images, classification results of individual ROIs, effects of calculating mean VI for each ROI on final accuracy, and trial classification on PET images without registration by MRI.

6.1 Cross validation results of registration

Inter-modality registration was a crucial step of our pipeline. Therefore, choosing a registration tool for this step has been particularly important. As mentioned in Chapter 4, FLIRT was the tool used for this step. This tool is validated by the authors and is published (Jenkinson and Smith, 2001), (Jenkinson et al., 2002). However, the results of registration between PET and MRI, using the SPM tool and FSL tool (FLIRT) were compared to the measured errors. To compare the errors, we used the same method that Kiebel et al. (1997) applied on AIR and SPM tools. The cross validation was executed on six subjects with FDG-PET and MRI from the ADNI database, including three AD and three NC images. Registration between PET and MRI using two tools (SPM and FLIRT) in four different configurations of cost function and mode is presented in Table 6.1 . Each iteration obtained a registration transformation matrix (RTM) ; in total, we had 24 RTMs for each tool. Figure 6.1 shows an example of the resulting registration between PET and MRI using FLIRT, and Figure 6.2 shows an example using SPM12. There is no common gold standard for registration between PET and MRI. Thus, to compare with the gold standard, we used the same method as similar works, using PET simulated based on corresponding MRI (Kiebel et al., 1997), (Grova et al., 2001).

The simulated PET images were generated by the method proposed by Kiebel et al. (1997). The sequences of this method are scalp editing and segmenting the MRI images into GM, WM, and CSF, which is done using the Seg3D tool version 1.10.0 (1993-2008 Scientific Computing and Imaging Institute, University of Utah). After that, we modified the GM, WM, and CSF intensities. Next, a rigid body or affine transformation and resampling to the PET voxel size was applied, and RTM was saved for further comparisons. At the end, 8 mm FWHM Gaussian filter was used to make the image smooth and to remove the noise. The only difference between our repeating the Kiebel method was doing 16 iterations for each image. For more details on the method, refer to the work by Kiebel et al. (1997). To choose

the best configuration (method and cost function) we compared the error of transformation matrices for 4 configurations in 16 iterations on 6 different subjects. The results are 96×4 matrices. For each subject we have 4 configurations which obtained 24 registration transformation matrices to compare the minimum landmark error. Table below present the min error of differentiation between the registration results and gold standard for each configuration. We obtained the same trend of the results for different iterations.

Table 6.1 Configuration of cost function and model of registration

Iteration	Cost function	model of registration	Results
1	mutual information	affine (12 parameters)	-0.89 0.05 0.03 167.72 -0.04 -0.85 -0.26 229.43 0.01 -0.19 0.87 -22.22
2	correlation ratio	rigid body (6 parameters)	0.84 -0.01 0.02 0.85 -0.03 -0.10
3	mutual information	rigid body (6 parameters)	0.96 -0.03 0.02 0.87 -0.04 -0.19
4	correlation ratio	affine (12 parameters)	0.85 -0.03 0.02 -0.52 0.02 0.79 0.23 -24.58 -0.03 -0.17 0.83 -25.92

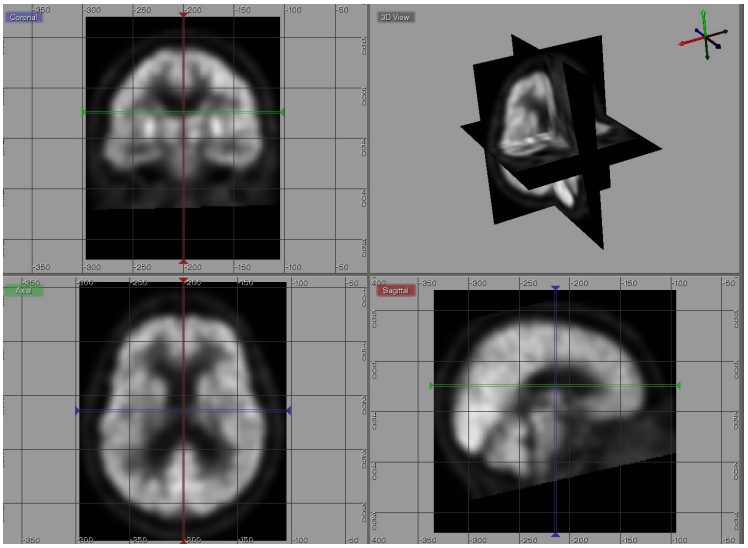

Figure 6.1 Example of result registration between PET and MRI using FLIRT.

To achieve the total error of registration, we compared nine members of RTM (translation, rotation, and scaling) to the transformation matrix, which was obtained by simulated PET.

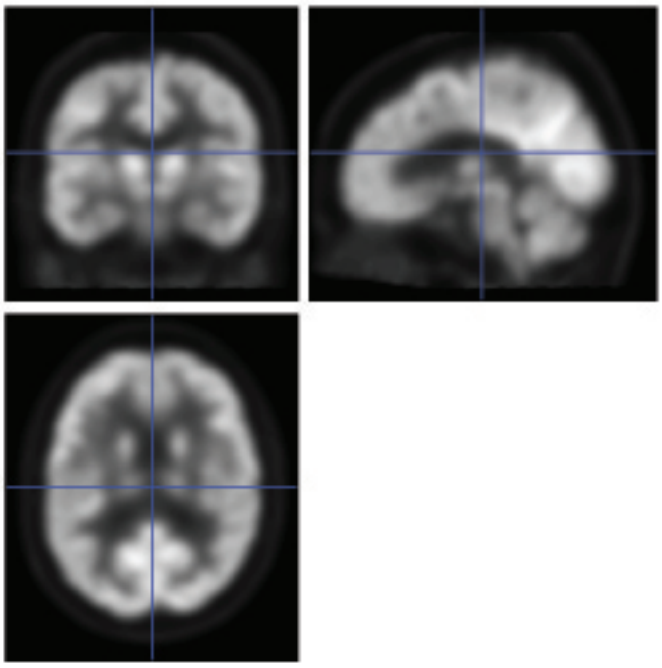

Figure 6.2 Example of result registration between PET and MRI using SPM12.

First, we chose the best configuration of registration, which gave a smaller error of transformation. Registration with affine with the correlation ratio cost function was chosen in both tools.

Table 6.2 Comparison registration error (SPM and FLIRT)

tool	Mean error of SPM			Mean error of FLIRT		
Registration	1.15	0.05	-0.06	0.98	0.04	-0.02
Transformation	-0.06	1.13	-0.26	-0.05	0.95	-0.25
Matrices	0.05	0.27	1.18	0.01	0.26	0.94

We then evaluated the results between registration tools (SPM and FLIRT). Table 6.2 illustrates the errors of registration. Finally, based on these results, we chose the FSL tool for our pipeline.

6.2 Classification Results

6.2.1 PET Images (1 mm)

We designed our pipeline independent of the resolution of images. We downloaded all images from ADNI in two resolutions (1 mm and 2 mm) for PET and MRI images. After obtaining

Table 6.3 Classification accuracy of FDG-PET images with 1 mm resolution using four classifiers.

	AD vs. NC		AD vs. EMCI		AD vs. LMCI		
Approache	I	II	I	II	I	II	
Linear-SVM	75.05	**83.33**	66.67	80.05	65.10	60.09	†/ † /†
PCA-SVM	66.67	75.12	61.67	61.67	53.33	61.01	†/ † /†
RBF-SVM	78.33	76.66	70.19	75.01	66.07	65.67	n.a.
RF	**86.35**	82.33	**82.36**	**80.39**	**73.21**	**68.33**	†/ † /†
	EMCI vs. NC		LMCI vs. NC		EMCI vs. LMCI		
Approache	I	II	I	II	I	II	
Linear-SVM	63.33	60.56	58.33	56.67	65.02	50.62	†/ † /†
PCA-SVM	55.01	64.52	50.25	51.67	65.02	53.52	†/ † /†
RBF-SVM	61.64	**65.01**	62.56	63.33	53.62	51.67	n.a.
RF	**66.67**	63.10	**65.22**	**65.38**	**65.22**	**72.46**	†/ † /†

our results, the results of the 2-mm images had higher accuracy. Nevertheless, the results of images with 1-mm resolution had acceptable accuracy in some classes. Table 6.3 details the summary of all results of 1-mm images. In this Table, † stands for $p<0.001$, approach I is multi-region and approach II represent whole brian method.

6.2.2 Individual Region of Interest

In this section, we display the classification results of linear SVM for 1-mm FDG-PET to test the effects of each ROI individually. We should mention that the results in Table 6.4 are not significant and only compare the effects of each region. The best result with 68% accuracy was for the lateral temporal lobe between AD and NC. Most of the regions obtained close to chance, indicating they are not reliable to classify the subjects individually

Table 6.4 Classification accuracy of each region of interest by linear SVM individually on FDG-PET image.

	AD vs. NC	AD vs. EMCI	AD vs. LMCI	EMCI vs. NC	LMCI vs. NC	EMCI vs. LMCI
Cingulum_Ant	63.27	**62.00**	45.71	52.64	50.98	**52.27**
Cingulum_Post	59.18	52.00	48.57	45.14	57.00	51.19
Frontal_Mid_Orb	53.06	53.37	51.67	55.56	55.10	49.52
Precuneus	63.33	48.33	50.00	**56.15**	51.28	42.00
Temporal_Mid	**68.00**	50.98	**56.00**	52.00	**59.42**	46.00

6.2.3 Mean Voxel Intensity

To test the other features studied in literature, the mean VI was tested for three classifiers (linear SVM, RBF-SVM, and RF). Table 6.5 presents the classification results of 2-mm FDG-PET images. These results were obtained using only the multi-region approach, and the mean VI were calculated by each region. As it shows, RF yielded the best accuracy ; however, RBF-SVM also was close to high accuracy.

Table 6.5 Classification accuracy of mean voxel intensity for the multi-region approach on FDG-PET images.

	AD vs. NC	AD vs. EMCI	AD vs. LMCI	EMCI vs. NC	LMCI vs. NC	EMCI vs. LMCI
Linear SVM	55.00	60.00	60.00	48.33	58.33	51.67
RBF-SVM	68.33	62.74	**66.07**	52.05	51.28	56.52
RF	**75.00**	**72.55**	60.71	**58.90**	**58.97**	**60.87**

6.2.4 PET Images without Registration by MRI

Registration between PET and MRI had a very important role in obtaining high accuracy because of helping to segment different brain anatomies precisely. To understand the importance of the MRI role, we executed the same pipeline on 2-mm PET images without registering to MRI. The results were relevant but not comparable with the MRI registered pipeline. The results classified by linear SVM are shown in Table 6.6

Table 6.6 Classification accuracy of non MRI registration using Linear SVM.

	AD vs. NC	AD vs. EMCI	AD vs. LMCI	EMCI vs. NC	LMCI vs. NC	EMCI vs. LMCI
Linear SVM	80.00	75.00	63.33	56.67	53.33	53.33

The average accuracy of all classes was 63.61%, which was lower than the average of 65.83% when we used MRI images to recognize the brain anatomies in the multi-region approach.

CHAPTER 7 GENERAL DISCUSSION

7.1 Evaluation of the Result Using ADNI Images

The results obtained in this study using the ADNI-PET images were similar to previous work (Gray et al., 2012), (Aidos et al., 2014a). We demonstrated that AV45-PET images as well as FDG-PET images had relevant information to obtain classification results that are comparable to the imaging and non-imaging classification of data. This important result was achieved using the ADNI database, which has been used in previous studies (Zhang et al., 2011a), (Hinrichs et al., 2009), and our results are close and in some cases better than the state-of-the-art technology. Based on our literature, there is no proposed method of classification for both AV45-PET and FDG-PET images with the same method that has yielded comparable results. In addition, the result of the combination of two time points demonstrated better performance in line with our state-of-the-art method.

The additional results of our experiments that were presented in Chapter 6 are much more than what we displayed in our submitted paper. As shown, two different resolutions were examined in all steps of our pipeline, which means our subjects were downloaded in 1-mm and 2-mm resolutions from the ADNI database. The PET and MRI images in 1 mm, despite including more voxels (7221032 voxels), did not obtain results better than the 2-mm images. It could be due to our method in the registration and segmentation that made the images uniform, specifically for atlas registration to have all images comparable in the atlas space.

Interpretation of our results was done using the diagnostic list of the ADNI database. Overall, 660 subjects had definitive diagnoses, including the MMSE score for each subject. We considered the conversion for all sample sets ; no conversion was reported among our data sample. Comparing the disease progression to the longitudinal MMSE score made us sure about the overall results of the classification accuracy. Higher accuracy in the second visit, especially for distinguishing between AD and NC, was completely logical because brain changes, such as atrophy and neuron loss, in patients with AD after approximately 12 months made a clear difference in the NC subjects, whereas these brain changes for discriminating between EMCI and LMCI were more intense than the baseline. However, the overall results of the combination of two time points were better than the single time point.

7.2 Effect of Data Processing on the Results

Data processing in our pipeline included registration and segmentation, which, based on our experiments, were crucial steps for obtaining higher accuracies. To choose the best scenario for obtaining the best results, we applied another version of our pipeline for PET images without MRI registration, and the results were not more accurate than when we registered PET images with the corresponding MRI (results presented in Chapter 6). Moreover, for the feature extraction step, we used the mean VI in each ROI individually, and it gave us a very simple matrix of 660×10, which was not a good representation of each class to train the classifiers. Finding the most relevant ROIs was a very effective step in the classification results. There are some studies that tested different brain regions to discover whether we can rely on those ROIs for classifying the PET images (Gray et al., 2012), (Carbonell et al., 2015). In this work, we selected our ROIs based on our literature and after testing, which gave us comparable results. In a comprehensive workshop of PET, which was held in McGill University (2016), we confirmed these ROIs for AV45-PET and FDG-PET by personal communication with Dr. Peter Herscovitch, chief of the PET Department at the NIH Clinical Center. As presented in Chapter 6, the individual effects of each region were not satisfactory. However, there were some regions that had more effects on the results. Therefore, after some testing, we decided to create a whole-brain mask including all ROIs.

We demonstrated the results of cross validation between the two tools of registration in Chapter 6. To achieve the more accurate results, multi-modal registration played a key role to properly align both the PET and MRI. The FLIRT tool can register intra- and inter-modal brain images without extracting or segmenting the whole volume of the brain, which is convenient for processing large cohorts of patients with the proposed pipeline using automated registration for all subjects.

In the atlas registration step, we were looking for an atlas with segments of brain images, which was included in our predefined ROIs. To achieve this purpose, we explored different available atlases, such as the Harvard-Oxford cortical and subcortical structural atlases, the Talairach atlas, the MNI152 structural atlas, and the automated anatomical labelling atlas. Among all four atlases, only the MNI152 atlas includes all 10 ROIs, which are labelled by the AAL atlas that segments the brain image into 116 cortical and subcortical regions. Therefore, the MNI152 atlas combined with AAL was selected for the purposes of our pipeline.

7.3 Comparison of Existing Classification Methods

Classification between AD and NC is relatively simple, while EMCI vs LMCI is the most difficult and has received relatively little attention in the previous studies. In fact, most publications discriminate the MCI and AD, with fewer attempts on EMCI or LMCI (Cabral and Silveira, 2013), (Zhang et al., 2011a), (Zhang et al., 2011b), (Rodrigues and Silveira, 2014). However, to obtain more relevant results, we conducted additional experiments to demonstrate that the models can indeed discriminate between early and late stages of MCI applied by four classifiers.

As we mentioned in our literature, different classification methods, primarily in the domain of AD using PET images used VI as a feature. There are several techniques to use VI ; some publications (like our proposed method) directly used the value of VI compared to other subjects' voxels (Habeck et al., 2008), (Zhang et al., 2011a). Previous studies showed, despite the passage of time and the improvement of imaging techniques, not only have the effects of using VI in classification not decreased, but VI has become one of the main features of PET images (Gray et al., 2013), (Aidos et al., 2014a), (Román and Pascual, 2012). This confirms the high diagnostic power of uptake values in discriminating between different cognitive stages, particularly by integrating a progression component using time series features to the analysis.

It is prevalent to apply more than one classifier, such as different kernels of SVMs or RF in many studies, regardless of using different material (PET or MRI images) (Cabral and Silveira, 2013), (Dolph et al., 2014), (Tong et al., 2017), whereas some studies were satisfied using only one, like SVM (Gray et al., 2012), (Liu et al., 2016). This is despite the fact that we used two classifiers in four methods (linear SVM, PCA-SVM, RBF-SVM, and RF), and they were tuned up by 10-fold cross validation.

We used PCA to reduce the dimension of our matrix for two approaches. In the first approach (multi-region approach), we selected 10 ROIs ; consequently, we had less voxels for each subject. To give an example, after excluding the non-ROIs voxels using our method, which is explained in Chapter 6, the matrix dimension is 660×179625. However, in the whole-brain approach, despite using a large volume of memory, the matrix has dimensions of 660×7221032, which are not suitable to train the classifiers. To solve this problem, we used PCA to reduce the dimensions. With different iterations, we found the optimum number of PCs, which was about the first 20 PCs. Then, we trained the linear SVM by the matrix of PCA reduced (660×20, 20 PCs for each subject). Except for some occasional cases, our results of PCA-SVM were not higher than other classifiers. We should mention that PCA-SVM was tested for the multi-region approach too, and its results are displayed in Chapter 5.

Our work proposed the pipeline for processing images, extracting the features and classifying the subjects based on FDG-PET images. In addition, our pipeline applied to AV45-PET images as well, which obtained comparable accuracy without changing on our methodology. In contrast, the work of Carbonell et al. (2015) used amyloid-PET images and more statistical information (MMSE, ADAS-Cog, CSF, gender, clinical classification and APOE genotype). The purpose of the classification approach in our work was discriminating between 6 different cognitive pair classes, whereas, the work of Carbonell et al. (2015) compared 2 pair classes, concentrating on high versus low level of amyloid. Carbonell and colleagues used the mean standard uptake value ratio (SUVr) as a feature. The authors tested different cut off values on mean SUVr for each region and composite of regions to find the optimal threshold. Nevertheless, in our work voxel intensity was used as a direct feature, which enabled us to discriminate between different classes by combining the 10 ROIs together as a target segment of whole image. In addition, our extracted ROIs from PET images based on our pipeline is automated by choosing the interest labels (according to the list of cortical brain structures), segmented regions will be available individual or combined. Regarding the methodology, we compared our work with similar works having used the same method of classification and extracting the features. Despite the fact that the paper of Carbonell et al (2015) reported high accuracy, they are not applying similar classifier (RDA classifier used), and there is no more details of the test and training data. In addition, they used different segmentation in order to extracting CSF and did not use structural segmentation for finding ROI, their target ROIs were instead segmented on whole cortical SUVr. They did not mention the performance metrics (only EMCI vs LMCI and AD vs NC) and how they calculated the accuracy of results. However, we can use RDA classifier in future work as it may give high accuracies.

7.4 Limitations and Future Work

Several limitations exist in this study. First, there are many other biomarkers and data sources that are useful for AD or MCI distinction, such as cortical thickness data, volume, voxel-wise tissue probability, density of GM, CSF, and APOE. As our hypothesis was using only PET images, the current study was limited to two modalities of MRI, PET (FDG and AV45). Second, the proposed method was only designed to compare the results of FDG-PET and AV45-PET, whereas the Pittsburgh compound B PET images have a great deal of information to discriminate between AD and NC (Fu et al., 2014), (Zhang et al., 2014). Third, we used VI as a feature, which was not appropriate for either the whole-brain approach or for 1-mm resolution images. Other feature selection methods, such as taking samples of subregions in each ROI, need further investigation. Fourth, we did not have the chance to use

anatomical segmentation methods in the subject space (in this work, we use atlas space) ; if so, we could achieve more precise regions without deforming the primary images.
Future work will involve covering the limitations as much as possible, mainly combining additional biomarkers in comparison with deep classifiers and other state-of-the-art AD classification approaches. The MRI scan has a cortical and subcortical variety information ; therefore, using multi-modal methods could have an accuracy-increasing benefit. In the context of AD, the method can improve the early detection of the disease with promising classification rates based on ground-truth knowledge.

CHAPTER 8 CONCLUSION AND RECOMMENDATIONS

In this work, we have introduced a new pipeline for classifying different stages of MCI and AD vs NC using PET images. Two common tracers, FDG-PET and AV45-PET, were under investigation and obtained the good results using the same pipeline. Our method included two approaches (multi-region and whole-brain) in two time points (baseline and second visit). Our results showed that we answered our research question. We extracted and selected some features from PET images to classify our subjects accurately. The methods used are valid and common ; however, it enabled us to obtain accurate results.

Because of the large number of voxels in the whole-brain approach, we were not able to combine the data of the two time points to be able to compare the results of the two approaches. Preprocessing the data plays an important role in achieving correct efficient classification. Thus, using more robust tools for co-registration between PET and MRI, such as ANT or SPM12 instead of FLIRT, despite having a large number of subjects and taking more time to register, may give more accurate results. In the same way, for segmentation based on atlas, we recommend using multi-atlas instead of single atlas methods, provided that different atlases include all ROIs.

As stated in some studies, the ANN has shown success in a variety of classification tasks, including PET. Therefore, in future work, we can try to use the ANN classifier to compare with our current results. Having the ability to classify different stages of MCI and differentiate AD vs NC, it seems possible to predict the progression of AD in subjects using longitudinal PET images.

REFERENCES

ADNI, "Alzheimer's Disease Neuroimaging Initiative." 2014. En ligne : http://adni.loni.usc.edu/.

H. Aidos, J. Duarte, et A. Fred, "Identifying regions of interest for discriminating Alzheimer's disease from mild cognitive impairment." *2014 IEEE International Conference on Image Processing, ICIP 2014*, pp. 21–25, 2014. En ligne : http://camoes.lx.it.pt/pia/GroupPapers/Alzheimer/IdentifyingregionsofinterestfordiscriminatingAlzheimer'sdiseasefrommildcognitiveimpairment.pdf

H. Aidos, A. L. N. Fred, H. Aidos, et A. Fred, "Finding Coherent Regions in PET Images for the Diagnosis of Alzheimer's Disease." *Proceedings of the International Conference on Bioimaging*, no. January 2015, pp. 12–18, 2014. En ligne : http://www.scitepress.org/DigitalLibrary/Link.aspx?doi=10.5220/0004802200120018

M. S. Albert, S. T. DeKosky, D. Dickson, B. Dubois, H. H. Feldman, N. C. Fox, A. Gamst, D. M. Holtzman, W. J. Jagust, R. C. Petersen, P. J. Snyder, M. C. Carrillo, B. Thies, et C. H. Phelps, "The diagnosis of mild cognitive impairment due to Alzheimer's disease : Recommendations from the National Institute on Aging-Alzheimer's Association workgroups on diagnostic guidelines for Alzheimer's disease." *Alzheimer's and Dementia*, vol. 7, no. 3, pp. 270–279, 2011. En ligne : http://dx.doi.org/10.1016/j.jalz.2011.03.008

G. E. Alexander et J. R. Moeller, "Application of the scaled subprofile model to functional imaging in neuropsychiatric disorders : A principal component approach to modeling brain function in disease." *Human Brain Mapping*, vol. 2, no. 1-2, pp. 79–94, 1994.

G. E. Alexander, K. Chen, P. Pietrini, S. I. Rapoport, et E. M. Reiman, "Longitudinal PET evaluation of cerebral metabolic decline in dementia : A potential outcome measure in Alzheimer's disease treatment studies", *American Journal of Psychiatry*, vol. 159, no. 5, pp. 738–745, 2002.

A. Alzheimer's Association, "2016 Alzheimer's Disease Facts and Figures,Report." 2016. En ligne : https://www.alz.org/documents_custom/2016\T1\textendashfacts\

T1\textendashand\T1\textendashfigures.pdf

L. G. Apostolova et P. M. Thompson, “Mapping progressive brain structural changes in early Alzheimer’s disease and mild cognitive impairment.” *Neuropsychologia*, vol. 46, no. 6, pp. 1597–1612, 2008.

J. Ashburner, “A fast diffeomorphic image registration algorithm.” *NeuroImage*, vol. 38, no. 1, pp. 95–113, 2007.

J. Ashburner et K. J. Friston, “Nonlinear spatial normalization using basis functions.” *Human Brain Mapping*, vol. 7, no. 4, pp. 254–266, 1999.

——, “Voxel-Based Morphometry—The Methods.” *NeuroImage*, vol. 11, no. 6, pp. 805–821, 2000. En ligne : http://linkinghub.elsevier.com/retrieve/pii/S1053811900905822

J. W. . L. S. Baker, S., “FDG-PET and memory tests best predict Alzheimer’s. Retrieved from aunt minnie.” *auntminnie, On line*, vol. 6, 2010. En ligne : http://www.auntminnie.com/index.aspx?sec=ser&sub=def&pag=dis&ItemID=91172

S. Barrack, *Neuroimaging biomarkers in Alzheimer’s disease.*, 1er éd. iMedPub, 2013.

R. J. Bateman, C. Xiong, T. L. S. Benzinger, A. M. Fagan, A. Goate, N. C. Fox, D. S. Marcus, N. J. Cairns, X. Xie, T. M. Blazey, D. M. Holtzman, A. Santacruz, V. Buckles, A. Oliver, K. Moulder, P. S. Aisen, B. Ghetti, W. E. Klunk, E. McDade, R. N. Martins, C. L. Masters, R. Mayeux, J. M. Ringman, M. N. Rossor, P. R. Schofield, R. A. Sperling, S. Salloway, et J. C. Morris, “Clinical and biomarker changes in dominantly inherited Alzheimer’s disease.” *The New England journal of medicine*, vol. 367, no. 9, pp. 795–804, 2012. En ligne : http://dx.doi.org/10.1056/NEJMoa1202753

C. M. Bauer, “Multimodal analysis in normal aging, mild cognitive impairment, and Alzheimer’s disease : Group differentiation, baseline cognition, and prediction of future cognitive decline.” *Dissertation Abstracts International : Section B : The Sciences and Engineering*, vol. 75, no. 2-B(E), pp. No–Specified, 2014. En ligne : http://gateway.proquest.com/openurl?url_ver=Z39.88-2004&rft_val_fmt=info:ofi/fmt:kev:mtx:dissertation&res_dat=xri:pqm&rft_dat=xri:pqdiss:35753075Cnhttp://ovidsp.ovid.com/ovidweb.cgi?T=JS&PAGE=reference&D=psyc11&NEWS=N&AN=2014-99160-291

O. Ben Ahmed, J. Benois-Pineau, M. Allard, C. Ben Amar, et G. Catheline, “Classification of Alzheimer’s disease subjects from MRI using hippocampal visual features.” *Multimedia Tools and Applications*, vol. 74, no. 4, pp. 1249–1266, 2014.

D. P. Bertsekas et J. N. Tsitsiklis, *Neuro-Dynamic Programming*, 1er éd. Athena Scientific, 1996.

C. M. Bishop, *Pattern Recognition and Machine Learning (Information Science and Statistics)*. New York, : Springer-Verlag, 2006.

brainimaging, "Feature extraction." 2017. En ligne : `http://brainimaging.waisman.wisc.edu/~oakes/teaching/coreg_software_comparison.html`

C. Brayne, "Research and Alzheimer's disease : an epidemiological perspective [editorial]." *Psychol.Med.*, vol. 23, no. 2, pp. 287–296, 1993.

L. Breiman, "Bagging Predictors." *Machine Learning*, vol. 24, no. 421, pp. 123–140, 1996.

——, "Random forests." *Machine Learning*, vol. 45, no. 1, pp. 5–32, 2001.

L. Breiman, J. Friedman, C. J. Stone, et R. Olshen, *Classification and Regression Trees*. Mathematics, 1984.

A. E. Budson et N. W. Kowall, *The Handbook of Alzheimer's Disease and Other Dementias*. Oxford, UK, : Wiley-Blackwell, 2011, ch. 1. Alzheimer's Disease., pp. 1–91.

T. Bylander, "Estimating generalization error on two-class datasets using out-of-bag estimates", *Machine Learning*, vol. 48, no. 1-3, pp. 287–297, 2002.

C. Cabral et M. Silveira, "Classification of Alzheimer's disease from FDG-PET images using favourite class ensembles." *Conference proceedings : Annual International Conference of the IEEE Engineering in Medicine and Biology Society. IEEE Engineering in Medicine and Biology Society. Annual Conference*, vol. 2013, pp. 2477–2480, 2013.

CaliSun, "What is the role of the Somatosensory Association Cortex." 2013. En ligne : `https://www.memrise.com/user/CaliSun/mems/created/page=7`

F. Carbonell, A. P. Zijdenbos, A. Charil, M. Grand'Maison, et B. J. Bedell, "Optimal Target Region for Subject Classification on the Basis of Amyloid PET Images." *Journal of nuclear medicine : official publication, Society of Nuclear Medicine*, vol. 56, no. 9, pp. 1351–8, 2015. En ligne : `http://www.ncbi.nlm.nih.gov/pubmed/26135108`

A. Chaddad, C. Desrosiers, et M. Toews, "LOCAL DISCRIMINATIVE CHARACTERIZATION OF MRI FOR ALZHEIMER ' S DISEASE´", *Isbi*, pp. 1–5, 2016.

J. M. Chalovich et E. Eisenberg, “Apolipoprotein E and Alzheimer disease : risk, mechanisms, and therapy.” *Biophysical Chemistry*, vol. 257, no. 5, pp. 2432–2437, 2005.

P. Chetsadaporn, M. Kolber, P. Ramchandra, M. Moghbel, S. Houshmand, M. Schöll, H. Bai, T. J. Werner, A. Alavi, et C. Buchpiguel, “Multimodality Imaging Approach in Alzheimer disease, Part I : Structural MRI, Functional MRI, Diffusion Tensor Imaging and Magnetization Transfer Imaging.” *Dementia & Neuropsychologia*, vol. 9, no. 4, pp. 318–329, 2015.

N. Chumchob et K. Chen, “A robust affine image registration method.” *International Journal of Numerical Analysis and Modeling*, vol. 6, no. 2, pp. 311–334, 2009.

M. Chupin, A. Hammers, R. Liu, O. Colliot, et al., “Automatic segmentation of the hippocampus and the amygdala driven by hybrid constraints : method and validation.” *Neuroimage*, vol. 46, no. 3, pp. 749–761, 2009.

D. L. Collins, a. P. Zijdenbos, V. Kollokian, J. G. Sled, N. J. Kabani, C. J. Holmes, et a. C. Evans, “Design and construction of a realistic digital brain phantom.” *IEEE transactions on medical imaging*, vol. 17, no. 3, pp. 463–468, 1998.

C. Cortes et V. Vapnik, “Support-Vector Networks.” *Machine Learning*, vol. 20, no. 3, pp. 273–297, 1995.

L. Crews et E. Masliah, “Molecular mechanisms of neurodegeneration in Alzheimer ’ s disease.” *HMG Advance Access*, vol. 19, no. 1, pp. 12–20, 2010.

G. Cybenko, “Approximation by superpositions of a sigmoidal function.” *Mathematics of Control, Signals and Systems*, vol. 2, p. 303–314, 1989.

P. Dayan et L. F. Abbott, “Theoretical Neuroscience : Computational and Mathematical Modeling of Neural Systems.” *MIT press, Computational Neuroscience*, p. 480, 2001.

S. De Santi, M. J. De Leon, H. Rusinek, A. Convit, C. Y. Tarshish, A. Roche, W. H. Tsui, E. Kandil, M. Boppana, K. Daisley, G. J. Wang, D. Schlyer, et J. Fowler, “Hippocampal formation glucose metabolism and volume losses in MCI and AD”, *Neurobiology of Aging*, vol. 22, no. 4, pp. 529–539, 2001.

R. S. Desikan, H. J. Cabral, C. P. Hess, W. P. Dillon, C. M. Glastonbury, M. W. Weiner, N. J. Schmansky, D. N. Greve, D. H. Salat, R. L. Buckner, et al., “Automated MRI measures identify individuals with mild cognitive impairment and Alzheimer’s disease.” *Brain*, p. awp123, 2009.

I. Despotovic, B. Goossens, et W. Philips, “MRI Segmentation of the Human Brain : Challenges , Methods , and Applications.” *Computational and Mathematical Methods in Medicine*, vol. 2015, p. 23.

M. M. Dessouky et T. E. Taha, “Selecting and Extracting Effective Features for Automated Diagnosis of Alzheimer ’ s Disease.” *International Journal of Computer Applications*, vol. 81, no. 4, pp. 17–28, 2013.

T. G. Dietterich, “Experimental comparison of three methods for constructing ensembles of decision trees : bagging, boosting, and randomization.” *Machine Learning*, vol. 40, no. 2, pp. 139–157, 2000. En ligne : `http://en.scientificcommons.org/426370985Cnuuid/7906280C-AEF8-405A-9A94-6BAA1DDAED1E`

C. V. Dolph, M. D. Samad, et K. M. Iftekharuddin, “Classification of Alzheimer’s disease using structural MRI.” *Proc MICCAI workshop challenge on computer-aided diagnosis of dementia based on structural MRI data*, pp. 31–37, 2014.

S. Duchesne, A. Caroli, C. Geroldi, C. Barillot, G. B. Frisoni, et D. L. Collins, “MRI-based automated computer classification of probable AD versus normal controls”, *IEEE Transactions on Medical Imaging*, vol. 27, no. 4, pp. 509–520, 2008.

R. Duda, P. Hart, et D. Stork, “Pattern Classification.” *New York : John Wiley, Section*, p. 680, 2001.

A. S. El-Baz, R. Acharya U, A. F. Laine, et J. S. Suri, *Multi Modality State-of-the-Art Medical Image Segmentation and Registration Methodologies - Volume II.* NewYork, USA, : Springer., 2015.

A. Elnakib, G. Gimel’farb, J. S. Suri, et A. S. El-Baz, *Multi Modality State-of-the-Art Medical Image Segmentation and Registration Methodologies - Volume II.* NewYork, USA, : Springer., 2015, ch. 1. Medical Image Segmentation : A Brief Survey., pp. 1689–1699.

B. Fischl, D. H. Salat, E. Busa, M. Albert, M. Dieterich, C. Haselgrove, A. Van Der Kouwe, R. Killiany, D. Kennedy, S. Klaveness, et al., “Whole brain segmentation : automated labeling of neuroanatomical structures in the human brain.” *Neuron*, vol. 33, no. 3, pp. 341–355, 2002.

B. Fischl, D. H. Salat, E. Busa, M. Albert, M. Dieterich, C. Haselgrove, A. van der Kouwe, R. Killiany, D. Kennedy, S. Klaveness, A. Montillo, N. Makris, B. Rosen, Dale, et M. Anders, “Whole Brain Segmentation : Neurotechnique Automated

Labeling of NeuroanatomicalStructures in the Human Brain." *Neuron*, vol. 33, no. 3, pp. 341–355, 2002. En ligne : http://eutils.ncbi.nlm.nih.gov/entrez/eutils/elink.fcgi?dbfrom=pubmed&id=11832223&retmode=ref&cmd=prlinks5Cnpapers2://publication/uuid/23BE8334-219B-4E46-AE68-C9D02B8AC109

Food and Drug Administration, "Update - New Fludeoxyglucose F 18 Injection PET Drug Approved in Less than 6 Months." 2014. En ligne : http://www.fda.gov/Drugs/DevelopmentApprovalProcess/Manufacturing/ucm182642.htm

N. L. Foster, J. L. Heidebrink, C. M. Clark, W. J. Jagust, S. E. Arnold, N. R. Barbas, C. S. DeCarli, R. Scott Turner, R. A. Koeppe, R. Higdon, et S. Minoshima, "FDG-PET improves accuracy in distinguishing frontotemporal dementia and Alzheimer's disease." *Brain*, vol. 130, no. 10, pp. 2616–2635, 2007.

N. C. Fox, P. A. Freeborough, et M. N. Rossor, "Visualisation and quantification of rates of atrophy in Alzheimer's disease." *Lancet*, vol. 348, no. 9020, pp. 94–97, 1996.

G. B. Frisoni, N. C. Fox, C. R. Jack, P. Scheltens, et P. M. Thompson, "The clinical use of structural MRI in Alzheimer disease." *Nature Reviews Neurol.*, vol. 6, no. 2, pp. 67–77, 2010. En ligne : http://www.nature.com/nrneurol/journal/v6/n2/abs/nrneurol.2009.215.html5Cnhttp://discovery.ucl.ac.uk/144642/5Cnhttp://dx.doi.org/10.1038/nrneurol.2009.215

K. J. Friston, J. Ashburner, C. D. Frith, J.-B. Poline, J. D. Heather, et R. S. J. Frackowiak, "Spatial registration and normalization of images." *Human Brain Mapping*, vol. 3, no. 3, pp. 165–189, 1995. En ligne : http://onlinelibrary.wiley.com/doi/10.1002/hbm.460030303/abstract5Cnhttp://doi.wiley.com/10.1002/hbm.460030303

L. Fu, L. Liu, J. Zhang, B. Xu, Y. Fan, et J. Tian, "Comparison of dual-biomarker PIB-PET and dual-tracer PET in AD diagnosis." *European Radiology*, vol. 24, no. 11, pp. 2800–2809, 2014.

S. Furber et S. Temple, "Neural systems engineering." *Journal of the Royal Society, Interface / the Royal Society*, vol. 4, no. 13, pp. 193–206, 2007.

F. H. Gage, "Structural plasticity of the adult brain." *Dialogues in Clinical Neuroscience*, vol. 6, no. 2, pp. 135–141, 2004.

K. J. Gorgolewski, G. Varoquaux, G. Rivera, Y. Schwartz, V. V. Sochat, S. S. Ghosh, C. Maumet, T. E. Nichols, J. B. Poline, T. Yarkoni, D. S. Margulies, et R. A. Poldrack,

"NeuroVault.org : A repository for sharing unthresholded statistical maps, parcellations, and atlases of the human brain." *NeuroImage*, vol. 124, no. April, pp. 1242–1244, 2016.

K. R. Gray, R. Wolz, R. A. Heckemann, P. Aljabar, A. Hammers, et D. Rueckert, "Multi-region analysis of longitudinal FDG-PET for the classification of Alzheimer's disease." *NeuroImage*, vol. 60, no. 1, pp. 221–229, 2012. En ligne : `http://dx.doi.org/10.1016/j.neuroimage.2011.12.071`

K. R. Gray, P. Aljabar, R. A. Heckemann, A. Hammers, et D. Rueckert, "Random forest-based similarity measures for multi-modal classification of Alzheimer's disease." *NeuroImage*, vol. 65, pp. 167–175, 2013. En ligne : `http://dx.doi.org/10.1016/j.neuroimage.2012.09.065`

C. Grova, A. Biraben, J. M. Scarabin, P. Jannin, I. Buvat, H. Benali, et B. Gibaud, "A methodology to validate MRI/SPECT registration methods using realistic simulated SPECT data." *Lecture Notes in Computer Science (including subseries Lecture Notes in Artificial Intelligence and Lecture Notes in Bioinformatics)*, vol. 2208, pp. 275–282, 2001.

G. Guo, "Support Vector Machines Applications." *Y. Ma and G. Guo (eds.), Support Vector Machines Applications, Springer.*, pp. 269–302, 2014. En ligne : `http://link.springer.com/10.1007/978-3-319-02300-7`

I. Guyon et A. Elisseeff, "Feature Extraction, Foundations and Applications : An introduction to feature extraction", *Studies in Fuzziness and Soft Computing*, vol. 207, pp. 1–25, 2006. En ligne : `http://eprints.pascal-network.org/archive/00002475/`

C. Habeck, N. L. Foster, R. Perneczky, A. Kurz, P. Alexopoulos, R. A. Koeppe, A. Drzezga, et Y. Stern, "Multivariate and univariate neuroimaging biomarkers of Alzheimer's disease." *NeuroImage*, vol. 40, no. 4, pp. 1503–1515, 2008.

A. Hammers, R. Allom, M. J. Koepp, S. L. Free, R. Myers, L. Lemieux, T. N. Mitchell, D. J. Brooks, et J. S. Duncan, "Three-dimensional maximum probability atlas of the human brain, with particular reference to the temporal lobe." *Human Brain Mapping*, vol. 19, no. 4, pp. 224–247, 2003.

R. A. Heckemann, J. V. Hajnal, P. Aljabar, D. Rueckert, et A. Hammers, "Automatic anatomical brain MRI segmentation combining label propagation and decision fusion." *NeuroImage*, vol. 33, no. 1, pp. 115–126, 2006.

A. Heyman, W. Wilkinson, J. Stafford, M. Helms, A. Sigmon, et T. Weinberg, “Alzheimer’s disease : a study of epidemiological aspects.” *Ann Neurol*, no. 15, p. 335–41, 1984.

C. Hinrichs, V. Singh, L. Mukherjee, G. Xu, M. K. Chung, et S. C. Johnson, “Spatially augmented LPboosting for AD classification with evaluations on the ADNI dataset.” *NeuroImage*, vol. 48, no. 1, pp. 138–149, 2009. En ligne : `http://dx.doi.org/10.1016/j.neuroimage.2009.05.056`

M. Hoffman, “Picture of the Brain, Human Anatomy.” 2014. En ligne : `http://www.webmd.com/brain/picture-of-the-brain#1`

K. Hornik, M. Stinchcombe, et H. White, “Multilayer feedforward networks are universal approximators”, *Neural Netw.*, vol. 2, no. 5, pp. 359–366, 1989.

K. Hornik, “Approximation capabilities of multilayer feedforward networks”, *Neural Networks*, vol. 4, no. 2, pp. 251–257, 1991.

R. Howlett et L. Jain, *Radial Basis Function Networks 2 New Advances in Design.* New York, : Springer-Verlag, 2001, vol. 67.

http ://www.edoctoronline.com, “2016 Alzheimer’s Disease Facts and Figures,Report.” 2016. En ligne : `http://www.edoctoronline.com/medical-atlas.asp?c=4&id=21701`

X. Hua, S. Lee, I. Yanovsky, A. D. Leow, Y.-y. Chou, A. J. Ho, J. Harvey, J. Kornak, N. Schuff, G. E. Alexander, et M. W. Weiner, “Optimizing power to track brain degeneration in Alzheimer’s disease and mild cognitive impairment with tensor-based morphometry : An ADNI study of 515 subjects.” *NIH Public Access*.

L. Ibanez, W. Schroeder, L. Ng, et J. Cates, “The ITK software guide.” 2005.

K. Ishii, T. Soma, A. K. Kono, K. Sofue, N. Miyamoto, T. Yoshikawa, E. Mori, et K. Murase, “Comparison of regional brain volume and glucose metabolism between patients with mild dementia with lewy bodies and those with mild Alzheimer’s disease”, *J Nucl Med*, vol. 48, no. 5, pp. 704–711, 2007.

C. R. Jack, M. M. Shiung, J. L. Gunter, P. C. O’Brien, S. D. Weigand, D. S. Knopman, B. F. Boeve, R. J. Ivnik, G. E. Smith, R. H. Cha, E. G. Tangalos, et R. C. Petersen, “Comparison of different MRI brain atrophy rate measures with clinical disease progression in AD.” *Neurology*, vol. 62, no. 4, pp. 591–600, 2004.

W. J. Jagust, “ADNI PET Core Report 2010.” *Alzheimer’s Dementia*, vol. 6, no. 3, pp. 221–229, 2010.

R. Jahn, “How neurons talk to each other.” 2016. En ligne : `https://www.mpg.de/10743509/how-neurons-talk-to-each-other`

Japan Association of Remote Sensing., “Image Processing - Classification.” pp. 208–225, 1996.

M. Jenkinson et S. Smith, “A global optimisation method for robust affine registration of brain images.” *Medical Image Analysis*, vol. 5, no. 2, pp. 143–156, 2001.

M. Jenkinson, P. Bannister, M. Brady, et S. Smith, “Improved optimization for the robust and accurate linear registration and motion correction of brain images.” *NeuroImage*, vol. 17, no. 2, pp. 825–841, 2002.

K. A. Johnson, N. C. Fox, R. A. Sperling, et W. E. Klunk, “Brain imaging in Alzheimer disease.” *Cold Spring Harbor Perspectives in Medicine*, vol. 2, no. 4, pp. 1–23, 2012.

S. Joshi, D. Shenoy, V. S. G.G., P. Rrashmi, K. Venugopal, et L. Patnaik, “Classification of Alzheimer’s Disease and Parkinson’s Disease by Using Machine Learning and Neural Network Methods.” *2010 Second International Conference on Machine Learning and Computing*, pp. 218–222, 2010. En ligne : `http://ieeexplore.ieee.org/lpdocs/epic03/wrapper.htm?arnumber=5460738`

R. N. Kalaria, G. E. Maestre, R. Arizaga, R. P. Friedland, D. Galasko, K. Hall, J. A. Luchsinger, A. Ogunniyi, E. K. Perry, F. Potocnik, M. Prince, R. Stewart, A. Wimo, Z. X. Zhang, et P. Antuono, “Alzheimer’s disease and vascular dementia in developing countries : prevalence, management, and risk factors.” *The Lancet Neurology*, vol. 7, no. 9, pp. 812–826, 2008.

H. Kalini, “Atlas-based image segmentation : A Survey.” *Neuroscience*, pp. 1–7, 2004.

R. Katzman, “Education and the prevalence of dementia and Alzheimer’s disease.” *Neurology*, no. 43, p. 13–20, 1993.

T. Kawachi, K. Ishii, S. Sakamoto, M. Sasaki, T. Mori, F. Yamashita, H. Matsuda, et E. Mori, “Comparison of the diagnostic performance of FDG-PET and VBM-MRI in very mild Alzheimer’s disease”, *European Journal of Nuclear Medicine and Molecular Imaging*, vol. 33, no. 7, pp. 801–809, 2006.

S. S. Keerthi et C.-J. Lin, “Asymptotic behaviors of support vector machines with Gaussian kernel.” *Neural computation*, vol. 15, no. 7, pp. 1667–89, 2003. En ligne : http://www.ncbi.nlm.nih.gov/pubmed/12816571

S. J. Kiebel, J. Ashburner, J. B. Poline, et K. J. Friston, “MRI and PET coregistration-a cross validation of statistical parametric mapping and automated image registration.” *NeuroImage*, vol. 5, no. 4 Pt 1, pp. 271–279, 1997.

Y. Y. Kim, H. J. Shin, M. J. Kim, et M. J. Lee, “Comparison of effective radiation doses from X-ray, CT, and PET/ CT in pediatric patients with neuroblastoma using a dose monitoring program”, *Diagnostic and Interventional Radiology*, vol. 22, no. 4, pp. 390–394, 2016.

J. S. Kippenhan, W. W. Barker, S. Pascal, J. Nagel, et R. Duara, “Evaluation of a neural-network classifier for PET scans of normal and Alzheimer’s disease subjects.” *Journal of Nuclear Medicine*, vol. 33, no. 8, pp. 1459–1467, 1992.

R. Kirwan, “Brain.” 2016. En ligne : http://www.infocomcanada.com/CMPI/Program%20Guide/brain.htm

S. Klein, M. Staring, K. Murphy, M. A. Viergever, et J. P. W. Pluim, “Elastix : A toolbox for intensity-based medical image registration.” *IEEE Transactions on Medical Imaging*, vol. 29, no. 1, pp. 196–205, 2010.

S. Klöppel, C. M. Stonnington, C. Chu, B. Draganski, I. Scahill, J. D. Rohrer, N. C. Fox, C. R. J. Jr, J. Ashburner, et R. S. J. Frackowiak, “UKPMC Funders Group Automatic classification of MR scans in Alzheimer ’ s disease”, *Brain*, vol. 131, no. Pt 3, pp. 681–689, 2008.

S. B. Kotsiantis, “Supervised machine learning : a review of classification techniques.” *Informatica (03505596)*, vol. 31, no. 3, 2007.

J. Lancaster, L. Rainey, J. Summerlin, et C. Freitas, “Automated labeling of the human brain : a preliminary report on the development and evaluation of a {...}.” *Human Brain Mapping*, vol. 242, pp. 238–242, 1997. En ligne : http://www3.interscience.wiley.com/journal/56443/abstract

J. L. Lancaster, L. H. Rainey, J. L. Summerlin, C. S. Freitas, P. T. Fox, A. C. Evans, A. W. Toga, et J. C. Mazziotta, “Automated labeling of the human brain : A preliminary report on the development and evaluation of a forward-transform method.” *Human Brain Mapping*, vol. 5, no. 4, pp. 238–242, 1997.

J. L. Lancaster, M. G. Woldorff, L. M. Parsons, M. Liotti, C. S. Freitas, L. Rainey, P. V. Kochunov, D. Nickerson, S. A. Mikiten, et P. T. Fox, "Automated Talairach Atlas labels for functional brain mapping." *Human Brain Mapping*, vol. 10, no. 3, pp. 120–131, 2000.

P. E. Lee, G. R. Hsiung, D. Seitz, S. S. Gill, et P. a. Rochon, "Cholinesterase inhibitors", *BC Medical Journal*, vol. 53, no. 8, pp. 404–408, 2011.

L. Lemieux, A. Hammers, T. Mackinnon, et R. S. N. Liu, "Automatic segmentation of the brain and intracranial cerebrospinal fluid in T1-weighted volume MRI scans of the head, and its application to serial cerebral and intracranial volumetry." *Magnetic Resonance in Medicine*, vol. 49, no. 5, pp. 872–884, 2003.

D. Lenzi, L. Serra, R. Perri, P. Pantano, G. L. Lenzi, E. Paulesu, C. Caltagirone, M. Bozzali, et E. Macaluso, "Single domain amnestic MCI : A multiple cognitive domains fMRI investigation." *Neurobiology of Aging*, vol. 32, no. 9, pp. 1542–1557, 2011. En ligne : `http://dx.doi.org/10.1016/j.neurobiolaging.2009.09.006`

A. Liaw et M. Wiener, "Classification and Regression by Random Forest." *R news*, vol. 2, no. December, pp. 18–22, 2002.

J. Liu, M. Li, W. Lan, F.-X. Wu, Y. Pan, et J. Wang, "Classification of Alzheimer's Disease Using Whole Brain Hierarchical Network." *IEEE/ACM transactions on computational biology and bioinformatics*, vol. 14, no. 8, pp. 1–10, 2016. En ligne : `http://www.ncbi.nlm.nih.gov/pubmed/27925595`

Y. Liu, L. Zhu, K. Plössl, S. R. Choi, H. Qiao, X. Sun, S. Li, Z. Zha, et H. F. Kung, "Optimization of automated radiosynthesis of [18F]AV-45 : A new PET imaging agent for Alzheimer's disease." *Nuclear Medicine and Biology*, vol. 37, no. 8, pp. 917–925, 2010.

H. Lodish, A. Berk, S. L. Zipursky, P. Matsudaira, D. Baltimore, et J. Darnell, "Molecular Cell Biology." 2000. En ligne : `https://www.ncbi.nlm.nih.gov/books/NBK21475/`

S. Love, "Neuropathological investigation of dementia : a guide for neurologists." *J Neurol Neurosurg Psychiatry*, vol. 76, pp. v8–14, 2005. En ligne : `http://dx.doi.org/10.1136/jnnp.2005.080754`

J. A. Luchsinger, M.-X. Tang, Y. Stern, S. Shea, et R. Mayeux, "Diabetes Mellitus and Risk of Alzheimer's Disease and Dementia with Stroke in a Multiethnic Cohort." *American Journal of Epidemiology*, vol. 154, no. 7, p. 635, 2001. En ligne : `http://dx.doi.org/10.1093/aje/154.7.635`

R. Maani, Y. H. Yang, et S. Kalra, “Voxel-based texture analysis of the brain”, *PLoS ONE*, vol. 10, no. 3, pp. 1–19, 2015.

P. J. Markiewicz, J. C. Matthews, J. Declerck, et K. Herholz, “Robustness of multivariate image analysis assessed by resampling techniques and applied to FDG-PET scans of patients with Alzheimer’s disease.” pp. 472–485, 2009.

I. Matsunari, M. Samuraki, W.-P. Chen, D. Yanase, N. Takeda, K. Ono, M. Yoshita, H. Matsuda, M. Yamada, et S. Kinuya, “Comparison of 18F-FDG PET and optimized voxel-based morphometry for detection of Alzheimer’s disease : aging effect on diagnostic performance.” *Journal of nuclear medicine : official publication, Society of Nuclear Medicine*, vol. 48, no. 12, pp. 1961–1970, 2007.

J. Maus, “PET-schema.png.” 2003. En ligne : `https://commons.wikimedia.org/wiki/File:PET-schema.png`

Mayo Clinic Staff, “Mild cognitive impairment.” 2017. En ligne : `http://www.mayoclinic.org/diseases-conditions/mild-cognitive-impairment/home/ovc-20206082`

G. M. McKhann, D. S. Knopman, H. Chertkow, B. T. Hyman, C. R. Jack, C. H. Kawas, W. E. Klunk, W. J. Koroshetz, J. J. Manly, R. Mayeux, R. C. Mohs, J. C. Morris, M. N. Rossor, P. Scheltens, M. C. Carrillo, B. Thies, S. Weintraub, et C. H. Phelps, “The diagnosis of dementia due to Alzheimer’s disease : Recommendations from the National Institute on Aging-Alzheimer’s Association workgroups on diagnostic guidelines for Alzheimer’s disease.” *Alzheimer’s and Dementia*, vol. 7, no. 3, pp. 263–269, 2011. En ligne : `http://dx.doi.org/10.1016/j.jalz.2011.03.005`

K. MILLER, Z. TAYLOR, et W. L. NOWINSKI, “Towards Computing Brain Deformations for Diagnosis, Prognosis and Neurosurgical Simulation”, *Journal of Mechanics in Medicine and Biology*, vol. 05, no. 01, pp. 105–121, 2005.

S. Miller, E. Fenstermacher, J. Bates, D. Blacker, et R. A. Sperling, “Hippocampal activation in adults with mild cognitive impairment predicts subsequent cogntive decline.” *J Neurol Neurosurg Psychiatry*, vol. 79, no. 6, pp. 630–635, 2009.

J. B. O. Mitchell, “Machine learning methods in chemoinformatics.” *Wiley Interdisciplinary Reviews : Computational Molecular Science*, vol. 4, no. October, pp. n/a–n/a, 2014. En ligne : `http://doi.wiley.com/10.1002/wcms.1183`

J.-P. Morin, C. Desrosiers, et L. Duong, “Atlas-based segmentation of brain magnetic

resonance imaging using random walks", *2012 IEEE Computer Society Conference on Computer Vision and Pattern Recognition Workshops*, pp. 44–49, 2012. En ligne : http://ieeexplore.ieee.org/lpdocs/epic03/wrapper.htm?arnumber=6239246

L. Mosconi, S. Sorbi, M. J. de Leon, Y. Li, B. Nacmias, P. S. Myoung, W. Tsui, A. Ginestroni, V. Bessi, M. Fayyazz, P. Caffarra, et A. Pupi, "Hypometabolism exceeds atrophy in presymptomatic early-onset familial Alzheimer's disease." *Journal of nuclear medicine*, vol. 47, no. 11, pp. 1778–1786, 2006.

L. Mucke, "Neuroscience : Alzheimer's disease." *Nature*, vol. 461, no. 7266, pp. 895–7, 2009. En ligne : http://dx.doi.org/10.1038/461895a

Neurodegenerative Diseases Research, "Neurodegenerative diseases." 2014. En ligne : http://www.neurodegenerationresearch.eu/about/what/

F. P. Oliveira et J. M. R. Tavares, "Medical image registration : A review." *Computer Methods in Biomechanics and Biomedical Engineering*, vol. 17, no. 2, pp. 73–93, 2014. En ligne : http://www.ncbi.nlm.nih.gov/pubmed/224353555Cnhttp://www.tandfonline.com/doi/abs/10.1080/10255842.2012.670855

Orthopaedics, "What is Magnetic Resonance Imaging." 2017. En ligne : http://www.orthopaedics.com.sg/treatments/magnetic-resonance-imaging-mri

B. R. Ott, R. A. Cohen, A. Gongvatana, C. Ozioma, C. E. Johanson, E. G. Stopa, et J. E. Donahue, "Brain ventricular volume and cerebrospinal fluid biomarkers of Alzheimer's disease." *Alzheimers Dis*, vol. 20, no. 2, pp. 647–657, 2011.

F. Pedersen, M. Bergstrom, E. Bengtsson, et E. Maripuu, "Principal component analysis of dynamic PET and gamma camera images : a methodology to visualize the signals in the presence of large noise." *1993 IEEE Conference Record Nuclear Science Symposium and Medical Imaging Conference*, pp. 1734–1738, 1993. En ligne : http://ieeexplore.ieee.org/lpdocs/epic03/wrapper.htm?arnumber=373589

D. P. Pelvig, H. Pakkenberg, A. K. Stark, et B. Pakkenberg, "Neocortical glial cell numbers in human brains." *Neurobiology of Aging*, vol. 29, no. 11, pp. 1754–1762, 2008.

R. C. Petersen, J. C. Stevens, M. Ganguli, E. G. Tangalos, J. L. Cummings, et S. T. Dekosky, "Practice parameter : Early detection of dementia : Mild Cognitive Impairment (an evidence-based review)." *Neurology*, vol. 56, pp. 1133–1142, 2001.

D. L. Pham, C. Xu, et J. L. Prince, “Current methods in medical image segmentation.” *Biomedical Engineering*, no. 2, pp. 315–37, 2000.

M. J. Pontecorvo et M. A. Mintun, “PET amyloid imaging as a tool for early diagnosis and identifying patients at risk for progression to Alzheimer’s disease.” *Alzheimer’s Research & Therapy*, vol. 3, no. 2, p. 11, 2011.

A. Pop, “Principal components analysis (PCA).” *Computers & Geosciences*, pp. 2–6, 1993. En ligne : `http://www.sciencedirect.com/science/article/pii/009830049390090R`

S. Przedborski, M. Vila, et V. Jackson-lewis, “Neurodegeneration : What is it and where are we ?” *J. Clin. Invest.*, vol. 111, no. 1, pp. 3–10, 2003.

S. Pushpa, P. Vinod, et C. Maple, “Creating a forest of binary search trees for a multiprocessor system.” *PARELEC 2006 - Proceedings : International Symposium on Parallel Computing in Electrical Engineering*, pp. 290–294, 2006.

A. Rao, Y. Lee, A. Gass, et A. Monsch, “Classification of Alzheimer’s Disease from structural MRI using sparse logistic regression with optional spatial regularization.” *Proceedings of the Annual International Conference of the IEEE Engineering in Medicine and Biology Society, EMBS*, no. 3, pp. 4499–4502, 2011.

D. B. Reisberg, “What Are the 7 Stages of Alzheimer’s Disease ?” 2016. En ligne : `http://www.alzheimers.net/stages-of-alzheimers-disease/`

E. Richard, B. A. Schmand, P. Eikelenboom, et W. A. Van Gool, “MRI and cerebrospinal fluid biomarkers for predicting progression to Alzheimer’s disease in patients with mild cognitive impairment : A diagnostic accuracy study.” *BMJ open*, vol. 3, no. 6, pp. 1–8, 2013. En ligne : `http://www.pubmedcentral.nih.gov/articlerender.fcgi?artid=3686215{&}tool=pmcentrez{&}rendertype=abstract`

M. D. Richard et R. P. Lippmann, “Neural network classifiers estimate Bayesian a posteriori probabilities.” *Neural computation*, vol. 3, no. 4, pp. 461–483, 1991.

E. D. Roberson et L. Mucke, “100 Years and Counting : Prospecs for Defeating Alzheimer’s Disease.” *Science*, vol. 314, no. 5800, pp. 781–784, 2013.

F. Rodrigues et M. Silveira, “Longitudinal FDG-PET features for the classification of Alzheimer’s disease.” *2014 36th Annual International Conference of the IEEE Engineering in Medicine and Biology Society, EMBC 2014*, pp. 1941–1944, 2014.

R. Rojas, *Neural Networks : A Systematic Introduction.* New York, NY, USA : Springer-Verlag New York, Inc., 1996.

G. Román et B. Pascual, "Contribution of Neuroimaging to the Diagnosis of Alzheimer's Disease and Vascular Dementia." *Archives of Medical Research*, vol. 43, no. 8, pp. 671–676, 2012.

L. Saint-Aubert, F. Nemmi, P. Péran, E. J. Barbeau, P. Payoux, F. Chollet, et J. Pariente, "Comparison between PET template-based method and MRI-based method for cortical quantification of florbetapir (AV-45) uptake in vivo." *European Journal of Nuclear Medicine and Molecular Imaging*, vol. 41, no. 5, pp. 836–843, 2014.

L. Saint-Aubert, E. J. Barbeau, P. Péran, F. Nemmi, C. Vervueren, H. Mirabel, P. Payoux, A. Hitzel, F. Bonneville, R. Gramada, M. Tafani, C. Vincent, M. Puel, S. Dechaumont, F. Chollet, et J. Pariente, "Cortical florbetapir-PET amyloid load in prodromal Alzheimer's disease patients." *EJNMMI research*, vol. 3, no. 1, p. 43, 2013. En ligne : `http://www.pubmedcentral.nih.gov/articlerender.fcgi?artid=3733998&tool=pmcentrez&rendertype=abstract`

D. Salas-Gonzalez, J. M. Górriz, J. Ramírez, I. A. Illán, M. López, F. Segovia, R. Chaves, P. Padilla, et C. G. Puntonet, "Feature selection using factor analysis for Alzheimer's diagnosis using 18F-FDG PET images." *Medical physics*, vol. 37, no. 11, pp. 6084–95, 2010. En ligne : `http://www.pubmedcentral.nih.gov/articlerender.fcgi?artid=2994934{&}tool=pmcentrez{&}rendertype=abstract`

E. Salmon, "Différentes facettes de la maladie de type Alzheimer", *Revue médicale de Liège*, vol. 63, no. 5, pp. 299–302, 2008.

A. Serrano-Pozo, M. P. Frosch, E. Masliah, et B. T. Hyman, "Neuropathological alterations in Alzheimer disease." *Cold Spring Harbor perspectives in medicine*, vol. 1, no. 1, pp. 1–23, 2011.

M. Silveira et J. Marques, "Boosting Alzheimer Disease Diagnosis using PET Images." *Proceedings of the 2010 20th IEEE International Conference on Pattern Recognition (ICPR)*, pp. 2556–2559, 2010.

D. H. Silverman, G. W. Small, C. Y. Chang, C. S. Lu, M. A. Kung De Aburto, W. Chen, J. Czernin, S. I. Rapoport, P. Pietrini, G. E. Alexander, M. B. Schapiro, W. J. Jagust, J. M. Hoffman, K. A. Welsh-Bohmer, A. Alavi, C. M. Clark, E. Salmon, M. J. De Leon, R. Mielke, J. L. Cummings, A. P. Kowell, S. S. Gambhir, C. K. Hoh, et M. E. Phelps,

"Positron emission tomography in evaluation of dementia : Regional brain metabolism and long-term outcome." *JAMA*, vol. 286, no. 17, pp. 2120–2127, 2001. En ligne : http://dx.doi.org/10.1001/jama.286.17.2120

D. Silverman, *PET in the Evaluation of Alzheimer's Disease and Related Disorders.*, 1er éd. New York : Springer Science and Business Media, 2009.

N. Smailagic, M. Vacante, C. Hyde, S. Martin, O. Ukoumunne, et C. Sachpekidis, "18F-FDG PET for the early diagnosis of Alzheimer's disease dementia and other dementias in people with mild cognitive impairment (MCI)." *Cochrane Database of Systematic Reviews*, no. 1, 2015. En ligne : http://onlinelibrary.wiley.com/doi/10.1002/14651858.CD010632.pub2/abstract

S. M. Smith, M. Jenkinson, M. W. Woolrich, C. F. Beckmann, T. E. J. Behrens, H. Johansen-Berg, P. R. Bannister, M. De Luca, I. Drobnjak, D. E. Flitney, R. K. Niazy, J. Saunders, J. Vickers, Y. Zhang, N. De Stefano, J. M. Brady, et P. M. Matthews, "Advances in functional and structural MR image analysis and implementation as FSL." *NeuroImage*, vol. 23, no. SUPPL. 1, pp. 208–219, 2004.

J. Stoeckel et G. Fung, "SVM Feature Selection for Classification of SPECT Images of Alzheimer's Disease Using Spatial Information." *Fifth IEEE International Conference on Data Mining (ICDM'05)*, vol. 11, no. 2, pp. 410–417, 2007. En ligne : http://ieeexplore.ieee.org/lpdocs/epic03/wrapper.htm?arnumber=1565706

K. Strimbu et J. a. Tavel, "What are Biomarkers ?" *Current Opinion in HIV and AIDS (LWW)*, vol. 5, no. 6, pp. 463–466, 2011.

E. Stühler et D. Merhof, "Principal Component Analysis Applied to SPECT and PET Data of Dementia Patients–A Review." *Principal Component Analysis : Multidisciplinary applications*, 2012. En ligne : http://nozdr.ru/data/media/biblioteka/kolxo3/M_Mathematics/MV_Probability/MVsa_Statisticsandapplications/SanguansatP.(ed.)Principalcomponentanalysis-multidisciplinaryapplications(InTech,2012)(ISBN9789535101291)(O)(212s)_MVsa_.pdf#page=179

H.-I. Suk et D. Shen, "Deep learning-based feature representation for AD/MCI classification." dans *International Conference on MICCAI*. Springer, 2013, pp. 583–590.

P. M. Thompson, K. M. Hayashi, G. I. De Zubicaray, A. L. Janke, S. E. Rose, J. Semple, M. S. Hong, D. H. Herman, D. Gravano, D. M. Doddrell, et A. W. Toga, "Mapping hip-

pocampal and ventricular change in Alzheimer disease." *NeuroImage*, vol. 22, no. 4, pp. 1754–1766, 2004.

L. Tilley, K. Morgan, et N. Kalsheker, "Genetic risk factors in Alzheimer's disease." *Journal of Clinical Pathology*, vol. 51, no. 6, pp. 293–304, 1998.

M. Toews, W. Wells, L. Collinsc, et T. Arbeld, "Feature-Based Morphometry : Discovering Group-related Anatomical Patterns", *Neuroimage*, vol. 49, no. 3, pp. 2318–2327, 2010.

T. Tong, K. Gray, Q. Gao, L. Chen, et D. Rueckert, "Multi-modal classification of Alzheimer's disease using nonlinear graph fusion." *Pattern Recognition*, vol. 63, no. September 2016, pp. 171–181, 2017. En ligne : `http://dx.doi.org/10.1016/j.patcog.2016.10.009`

S. L. Tyas, J. Manfreda, L. A. Strain, et P. R. Montgomery, "Risk factors for Alzheimer's disease : a population-based, longitudinal study in Manitoba, Canada." *International journal of epidemiology*, vol. 30, no. 3, pp. 590–7, 2001. En ligne : `http://www.ncbi.nlm.nih.gov/pubmed/11416089`

N. Tzourio-Mazoyer, B. Landeau, D. Papathanassiou, F. Crivello, O. Etard, N. Delcroix, B. Mazoyer, et M. Joliot, "Automated anatomical labeling of activations in SPM using a macroscopic anatomical parcellation of the MNI MRI single-subject brain." *NeuroImage*, vol. 15, no. 1, pp. 273–289, 2002.

L. A. Van de Pol, E. S. C. Korf, W. M. Van der Flier, H. R. Brashear, N. C. Fox, F. Barkhof, et P. Scheltens, "Magnetic resonance imaging predictors of cognition in mild cognitive impairment." *Archives of Neurology*, vol. 64, no. 7, pp. 1023–1028, 2007. En ligne : `http://search.ebscohost.com/login.aspx?direct=true&db=psyh&AN=2007-11296-006&lang=de&site=ehost-live&scope=site`

W. F. Velicer, "Determining the number of components from the matrix of partial correlations", *Psychometrika*, vol. 41, no. 3, pp. 321–327, 1976.

P. Vemuri, H. J. Wiste, S. D. Weigand, D. S. Knopman, J. Q. Trojanowski, L. M. Shaw, M. A. Bernstein, P. S. Aisen, M. Weiner, R. C. Petersen, et C. R. Jack, "Serial MRI and CSF biomarkers in normal aging, MCI, and AD." *Neurology*, vol. 75, no. 2, pp. 143–151, 2010.

P. Vemuri et C. Jack, "Role of structural MRI in Alzheimer's disease." *Alzheimer's Research & Therapy*, vol. 2, no. 4, p. 23, 2010. En ligne : `http://alzres.com/content/2/4/23`

A. G. Vlassenko, T. L. S. Benzinger, et J. C. Morris, "PET amyloid-beta imaging in preclinical Alzheimer's disease." *Biochimica et Biophysica Acta - Molecular Basis of Disease*, vol. 1822, no. 3, pp. 370–379, 2012. En ligne : `http://dx.doi.org/10.1016/j.bbadis.2011.11.005`

C. Wachinger, M. Toews, G. Langs, W. Wells IIIi, et P. Golland, "Keypoint Transfer Segmentation", *Information Processing in Medical Imaging*, vol. 9123, pp. 233–245, 2015.

K. B. Walhovd, A. M. Fjell, J. Brewer, L. K. McEvoy, C. Fennema-Notestine, D. J. Hagler, R. G. Jennings, D. Karow, A. Dale, et T. A. D. N. Initiative, "Combining MRI, PET and CSF biomarkers in diagnosis and prognosis of Alzheimer's disease." *American Journal of Neuroradiology*, vol. 31, no. 2, p. 347, 2010.

C. Watson, M. Kirkcaldie, et G. Paxinos, *The Brain : An Introduction to Functional Neuroanatomy.* Elsevier Science Publishing Co Inc, 2010.

M. P. Wattjes, "Structural MRI." *International Psychogeriatrics*, vol. 23, no. S2, p. S13–S24, 2011.

M. Weiner et Z. Khachaturian, "The Use of MRI and PET for Clinical Diagnosis of Dementia and Investigation of Cognitive Impairment : A Consensus Report." *Alzheimer's Association, Chicago, IL*, no. 1, pp. 1–15, 2005. En ligne : `http://www.alz.co.il/pdf/603333.pdf`

E. Westman, A. Simmons, J. S. Muehlboeck, P. Mecocci, B. Vellas, M. Tsolaki, I. Kloszewska, H. Soininen, M. W. Weiner, S. Lovestone, C. Spenger, et L. O. Wahlund, "AddNeuroMed and ADNI : Similar patterns of Alzheimer's atrophy and automated MRI classification accuracy in Europe and North America." *NeuroImage*, vol. 58, no. 3, pp. 818–828, 2011.

R. Wolz, V. Julkunen, J. Koikkalainen, E. Niskanen, D. P. Zhang, D. Rueckert, H. Soininen, et J. Lötjönen, "Multi-method analysis of MRI images in early diagnostics of Alzheimer's disease." *PLoS ONE*, vol. 6, no. 10, pp. 1–9, 2011.

R. P. Woods, S. T. Grafton, C. J. Holmes, S. R. Cherry, et J. C. Mazziotta, "Automated Image Registration : I. General methods and intrasubject, intramodality validation." *Journal of computer assisted tomography*, vol. 22, no. February 1998, pp. 139–152, 1998.

L. Xu, X. Wu, K. Chen, et L. Yao, "Multi-modality sparse representation-based classification for Alzheimer's disease and mild cognitive impairment." *Computer Methods*

and Programs in Biomedicine, vol. 122, no. 2, pp. 182–190, 2015. En ligne : http://dx.doi.org/10.1016/j.cmpb.2015.08.004

D. Zhang et D. Shen, "Predicting future clinical changes of MCI patients using longitudinal and multimodal biomarkers", *PLoS ONE*, vol. 7, no. 3, 2012.

D. Zhang, Y. Wang, L. Zhou, H. Yuan, et D. Shen, "Multimodal classification of Alzheimer's disease and mild cognitive impairment." *NeuroImage*, vol. 55, no. 3, pp. 856–867, 2011. En ligne : http://dx.doi.org/10.1016/j.neuroimage.2011.01.008

D. Zhang, Y. Wang, L. Zhou, H. Yuan, D. Shen, et al., "Multimodal classification of Alzheimer's disease and mild cognitive impairment." *Neuroimage*, vol. 55, no. 3, pp. 856–867, 2011.

S. Zhang, N. Smailagic, C. Hyde, N.-S. Ah, Y. Takwoingi, R. Mcshane, et J. Feng, "11C-PIB-PET for the early diagnosis of Alzheimer's disease dementia and other dementias in people with mild cognitive impairment (MCI) (Review)." *Cochrane Database of Systematic Reviews*, no. 7, pp. 10–12, 2014.

B. Zitová et J. Flusser, "Image registration methods : A survey." *Image and Vision Computing*, vol. 21, no. 11, pp. 977–1000, 2003.